

UNIVERSITÉ DE SAVOIE,
LABORATOIRE D'ANNECY-LE-VIEUX DE PHYSIQUE THÉORIQUE

THÈSE

présentée pour obtenir le grade de

DOCTEUR EN PHYSIQUE
DE L'UNIVERSITÉ DE SAVOIE
Spécialité: Physique Théorique

par

LÊ Đức Ninh

Sujet :

**ONE-LOOP YUKAWA CORRECTIONS TO THE
PROCESS $pp \rightarrow b\bar{b}H$ IN THE STANDARD MODEL AT
THE LHC: LANDAU SINGULARITIES.**

Soutenue le 22 Juillet 2008 après avis des rapporteurs :

Mr. Guido ALTARELLI

Mr. Ansgar DENNER

devant la commission d'examen composée de :

Mr. Guido ALTARELLI Rapporteur

Mr. Patrick AURENCHE

Mr. Fawzi BOUDJEMA Directeur de thèse

Mr. Ansgar DENNER Rapporteur

Mr. Luc FRAPPAT Président du jury

Mr. HOÀNG Ngọc Long Co-directeur de thèse

Mr. NGUYỄN Anh Kỳ

Résumé

Le sujet de ma thèse recouvre deux aspects. En premier lieu, l'objectif était d'étudier et d'améliorer les méthodes de calcul à une boucle pour les corrections radiatives dans le cadre des théories de champs perturbatives. En second lieu, l'objectif était d'appliquer ces techniques pour calculer les effets dominants des corrections radiatives électrofaibles au processus important de production de Higgs associé à deux quarks bottom au LHC (Large Hadron Collider) du CERN. L'étude concerne le Higgs du Modèle Standard.

Le premier objectif est d'importance plutôt théorique. Bien que la méthode générale pour le calcul à une boucle des corrections radiatives dans le modèle standard soit, en principe, bien compris par le biais de la renormalisation, il y a un certain nombre de difficultés techniques. Ces difficultés sont liées aux intégrales de boucle, intégration sur les impulsions des particules virtuelles. En particulier les intégrales dites tensorielles peuvent être "réduites" en intégrales scalaires. Ceci revient à exprimer ces intégrales tensorielles sur une base d'intégrales scalaires pour lesquels des bibliothèques numériques existent. Cependant cette réduction du rang de l'intégrale alourdit énormément les expressions analytiques surtout lorsqu'il s'agit de processus impliquant plus de 4 particules externes, comme dans le cas de notre application, jusqu'à rendre le code pour les amplitudes de transition pratiquement inexploitable même avec des ordinateurs puissants. Dans cette thèse, nous avons étudié ce problème et réalisé que tout le calcul peut être facilement optimisé si l'on utilise la méthode des amplitudes d'hélicité. Un autre problème est lié aux propriétés analytiques des intégrales scalaires. Une partie importante de cette thèse est consacrée à ce problème et à l'étude des équations de Landau. Nous avons trouvé des effets significatifs en raison de singularités de Landau dans le processus de production de Higgs associé à deux quarks bottom au LHC.

Le deuxième objectif est d'ordre pratique avec des conséquences au niveau phénoménologique et expérimental importants puisqu'il s'agit de raffiner les prédictions concernant le taux de production du Higgs en association avec des quarks b au LHC. L'intérêt de ce processus est de tester le mécanisme de génération de masses en sondant le couplage de Yukawa du Higgs au quark b. Dans cette thèse, nous avons calculé les corrections électrofaibles à ce processus. On peut résumer les résultats comme suit. Si la masse du Higgs est d'environ 120 GeV, la correction au premier ordre dominant est petite de l'ordre d'environ -4% . Si la masse de Higgs est d'environ 160 GeV, seuil de production d'une paire de W par le Higgs, les corrections électrofaibles bénéficient du couplage fort du Yukawa du top et sont amplifiées par la singularité de Landau conduisant à une importante correction d'environ 50%. Ce phénomène important est soigneusement étudiée dans cette thèse.

Tóm tắt

Mục đích của luận án này bao gồm hai phần chính. Phần thứ nhất liên quan đến việc nghiên cứu các phương pháp tính bổ đính vòng trong khuôn khổ của lý thuyết nhiễu loạn. Phần thứ hai bao gồm việc vận dụng các phương pháp trên để tính toán bổ đính liên quan đến tương tác yếu ở mức một vòng cho quá trình $pp \rightarrow b\bar{b}H$ tại máy gia tốc LHC. Các tính toán trong luận án này giới hạn trong khuôn khổ của mô hình chuẩn.

Mục đích thứ nhất là quan trọng về mặt lý thuyết. Mặc dù cách thức tính bổ đính một vòng trong lý thuyết trường nhiễu loạn, về mặt nguyên tắc, đã được hiểu một cách rõ ràng thông qua việc tái chuẩn hoá. Trong thực tế, quy trình đó biểu lộ nhiều khó khăn liên quan đến việc tính tích phân vòng. Phương pháp giải tích gặp nhiều khó khăn khi các tính toán có nhiều hơn 4 hạt ở trạng thái ngoài. Đó là vì biểu thức đại số của biên độ tán xạ trở nên rất phức tạp và khó xử lý. Trong luận án này, chúng tôi đã nghiên cứu vấn đề này và nhận thấy rằng việc tính toán sẽ đơn giản hơn rất nhiều nếu sử dụng phương pháp biên độ tán xạ phân cực. Một vấn đề khác liên quan đến tính chất giải tích của tích phân vòng. Một phần quan trọng của luận án được dành để nghiên cứu vấn đề này bằng cách sử dụng phương trình Landau. Chúng tôi đã tìm thấy những hiệu ứng quan trọng của dị thường Landau trong quá trình $pp \rightarrow b\bar{b}H$.

Mục đích thứ hai là quan trọng về mặt thực nghiệm. Quá trình $pp \rightarrow b\bar{b}H$ tại máy gia tốc LHC là rất quan trọng trong việc xác định hệ số tương tác giữa Higgs và quark b. Nếu hệ số tương tác này là lớn như tiên đoán của mô hình Siêu đối xứng tối thiểu thì tiết diện tán xạ sẽ rất lớn. Trong luận án này, dựa vào các phương pháp lý thuyết thảo luận ở trên, chúng tôi đã tính toán các bổ đính chính của tương tác yếu. Kết quả là như sau. Nếu khối lượng của hạt Higgs khoảng 120GeV thì bổ đính ở mức một vòng là nhỏ, khoảng -4% . Nếu khối lượng của hạt Higgs vào khoảng 160GeV thì bổ đính trên được làm tăng thêm nhiều bởi dị thường Landau, khoảng 50%. Hiện tượng quan trọng này được nghiên cứu kỹ trong luận án.

Table of Contents

Table of Contents	i
Abstract	v
Acknowledgements	vii
Introduction	1
1 The Standard Model and beyond	9
1.1 QCD	11
1.2 The Glashow-Salam-Weinberg Model	14
1.2.1 Gauge sector	14
1.2.2 Fermionic gauge sector	15
1.2.3 Higgs sector	15
1.2.4 Fermionic scalar sector	16
1.2.5 Quantisation: Gauge-fixing and Ghost Lagrangian	17
1.2.6 One-loop renormalisation	18
1.3 Higgs Feynman Rules	22
1.4 Problems of the Standard Model	25
1.5 Minimal Supersymmetric Standard Model	26
1.5.1 The Higgs sector of the MSSM	28

1.5.2	Higgs couplings to gauge bosons and heavy quarks	30
2	Standard Model Higgs production at the LHC	31
2.1	The Large Hadron Collider	31
2.2	SM Higgs production at the LHC	33
2.3	Experimental signatures of the SM Higgs	36
2.4	Summary and outlook	38
3	Standard Model $b\bar{b}H$ production at the LHC	41
3.1	Motivation	41
3.2	General considerations	43
3.2.1	Leading order considerations	43
3.2.2	Electroweak Yukawa-type contributions, novel characteristics .	45
3.2.3	Three classes of diagrams and the chiral structure at one-loop	47
3.3	Renormalisation	50
3.4	Calculation details	53
3.4.1	Loop integrals, Gram determinants and phase space integrals .	54
3.4.2	Checks on the results	55
3.5	Results: $M_H < 2M_W$	57
3.5.1	Input parameters and kinematical cuts	57
3.5.2	NLO EW correction with $\lambda_{bbH} \neq 0$	57
3.5.3	EW correction in the limit of vanishing λ_{bbH}	60
3.6	Summary	62
4	Landau singularities	65
4.1	Singularities of complex integrals	66
4.2	Landau equations for one-loop integrals	70
4.3	Necessary and sufficient conditions for Landau singularities	74
4.4	Nature of Landau singularities	78

4.4.1	Nature of leading Landau singularities	78
4.4.2	Nature of sub-LLS	82
4.5	Conditions for leading Landau singularities to terminate	87
4.6	Special solutions of Landau equations	89
4.6.1	Infrared and collinear divergences	89
4.6.2	Double parton scattering singularity	91
5	SM $b\bar{b}H$ production at the LHC: $M_H \geq 2M_W$	95
5.1	Motivation	95
5.2	Landau singularities in $gg \rightarrow b\bar{b}H$	96
5.2.1	Three point function	96
5.2.2	Four point function	99
5.2.3	Conditions on external parameters to have LLS	106
5.3	The width as a regulator of Landau singularities	113
5.4	Calculation and checks	114
5.5	Results in the limit of vanishing $\lambda_{b\bar{b}H}$	116
5.5.1	Total cross section	117
5.5.2	Distributions	119
5.6	Results at NLO with $\lambda_{b\bar{b}H} \neq 0$	123
5.6.1	Width effect at NLO	123
5.6.2	NLO corrections with $m_b \neq 0$	124
5.7	Summary	126
6	Conclusions	129
A	The helicity amplitude method	133
A.1	The method	133
A.2	Transversality and gauge invariance	136

B Optimization with FORM	139
B.1 Optimization	139
B.2 Technical details	142
B.3 Automation with FORM	145
C Phase space integral	149
C.1 $2 \rightarrow 3$ phase space integral	149
C.2 Numerical integration with BASES	154
D Mathematics	157
D.1 Logarithms and Powers	157
D.2 Dilogarithms	158
D.3 Gamma and Beta functions	159
D.4 Integrals	160
E Scalar box integrals with complex masses	163
E.1 Integral with two opposite lightlike external momenta	164
E.2 Integral with two adjacent lightlike external momenta	168
Bibliography	173

Abstract

The aim of this thesis is twofold. First, to study methods to calculate one-loop corrections in the context of perturbative theories. Second, to apply those methods to calculate the leading electroweak (EW) corrections to the important process of Higgs production associated with two bottom quarks at the CERN Large Hadron Collider (LHC). Our study is restricted to the Standard Model (SM).

The first aim is of theoretical importance. Though the general method to calculate one-loop corrections in the SM is, in principle, well understood by means of renormalisation, it presents a number of technical difficulties. They are all related to loop integrals. The analytical method making use of various techniques to reduce all the tensorial integrals in terms of a basis of scalar integrals is most widely used nowadays. A problem with this method is that for processes with more than 4 external particles the amplitude expressions are extremely cumbersome and very difficult to handle even with powerful computers. In this thesis, we have studied this problem and realised that the whole calculation can be easily optimised if one uses the helicity amplitude method. Another general problem is related to the analytic properties of the scalar loop integrals. An important part of this thesis is devoted to studying this by using Landau equations. We found significant effects due to Landau singularities in the process of Higgs production associated with two bottom quarks at the LHC.

The second aim is of practical (experimental) importance. Higgs production associated with bottom quarks at the LHC is a very important process to understand the

bottom-Higgs Yukawa coupling. If this coupling is strongly enhanced as predicted by the Minimal Supersymmetric Standard Model (MSSM) then this process can have a very large cross section. In this thesis, based on the theoretical study mentioned above, we have calculated the leading EW corrections to this process. The result is the following. If the Higgs mass is about 120GeV then the next-to-leading order (NLO) correction is small, about -4% . If the Higgs mass is about 160GeV then the EW correction is strongly enhanced by the Landau singularities, leading to a significant correction of about 50%. This important phenomenon is carefully studied in this thesis.

Acknowledgements

I would like to thank Fawzi BOUDJEMA, my friendly supervisor, for accepting me as his student, giving me an interesting topic, many useful suggestions and constant support during this research. In particular, he has suggested and encouraged me a lot to attack the difficult problem of Landau singularities. His enthusiasm for physics was always great and it inspired me a lot. By guiding me to finish this thesis, he has done so much to mature my approach to physics.

I admire Patrick AURENCHE for his personal character and physical understanding. It was always a great pleasure for me to see and talk to him. In every physical discussion since the first time we met in Hanoi (2003), I have learnt something new from him. The way he attacks any physical problem is so simple and pedagogical. I thank him for bringing me to Annecy (the most beautiful city I have ever seen), filling my Ph.D years with so many beautiful weekends at his house. I will never forget the trips to Lamastre. He has carefully read the manuscript and given me a lot of suggestions. Without his help and continuous support I would not be the person I am today. Thanks, Patrick!

I am deeply indebted to Guido ALTARELLI for his guidance, support and a lot of fruitful discussions during the one-year period I was at CERN. He has also spent time and effort to read the manuscript as a rapporteur.

Ansgar DENNER, as a rapporteur, has carefully read the manuscript and given me many comments and suggestions which improved a lot the thesis. I greatly appreciate it and thank him so much.

I am grateful to HOÀNG Ngọc Long for his continuous encouragement and support. He

has read the manuscript and given me valuable comments. I thank NGUYỄN Anh Kỳ for suggesting me to apply for the CERN Marie Curie fellowship and constant support. The help of the Institute of Physics in Hà Nội is greatly acknowledged.

For interesting discussions and help I would like to thank Nans BARO, James BEDFORD, Geneviève BÉLANGER, Christophe BERNICOT, Thomas BINOTH, Nouredine BOUAYED, ĐÀO Thị Nhung, Cedric DELAUNAY, Ansgar DENNER, Stefan DITTMAIER, ĐỖ Hoàng Sơn, John ELLIS, Luc FRAPPAT, Junpei FUJIMOTO, Jean-Philippe GUILLET, Thomas HAHN, Wolfgang HOLLIK, Kiyoshi KATO, Yoshimasa KURIHARA, Mühlleitner MARGARETE, Zoltan NAGY, Éric PILON, Grégory SANGUINETTI, Pietro SLAVICH, Peter UWER, Jos VERMASEREN, VŨ Anh Tuấn, John WARD and Fukuko YUASA. Special thanks go to Éric PILON for many fruitful discussions and explaining me useful mathematical tricks related to Landau singularities. Other special thanks go to YUASA-san for comparisons between her numerical code and our code for the four-point function with complex masses.

I would like to thank Jean-Philippe GUILLET for his help with the computer system and his suggestion to use Perl.

ĐỖ Hoàng Sơn is very good at computer and Linux operating system. He has improved both my computer and my knowledge of it. Thanks, Sơn!

I acknowledge the financial support of LAPTH, *Rencontres du Vietnam* sponsored by Odon VALLET and the *Marie Curie Early Stage Training Grant of the European Commission*. In particular, I am grateful to TRẦN Thanh Vân for his support.

Dominique TURC-POENCIER, Véronique JONNERY, Virginie MALAVAL, Nanie PERLIN, Diana DE TOTH and Suzy VASCOTTO make CERN and LAPTH really special places and I thank them for their help.

Last, but by no means least I owe a great debt to my parents NGUYỄN Thị Thắm and LÊ Trần Phương, my sister LÊ Thị Nam and her husband LÊ Quang Đông, and my wife ĐÀO Thị Nhung, for their invaluable love.

Introduction

In the realm of high energy physics, the Standard Model (SM) of particle physics [1, 2, 3, 4, 5, 6, 7] is the highest achievement to date. Almost all its predictions have been verified by various experiments [8, 9]. The only prediction of the SM which has not been confirmed by any experiment is the existence of a scalar fundamental particle called the Higgs boson. The fact that we have never observed any fundamental scalar particle in nature so far makes this the truly greatest challenge faced by physicists today. For this greatest challenge we have the world largest particle accelerator to date, the CERN Large Hadron Collider (LHC) [10]. The LHC collides two proton beams with a center-of-mass energy up to 14TeV and is expected to start this year. It is our belief that the Higgs boson will be found within a few years.

The prominent feature of the Higgs boson is that it couples mainly to heavy particles with large couplings. This makes the theoretical calculations of the Higgs production rates as perturbative expansions in those large couplings complicated. The convergence rate of the perturbative expansion is slow and one cannot rely merely on the leading order (LO) result. Loop calculations are therefore mandatory. The most famous example is the Higgs production mechanism via gluon fusion, the Higgs discovery channel. The LO contribution in this example is already at one-loop level. The two-loop contribution, mainly due to the gluon radiation in the initial state and the QCD virtual corrections, increases the total cross section by about 60% for a Higgs mass about 100GeV at the LHC [11]. Indeed, loop calculations are required in order to understand the structure of perturbative field theory and the uncertainties of the

theoretical predictions. The only way to reduce the error of a theoretical prediction so that it can be comparable to the small error (say 10%) of precision measurements nowadays is to pick up higher order terms, *i.e.* loop corrections.

There are two methods to calculate loop integrals: analytical and numerical methods. The traditional analytical method decomposes each Feynman diagram's numerator into a sum of scalar and tensorial Passarino-Veltman functions. The advantage is that the whole calculation of cross sections involving the numerical integration over phase space is faster. The disadvantage is that the numerator decomposition usually results in huge algebraic expressions with various spurious singularities, among them the inverse of the Gram determinant (defined as $\det(G) = \det(2p_i \cdot p_j)$ with p_i are external momenta) which can vanish in some region of phase space. Recently, Denner and Dittmaier have developed a numerically stable method for reducing one-loop tensor integrals [12, 13], which has been used in various electroweak processes including the $e^+e^- \rightarrow 4$ fermions process [14, 15]. For the numerical method, the loop integration should be performed along with the integrations over the momenta of final state particles. In this method one should not decompose the various numerators but rather combine various terms in one common denominator. Thus the algebraic expression of the integrand is much simpler this way and no spurious singularities appear. The disadvantage is that the number of integration variables is large resulting in large integration errors. In both methods, the ultra-violet (UV)-, infrared (IR)- and collinear- divergences have to be subtracted before performing the numerical integration.

Recently, there has appeared *on-shell methods* to calculate one-loop multi-leg QCD processes (see [16] for a review). These methods are analytical but very different from traditional methods based on Passarino-Veltman reduction technique. On-shell methods have already led to a host of new results at one loop, including the computation of non-trivial amplitudes in QCD with an arbitrary number of external legs [17, 18, 19]. These methods work as follows. A generic one-loop amplitude can be expressed in terms of a set of scalar master integrals multiplied by various rational coefficients,

along with the additional purely rational terms. The relevant master integrals consist of box, triangle, bubble and (for massive particles) tadpole integrals. All these basic integrals are known analytically. The purely rational terms have their origin in the difference between $D = 4 - 2\varepsilon$ and four dimensions when using dimensional regularization. One way to calculate the rational terms is to use on-shell recursion [20, 21] to construct the rational remainder from the loop amplitudes' factorization poles [22, 17, 16]. The various rational coefficients are determined by using generalized unitarity cuts [23, 24]. The evaluation is carried out in the context of the spinor formalism. Like the traditional analytical method, spurious singularities occur in intermediate steps. However, it is claimed in [16] that they can be under control. More detailed studies on this important issue are necessary to confirm this statement though. On-shell methods can also deal with massive internal/external particles [25] and hence can be used for electroweak processes. It is not clear for us whether these on-shell methods can be extended to include the case of internal unstable particles.

Although the on-shell methods differ from the traditional analytical methods in many respects, they have a common feature that one-loop amplitudes are expressed in terms of a set of basic scalar loop integrals. One may wonder if there is a method to express a one-loop amplitude in terms of tree-level amplitudes? The answer was known 45 years ago by Feynman [26, 27]. Feynman has proved that any diagram with closed loops can be expressed in terms of sums (actually phase-space integrals) of tree diagrams. This is called the Feynman Tree Theorem (FTT) whose very simple proof can be found in [27]. This theorem can be used in several ways. The simplest application is to calculate scalar loop integrals needed by other analytical methods described above. The best application is to calculate loop corrections for physical processes. Feynman has shown that this important application can be realized for many processes. Let us explain this a little bit more. After making use of the FTT, one has a lot of tree diagrams obtained by cutting a N -point one-loop diagram with multiple cuts (single-cut, double-cut, \dots , N -cut). One can re-organize this result as a sum of sets of tree diagrams, each set representing the complete set of tree diagrams

expected for some given physical process. In this way, one obtains relations among the diagrams for various processes. Surprisingly, no one has applied this FTT to calculate QCD/EW one-loop corrections to important processes at colliders, to the best of our knowledge. However, there is ongoing effort in this direction by Catani, Gleisberg, Krauss, Rodrigo and Winter. They have very recently proposed a method to numerically compute multi-leg one-loop cross sections in perturbative field theories [28]. The method relies on the so-called duality relation between one-loop integrals and phase space integrals. This duality relation is very similar to the FTT. The main difference is that the duality relation involves only single cuts of the one-loop diagrams. Interestingly, the duality relation can be applied to one-loop diagrams with internal complex masses [28].

In general, Higgs production processes involve unstable internal particles. If these unstable particles can be on-shell then the width effect can be relevant and therefore must be taken into account. In particular, scalar box integrals with unstable internal particles can develop a Landau singularity (to be discussed below) which is not integrable at one-loop amplitude square level. In this case, the internal widths are regulators as they move the singularity outside the physical region. Thus, a good method to calculate one-loop corrections must be able to handle internal complex masses.

Independent of calculation methods, the analytic structure of S-matrix is intrinsic and is related to fundamental properties like unitarity and causality [29]. Analytic properties of S-matrix can be studied by using Landau equations [30, 29] applied to an individual Feynman diagram. Landau equations are necessary and sufficient conditions for the appearance of a pinch singularity of Feynman loop integrals [31]. Solutions of Landau equations are singularities of the loop integral as a function of internal masses and external momenta, called Landau singularities. These singularities occur when internal particles are on-shell. They can be finite like the famous normal threshold in the case of one-loop two-point function. The normal thresholds

are branch points [29]. Landau singularities can be divergent like in the case of three-point and four-point functions. The former is integrable but the latter is not at the level of one-loop amplitude squared. This four-point Landau divergence can be due to the presence of internal unstable particles and hence must be regularized by taking into account their widths. A detailed account on this topic is given in chapters 4 and 5.

The main calculation of this thesis is to compute the leading electroweak one-loop correction to Higgs production associated with two bottom quarks at the LHC in the SM. Our calculation involves 8 tree-level diagrams and 115 one-loop diagrams with 8 pentagons. The loop integrals include 2-point, 3-point, 4-point and 5-point functions which contain internal unstable particles, namely the top-quark and the W gauge boson. Interestingly, Landau singularities occur in all those functions. We follow the traditional analytical method of Veltman and Passarino [32] to calculate the one-loop corrections. For the 5-point function part, we have adapted the new reduction method of Denner and Dittmaier [12], which replaces the inverse of vanishing Gram determinant with the inverse of the Landau determinant and hence replaces the spurious Gram singularities with the true Landau singularities of loop integrals. In our opinion, this is one of the best ways to deal with those spurious Gram singularities. However, as will be explained in chapter 4, the condition of vanishing Landau determinant is necessary but not sufficient for a Landau singularity to actually occur in the physical region. Thus, spurious singularities can still be encountered but very rarely. This new reduction method for 5-point functions has been implemented in the library LoopTools [33, 34] based on the library FF [35]. Our calculation has proved the efficiency of this method. The reason for us to choose this traditional method is that our calculation involves massive internal particles. Furthermore, in order to deal with Landau singularities, our calculation must include also complex masses. Although the calculation method is well understood, the difficulty is that we have to handle very huge algebraic expressions since we have to expand the numerator of each Feynman diagram. Thus, we cannot use the traditional amplitude squared method

as it will result in extremely enormous algebraic expressions of the total amplitude squared. Fortunately, there is a very efficient way to organize the calculation based on the helicity amplitude method (HAM) [36]. Using this HAM, one just needs to calculate all the independent helicity amplitudes which are complex numbers. This way of calculating makes it very easy to divide the whole complicated computation into independent blocks therefore factorizes out terms that occur several times in the calculation.

Our calculation consists of two parts. In the first part, we calculate the NLO corrections, *i.e.* the interference terms between tree-level and one-loop amplitudes. Although Landau singularities do appear in many one-loop diagrams, they are integrable hence do not cause any problem of numerical instability. The bottom-quark mass is kept in this calculation. In the second part, we calculate the one-loop correction in the limit of massless bottom-quark therefore the bottom-Higgs Yukawa coupling vanishes. The process is loop induced and we have to calculate one-loop amplitude squared. In this calculation, the Landau singularity of a scalar four-point function is not integrable and causes a severe problem of numerical instability if $M_H \geq 2M_W$. This problem is solved by introducing a width for the top-quark and W gauge boson in the loop diagrams. It turns out that the width effect is large if M_H is around $2M_W$.

Although the main calculation of this thesis is for a very specific process, we have gained several insights that can be equally used for other practical calculations. First of all, the method to optimise complicated loop calculations using the HAM is general. Second, the method to check the final/intermediate results by using QCD gauge invariance in the framework of the HAM can be used for any process with at least one gluon in the external states. Third, some general results related to Landau singularities are new and can be used for practical purposes. They are equations (4.27) and (4.49). Finally, we have applied the loop calculation method of 't Hooft and Veltman to write down explicitly two formulae to calculate scalar box integrals with complex internal masses. They are equations (E.15) and (E.40). The restriction

is that at least two external momenta are lightlike. We have implemented those two formulae into the library LoopTools.

The outline of this thesis is as follows. First, a short review of the SM including QCD is presented in chapter 1. We pay special attention to the one-loop renormalisation of the EW part and the Higgs sector. We also give a short introduction to the Minimal Supersymmetric Standard Model and discuss its Higgs sector in the same chapter. In chapter 2 we discuss the dominant mechanisms for SM Higgs production at the LHC and Higgs signatures at the colliders. In chapter 3 we present the main calculation of this thesis, one-loop Yukawa corrections to the SM process $pp \rightarrow b\bar{b}H$ at the LHC, for the case $M_H \leq 150\text{GeV}$. There are two reasons to start with small values of the Higgs mass: it is preferred by the latest EW data and there is no problem of numerical instability related to Landau singularities. The framework of a one-loop calculation based on the helicity amplitude method is also given in this chapter. In chapter 4 we explain in detail the Landau singularities of a general one-loop Feynman diagram. We emphasize the conditions to have a Landau singularity and its nature. In chapter 5, we complete the study of chapter 3 for larger values of M_H , up to 250GeV . We show that the one-loop process $gg \rightarrow b\bar{b}H$ is an ideal example for understanding Landau singularities. It contains several types of Landau singularities related to two-point, three-point and four-point functions. The conclusions are given in chapter 6.

This thesis includes several appendices. In appendix A we explain the helicity amplitude method and how to check the correctness of the result by using QCD gauge invariance. In appendix B we show how to optimise the calculation of various one-loop helicity amplitudes and how that can be easily achieved by using FORM. Appendix C concerns the phase space integral of $2 \rightarrow 3$ process. We explain how to use the Fortran routine BASES [37] to do numerical integration. Appendix D gives useful mathematical formulae related to loop integrals. In appendix E we explain the analytical calculation of scalar one-loop four-point integrals with complex internal masses. The restriction is that at least two external momenta are lightlike.

Chapter 1

The Standard Model and beyond

The Glashow-Salam-Weinberg (GSW) model of the electroweak interaction was proposed by Glashow [1], Weinberg [2] and Salam [3] for leptons and extended to the hadronic degrees of freedom by Glashow, Iliopoulos and Maiani [38]. The GSW model is a Yang-Mills theory [39] based on the symmetry group $SU(2)_L \times U(1)_Y$. It describes the electromagnetic and weak interactions of the known 6 leptons and 6 quarks. The electromagnetic interaction is mediated by a massless gauge boson, the photon (γ). The short-range weak interaction is carried by 2 massive gauge bosons, Z and W . The strong interaction, mediated by the massless gluon, is also a Yang-Mills theory based on the gauge group $SU(3)_C$. This is known as Quantum chromodynamics (abbreviated as QCD) [4, 5, 6, 7]. The Standard Model of particle physics is just a trivial combination of GSW model and QCD. The particle content of the SM is listed in Table. 1.1. There is an additional scalar field called the Higgs boson (H), the only remnant of the spontaneous symmetry breaking (SSB) mechanism invented by Brout, Englert, Guralnik, Hagen, Higgs and Kibble [40, 41, 42, 43, 44]. The SSB mechanism is responsible for explaining the mass spectrum of the SM.

To date, almost all experimental tests of the three forces described by the Standard Model agree with its predictions [8, 9, 45]. The measurements of M_W and M_Z together

Table 1.1: Particle content of the standard model

	Particles	Spin	Electric charge
Leptons	(e, μ, τ)	1/2	-1
	$(\nu_e, \nu_\mu, \nu_\tau)$	1/2	0
Quarks	(u, c, t)	1/2	2/3
	(d, s, b)	1/2	-1/3
Gauge bosons	gluon (g)	1	0
	(γ, Z)	1	0
	W^\pm	1	± 1
Higgs	H	0	0

with the fact that their relation $M_W^2 = M_Z^2 c_W^2$ (with $c_W^2 \approx 0.77$ defined in Eq. (1.10)) has been experimentally proven imply two things. First, the existence of massive gauge bosons means that the local gauge symmetry is broken. Second, the mass relation indicates that the effective Higgs (be it fundamental or composite) is isospin doublet [45]. Experiments have also confirmed that couplings that are mass-independent like the ones of quarks and leptons to the W^\pm and Z gauge bosons or triple couplings among electroweak gauge bosons agree with those described by the gauge symmetry [45]. It means that the only sector which remains untested is the mass couplings or in other words the nature of SSB mechanism.

The primary goal of the LHC is to find the scalar Higgs boson and to understand its properties. The main drawback here is that we do not know the value of the Higgs mass which uniquely defines the Higgs profile. The LEP direct searches for the Higgs and precision electroweak measurements lead to the conclusion that $114\text{GeV} < M_H < 190\text{GeV}$ [9]. The most prominent property of the Higgs is that it couples mainly to heavy particles at tree level. This has two consequences at the LHC: the Higgs production cross section is small and the Higgs decay product is very complicated and usually suffers from huge QCD background. Thus, it is completely understandable that searching for the Higgs is not an easy task, even at the LHC.

1.1 QCD

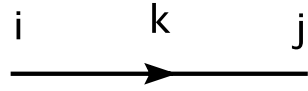
The classical QCD Lagrangian reads

$$\mathcal{L}_{QCD} = \bar{\psi}(i\not{D} - m)\psi - \frac{1}{2} \text{Tr} F_{\mu\nu} F^{\mu\nu}, \quad (1.1)$$

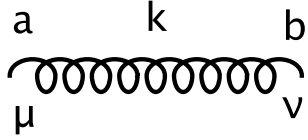
where

$$\begin{aligned} \not{D} &= \gamma^\mu D_\mu, \quad D_\mu = \partial_\mu - ig_s \mathcal{A}_\mu, \quad \mathcal{A}_\mu = A_\mu^a T_a, \\ F_{\mu\nu} &= \partial_\mu \mathcal{A}_\nu - \partial_\nu \mathcal{A}_\mu - ig_s [\mathcal{A}_\mu, \mathcal{A}_\nu], \end{aligned} \quad (1.2)$$

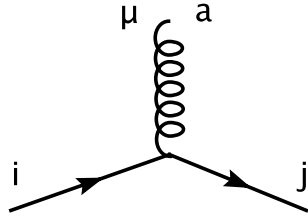
with $a = 1, \dots, 8$; ψ is a fermion field belonging to the triplet representation of $SU(3)_C$ group; A the gauge boson field and g_s is the strong coupling; T_a are Gell-Mann generators. The corresponding Feynman rules in the 't Hooft-Feynman gauge read:



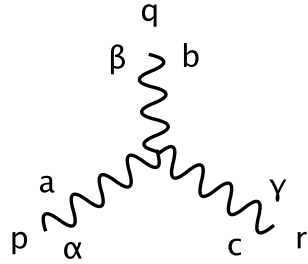
$$\frac{-\delta_{ij}}{\not{k} - m + i\epsilon}$$



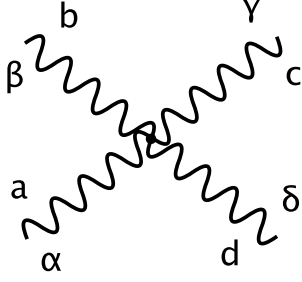
$$\frac{\delta_{ab} g_{\mu\nu}}{k^2 + i\epsilon}$$



$$g_s \gamma^\mu (T_a)_{ji}$$



$$-ig_s f^{abc} [(p-q)_\gamma g_{\alpha\beta} + (q-r)_\alpha g_{\beta\gamma} + (r-p)_\beta g_{\alpha\gamma}]$$

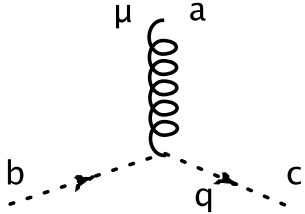


$$\begin{aligned}
& g_s^2 f^{abe} f^{cde} (g_{\alpha\gamma} g_{\beta\delta} - g_{\alpha\delta} g_{\beta\gamma}) \\
& + g_s^2 f^{ace} f^{bde} (g_{\alpha\beta} g_{\gamma\delta} - g_{\alpha\delta} g_{\beta\gamma}) \\
& + g_s^2 f^{ade} f^{bce} (g_{\alpha\beta} g_{\gamma\delta} - g_{\alpha\gamma} g_{\beta\delta})
\end{aligned}$$

We have adopted the Feynman rules of [46, 47] (derived by using \mathcal{L}) which differ from the normal Feynman rules (derived by using $i\mathcal{L}$) by a factor i . One can use those Feynman rules to calculate tree-level QCD processes or QED-like processes by keeping in mind that the gluon has only two transverse polarisation components. However, in a general situation where a loop calculation is involved one needs to quantize the classical Lagrangian (1.1). The covariant quantization following the Faddeev-Popov method [48] introduces unphysical scalar Faddeev-Popov ghosts with additional Feynman rules:



$$\frac{-\delta_{ab}}{k^2}$$



$$-igf^{abc}q^\alpha$$

The main difference between QCD and QED is that the gluon couples to itself while the photon does not. In QED, only the transverse photon can couple to the electron hence the unphysical components (longitudinal and scalar polarisations) decouple from the theory and the Faddeev-Popov ghosts do not appear. The same thing happens for the gluon-quark coupling. However, an external transverse gluon can couple to its unphysical states via its triple and quartic self couplings. Those unphysical states, in some situation, can propagate as internal particles without coupling to any

quarks and give an unphysical contribution to the final result. In that situation, one has to take into account also the ghost contribution for compensation.

Indeed, there is another way to calculate QCD processes by taking into account only the physical contribution, *i.e.* only the transverse gluon components involve and no ghosts appear. This is called the axial (non-covariant) gauge [49]. The main difference compared to the above covariant gauge is with the form of the gluon propagator. The covariant propagator includes the unphysical polarisation states via¹

$$g_{\mu\nu} = \epsilon_\mu^- \epsilon_\nu^{+*} + \epsilon_\mu^+ \epsilon_\nu^{-*} - \sum_{i=1}^2 \epsilon_{i\mu} \epsilon_{i\nu}^*, \quad (1.3)$$

where ϵ_μ^\pm are two unphysical polarisation states and $\epsilon_{i\mu}$ with $i = 1, 2$ are the two transverse polarisation states. In the axial gauge, the gluon propagator takes the form

$$\begin{aligned} P_{\mu\nu} &= -\frac{\delta_{ab}}{k^2 + i\epsilon} \sum_{i=1}^2 \epsilon_{i\mu} \epsilon_{i\nu}^* \\ &= -\frac{\delta_{ab}}{k^2 + i\epsilon} \left[-g_{\mu\nu} + \frac{k_\mu n_\nu + k_\nu n_\mu}{n.k} \right] \end{aligned} \quad (1.4)$$

with $n^2 = 0$ and $n.k \neq 0$, which includes only the transverse polarisation states. The main drawback of this axial gauge is that the propagator's numerator becomes very complicated.

The main calculation of this thesis is to compute the one-loop electroweak corrections to the process $gg \rightarrow b\bar{b}H$. Though the triple gluon coupling does appear in various Feynman diagrams, it always couples to a fermion line hence the virtually unphysical polarisation states cannot contribute and the ghosts do not show up. We will therefore use the covariant Feynman rules and take into account only the contribution of the transverse polarisation states of the initial gluons².

¹See p.511 of [50].

²If one follows the traditional amplitude squared method and wants to use the polarisation sum identity $\sum \epsilon_\mu \epsilon_\nu = -g_{\mu\nu}$ then one has to consider the Feynman diagrams with two ghosts in the initial state.

1.2 The Glashow-Salam-Weinberg Model

The classical Lagrangian of the GSW model is composed of a gauge, a Higgs, a fermion and a Yukawa part ³

$$\mathcal{L}_C = \mathcal{L}_G + \mathcal{L}_H + \mathcal{L}_F + \mathcal{L}_Y. \quad (1.5)$$

Each of them is separately gauge invariant and specified as follows:

1.2.1 Gauge sector

The Lagrangian of the gauge part of the group $SU(2)_L \times U(1)_Y$ reads

$$\mathcal{L}_G = -\frac{1}{4}(\partial_\mu W_\nu^a - \partial_\nu W_\mu^a + g\epsilon^{abc}W_\mu^b W_\nu^c)^2 - \frac{1}{4}(\partial_\mu B_\nu - \partial_\nu B_\mu)^2, \quad (1.6)$$

where $a, b, c \in \{1, 2, 3\}$, W_μ^a are the 3 gauge fields of the $SU(2)$ group, B_μ is the $U(1)$ gauge field, the $SU(2)$ gauge coupling g , the $U(1)$ gauge coupling g' and ϵ^{abc} are the totally antisymmetric structure constants of $SU(2)$. The covariant derivative is given by

$$D_\mu = \partial_\mu - igT^a W_\mu^a - ig'Y B_\mu, \quad (1.7)$$

where $T^a = \sigma^a/2$ with σ^a are the usual Pauli matrices, the hypercharge according to the Gell-Mann Nishijima relation

$$Q = T^3 + Y. \quad (1.8)$$

The physical fields W^\pm, Z, A relate to the W^a and B fields as

$$\begin{cases} W_\mu^\pm &= \frac{W_\mu^1 \mp iW_\mu^2}{\sqrt{2}} \\ Z_\mu &= c_W W_\mu^3 - s_W W_\mu^0 \\ A_\mu &= s_W W_\mu^3 + c_W W_\mu^0, \end{cases} \quad (1.9)$$

³For more technical details of the GSW model, its one-loop renormalisation prescription and Feynman rules, we refer to [51, 46, 47].

with

$$c_W = \frac{g}{\sqrt{g^2 + g'^2}}, \quad s_W = \frac{g'}{\sqrt{g^2 + g'^2}}, \quad (1.10)$$

the electromagnetic coupling e

$$e = \frac{gg'}{\sqrt{g^2 + g'^2}}, \quad g = \frac{e}{s_W}, \quad g' = \frac{e}{c_W}. \quad (1.11)$$

1.2.2 Fermionic gauge sector

Left-handed fermions L of each generation belong to $SU(2)_L$ doublets while right-handed fermions R are in $SU(2)_L$ singlets. The fermionic gauge Lagrangian is just

$$\mathcal{L}_F = i \sum \bar{L} \gamma^\mu D_\mu L + i \sum \bar{R} \gamma^\mu D_\mu R, \quad (1.12)$$

where the sum is assumed over all doublets and singlets of the three generations. Note that in the covariant derivative D_μ acting on right-handed fermions the term involving g is absent since they are $SU(2)_L$ singlets. Neutrinos are left-handed in the SM. Fermionic mass terms are forbidden by gauge invariance. They are introduced through the interaction with the scalar Higgs doublet.

1.2.3 Higgs sector

Mass terms for both the gauge bosons and fermions are generated in a gauge invariant way through the Higgs mechanism. To that effect one introduces minimally a complex scalar $SU(2)$ doublet field with hypercharge $Y = 1/2$

$$\Phi = \begin{pmatrix} \phi^+ \\ \phi^0 \end{pmatrix} = \begin{pmatrix} i\chi^+ \\ (v + H - i\chi_3)/\sqrt{2} \end{pmatrix}, \quad \langle 0 | \Phi | 0 \rangle = v/\sqrt{2}, \quad (1.13)$$

where the electrically neutral component has been given a non-zero vacuum expectation value v to break spontaneously the gauge symmetry $SU(2)_L \times U(1)_Y$ down to $U(1)_Q$. The scalar Lagrangian writes

$$\mathcal{L}_H = (D_\mu \Phi)^\dagger (D^\mu \Phi) - V(\Phi), \quad V(\Phi) = -\mu^2 \Phi^\dagger \Phi + \lambda (\Phi^\dagger \Phi)^2. \quad (1.14)$$

After rewriting \mathcal{L}_H in terms of χ^\pm , χ_3 , H and imposing the minimum condition on the potential $V(\Phi)$ one sees that χ^\pm and χ_3 are massless while the Higgs boson obtains a mass

$$M_H^2 = 2\mu^2, \quad \mu^2 = \lambda v^2. \quad (1.15)$$

χ^\pm , χ_3 are called the Nambu-Goldstone bosons. They are unphysical degrees of freedom and get absorbed by the W^\pm and Z to give the latter masses given by

$$M_W = \frac{ev}{2s_W}, \quad M_Z = \frac{ev}{2s_W c_W}. \quad (1.16)$$

1.2.4 Fermionic scalar sector

Fermion masses require the introduction of Yukawa interactions of fermions and the scalar Higgs doublet

$$\mathcal{L}_Y = - \sum_{up} f_U^{ij} \bar{L}^i \tilde{\Phi} R_U^j - \sum_{down} f_D^{ij} \bar{L}^i \Phi R_D^j + (h.c.), \quad M_{U,D}^{ij} = \frac{f_{U,D}^{ij} v}{\sqrt{2}}, \quad (1.17)$$

where $f_{U,D}^{ij}$ with $i, j \in \{1, 2, 3\}$ the generation indices are Yukawa couplings, $\tilde{\Phi} = i\sigma_2 \Phi^*$. Neutrinos, which are only right-handed, do not couple to the Higgs boson and thus are massless in the SM. The diagonalization of the fermion mass matrices $M_{U,D}^{ij}$ introduces a matrix into the quark-W-boson couplings, the unitary quark mixing matrix [8]

$$V = \begin{pmatrix} V_{ud} & V_{us} & V_{ub} \\ V_{cd} & V_{cs} & V_{cb} \\ V_{td} & V_{ts} & V_{tb} \end{pmatrix} = \begin{pmatrix} 0.97383 & 0.2272 & 0.00396 \\ 0.2271 & 0.97296 & 0.04221 \\ 0.00814 & 0.04161 & 0.9991 \end{pmatrix}, \quad (1.18)$$

which is well-known as Cabibbo-Kobayashi-Maskawa (CKM) matrix. There is no corresponding matrix in the lepton sector as the neutrinos are massless in the SM.

For later reference, we define $\lambda_f = \sqrt{2}m_f/v$ where m_f is the physical mass of a fermion.

1.2.5 Quantisation: Gauge-fixing and Ghost Lagrangian

The classical Lagrangian \mathcal{L}_C has gauge freedom. A Lorentz invariant quantisation requires a gauge fixing (otherwise the propagators of gauge fields are not well-defined). The 't Hooft linear gauge fixing terms read

$$\begin{aligned} F^A &= (\xi^A)^{-1/2} \partial^\mu A_\mu, \\ F^Z &= (\xi_1^Z)^{-1/2} \partial^\mu Z_\mu - M_Z (\xi_2^Z)^{1/2} \chi_3, \\ F^\pm &= (\xi_1^W)^{-1/2} \partial^\mu W_\mu^\pm + M_W (\xi_2^W)^{1/2} \chi^\pm. \end{aligned} \quad (1.19)$$

This leads to a gauge fixing Lagrangian

$$\mathcal{L}_{fix} = -\frac{1}{2} [(F^A)^2 + (F^Z)^2 + 2F^+ F^-]. \quad (1.20)$$

\mathcal{L}_{fix} involves the unphysical components of the gauge fields, *i.e.* field components with negative norm, which lead to a serious problem that the theory is not gauge invariant and violates unitarity. In order to compensate their effects one introduces Faddeev Popov ghosts $u^\alpha(x)$, $\bar{u}^\alpha(x)$ ($\alpha = A, Z, W^\pm$) with the Lagrangian

$$\mathcal{L}_{ghost} = \bar{u}^\alpha(x) \frac{\delta F^\alpha}{\delta \theta^\beta(x)} u^\beta(x), \quad (1.21)$$

where $\frac{\delta F^\alpha}{\delta \theta^\beta(x)}$ is the variation of the gauge fixing operators F^α under infinitesimal gauge transformation parameter $\theta^\beta(x)$. An element of the $SU(2)_L \times U(1)_Y$ group has a typical form $G = e^{-igT^\alpha \theta_\alpha(x) - ig'Y \theta_Y(x)}$. Faddeev Popov ghosts are scalar fields following anticommutation rules and belonging to the adjoint representation of the gauge group.

In a practical calculation, the final result does not depend on gauge parameters. Thus one can choose for these parameters some special values to make the calculation simpler. For tree-level calculations, one can think of the unitary gauge $\xi^Z = \xi^W = \infty$ where the Nambu-Goldstone bosons and ghosts do not appear and the number of Feynman diagrams is minimized. For general one-loop calculations, it is more convenient to use the 't Hooft Feynman gauge $\xi^A = \xi^Z = \xi^W = 1$ where the numerator structure is simplest.

It is worth knowing that the 't Hooft linear gauge fixing terms defined in Eq. (1.19) can be generalised to include non-linear terms as follows [52, 47]

$$\begin{aligned} F^Z &= (\xi_Z)^{-1/2} \left[\partial^\mu Z_\mu + M_Z \xi'_Z \chi_3 + \frac{g}{2c_W} \xi'_Z \tilde{\epsilon} H \chi_3 \right], \\ F^\pm &= (\xi_W)^{-1/2} \left[\partial^\mu W_\mu^\pm + M_W \xi'_W \chi^\pm \right. \\ &\quad \left. \mp (ie\tilde{\alpha} A_\mu + igc_W \tilde{\beta} Z_\mu) W^{\mu\pm} + \frac{g}{2} \xi'_W (\tilde{\delta} H \pm i\tilde{\kappa} \chi_3) \chi^\pm \right], \end{aligned} \quad (1.22)$$

with the gauge fixing term for the photon F^A remains unchanged. It is simplest to choose $\xi'_{Z,W} = \xi_{Z,W}$. Those non-linear fixing terms involve five extra arbitrary parameters $\zeta = (\tilde{\alpha}, \tilde{\beta}, \tilde{\delta}, \tilde{\kappa}, \tilde{\epsilon})$. The advantage of this non-linear gauge is twofold. First, in an automatic calculation involving a lot of Feynman diagrams one can perform the gauge-parameter independence checks to find bugs. Second, for some specific calculations involving gauge and scalar fields one can kill some triple and quartic vertices by judiciously choosing some of those gauge parameters and thus reduce the number of Feynman diagrams. This is based on the fact that the new gauge parameters modify some vertices involving the gauge, scalar and ghost sector and at the same time introduce new quartic vertices [47]. In the most general case, the Feynman rules with non-linear gauge are much more complicated than those with 't Hooft linear gauge, however.

With \mathcal{L}_{fix} and \mathcal{L}_{ghost} the complete renormalisable Lagrangian of the GSW model reads

$$\mathcal{L}_{GSW} = \mathcal{L}_C + \mathcal{L}_{fix} + \mathcal{L}_{ghost}. \quad (1.23)$$

1.2.6 One-loop renormalisation

Given the full Lagrangian \mathcal{L}_{GSW} above, one proceeds to calculate the cross section of some physical process. In the framework of perturbative theory this can be done order by order. At tree level, the cross section is a function of a set of input parameters which appear in \mathcal{L}_{GSW} . These parameters can be chosen to be

$O = \{e, M_W, M_Z, M_H, M_{U,D}^{ij}\}$ which have to be determined experimentally. There are direct relations between these parameters and physical observables at tree level. However, these direct relations are destroyed when one considers loop corrections. Let us look at the case of M_W as an example. The tree-level W mass is directly related to the Fermi constant G_μ through

$$s_W^2 M_W^2 = \frac{\pi\alpha}{\sqrt{2}G_\mu}. \quad (1.24)$$

When one takes into account higher order corrections, this becomes [53, 54, 55]

$$s_W^2 M_W^2 = \frac{\pi\alpha}{\sqrt{2}G_\mu} \frac{1}{1 - \Delta r}, \quad (1.25)$$

where Δr containing all loop effect is a complicated function of M_W and other input parameters. A question arises naturally, how to calculate Δr or some cross section at one-loop level? The answer is the following. If we just use the Lagrangian given in Eq. (1.23), follow the corresponding Feynman rules to calculate all the relevant one-loop Feynman diagrams then we will end up with something infinite. This is because there are a lot of one-loop diagrams being UV-divergent. This problem can be solved if \mathcal{L}_{GSW} is renormalisable. The renormalisability of nonabelian gauge theories with spontaneous symmetry breaking and thus the GSW model was proven by 't Hooft [56, 57]. The idea of renormalisation is that we have to get rid of all UV-divergence terms originating from one-loop diagrams by redefining a finite number of fundamental input parameters O in the original Lagrangian \mathcal{L}_{GSW} . This is done as follows

$$\begin{aligned} e &\rightarrow (1 + \delta Y)e, \\ M &\rightarrow M + \delta M, \\ \psi &\rightarrow (1 + \delta Z^{1/2})\psi. \end{aligned} \quad (1.26)$$

The latter is called wave function renormalisation. The renormalisation constants δY , δM and $\delta Z^{1/2}$ are fixed by using renormalisation conditions to be discussed later. The one-loop renormalised Lagrangian writes

$$\mathcal{L}_{GSW}^{1-loop} = \mathcal{L}_{GSW} + \delta\mathcal{L}_{GSW}. \quad (1.27)$$

The parameters O in $\mathcal{L}_{GSW}^{1-loop}$ are now called the renormalised parameters determined from experiments. From this renormalised Lagrangian one can write down the corresponding Feynman rules and use them to calculate Δr or any cross section at one loop. The results are guaranteed to be finite by 't Hooft.

We now discuss the renormalisation conditions which define a renormalisation scheme. In this thesis, we stick with the on-shell scheme where all renormalisation conditions are formulated on mass shell external fields. To fix δY , one imposes a condition on the e^+e^-A vertex as in QED. The condition reads

$$(e^+e^-A \text{ one-loop term} + e^+e^-A \text{ counterterm})|_{q=0, p_{\pm}^2=m_e^2}=0, \quad (1.28)$$

where q is the photon momentum, p_{\pm} are the momenta of e^{\pm} respectively. All δM s are fixed by the requirement that the corresponding renormalised mass parameter is equal to the physical mass which is the single pole of the two-point Green function. This translates into the condition that the real part of the inverse of the corresponding propagator is zero. $\delta Z^{1/2}$ s are found by requiring that the residue of the propagator at the pole is 1. To be explicit we look at the cases of Higgs boson, fermions and gauge bosons, which will be useful for our main calculation of $pp \rightarrow b\bar{b}H$. The Higgs one-particle irreducible two-point function is $\tilde{\Pi}^H(q^2)$ with q the Higgs momentum. One calculates this function by using Eq. (1.27)

$$\tilde{\Pi}^H(q^2) = \Pi^H(q^2) + \hat{\Pi}^H(q^2) \quad (1.29)$$

where the counterterm contribution is denoted by a caret, the full contribution is denoted by a tilde. The two renormalisation conditions read

$$\text{Re } \tilde{\Pi}^H(M_H^2) = 0, \quad \frac{d}{dq^2} \text{Re } \tilde{\Pi}^H(q^2) \Big|_{q^2=M_H^2} = 0. \quad (1.30)$$

This gives

$$\delta Z_H^{1/2} = -\frac{1}{2} \frac{d}{dq^2} \text{Re } \Pi^H(q^2) \Big|_{q^2=M_H^2}. \quad (1.31)$$

For a fermion with $\psi = \psi_L + \psi_R$ ($\psi_{L,R} = P_{L,R}\psi$ with $P_{L,R} = \frac{1}{2}(1 \mp \gamma_5)$, respectively), the one-particle irreducible two-point function takes the form

$$\begin{aligned}\tilde{\Sigma}(q^2) &= \Sigma(q^2) + \hat{\Sigma}(q^2), \\ \Sigma(q^2) &= K_1 + K_\gamma \not{q} + K_{5\gamma} \not{q} \gamma_5, \\ \hat{\Sigma}(q^2) &= \hat{K}_1 + \hat{K}_\gamma \not{q} + \hat{K}_{5\gamma} \not{q} \gamma_5,\end{aligned}\tag{1.32}$$

with

$$\begin{aligned}\hat{K}_1 &= -m_f(\delta Z_{fL}^{1/2} + \delta Z_{fR}^{1/2}) - \delta m_f, \\ \hat{K}_\gamma &= (\delta Z_{fL}^{1/2} + \delta Z_{fR}^{1/2}), \\ \hat{K}_{5\gamma} &= -(\delta Z_{fL}^{1/2} - \delta Z_{fR}^{1/2}).\end{aligned}\tag{1.33}$$

The two renormalisation conditions become

$$\begin{cases} m_f \operatorname{Re} \tilde{K}_\gamma(m_f^2) + \operatorname{Re} \tilde{K}_1(m_f^2) = 0 & \text{and} & \operatorname{Re} \tilde{K}_{5\gamma}(m_f^2) = 0 \\ \frac{d}{dq} \operatorname{Re} [\not{q} \tilde{K}_\gamma(q^2) + \tilde{K}_1(q^2)]_{\not{q}=m_f} = 0. \end{cases}\tag{1.34}$$

This gives

$$\begin{aligned}\delta m_f &= \operatorname{Re} \left(m_f K_\gamma(m_f^2) + K_1(m_f^2) \right), \\ \delta Z_{fL}^{1/2} &= \frac{1}{2} \operatorname{Re} \left(K_{5\gamma}(m_f^2) - K_\gamma(m_f^2) \right) - m_f \frac{d}{dq^2} \left(m_f \operatorname{Re} K_\gamma(q^2) + \operatorname{Re} K_1(q^2) \right) \Big|_{q^2=m_f^2}, \\ \delta Z_{fR}^{1/2} &= -\frac{1}{2} \operatorname{Re} \left(K_{5\gamma}(m_f^2) + K_\gamma(m_f^2) \right) - m_f \frac{d}{dq^2} \left(m_f \operatorname{Re} K_\gamma(q^2) + \operatorname{Re} K_1(q^2) \right) \Big|_{q^2=m_f^2}.\end{aligned}\tag{1.35}$$

For gauge bosons, the one-particle irreducible two-point functions write⁴

$$\begin{aligned}\tilde{\Pi}_T^V &= \Pi_T^V + \hat{\Pi}_T^V, \\ \Pi_{\mu\nu}^V(q^2) &= (g_{\mu\nu} - \frac{q_\mu q_\nu}{q^2}) \Pi_T^V(q^2) + \frac{q_\mu q_\nu}{q^2} \Pi_L^V(q^2), \\ \hat{\Pi}_{\mu\nu}^V(q^2) &= (g_{\mu\nu} - \frac{q_\mu q_\nu}{q^2}) \hat{\Pi}_T^V(q^2) + \frac{q_\mu q_\nu}{q^2} \hat{\Pi}_L^V(q^2), \\ \hat{\Pi}_T^V &= \delta M_V^2 + 2(M_V^2 - q^2) \delta Z_V^{1/2}, \quad \hat{\Pi}_L^V = \delta M_V^2 + 2M_V^2 \delta Z_V^{1/2},\end{aligned}\tag{1.36}$$

⁴For massless gauge bosons like the photon, the longitudinal part Π_L^V vanishes.

where $V = W, Z$. We do not touch the photon⁵ since it is irrelevant to the calculations in this thesis, which are only related to the Yukawa sector. It is sufficient to impose the two renormalisation conditions (for the pole-position and residue) on the transverse part $\Pi_T^V(q^2)$ to determine δM_V^2 and $\delta Z_V^{1/2}$. The longitudinal part is automatically renormalised when the transverse part is, if the theory is renormalisable. The two conditions write

$$\text{Re } \tilde{\Pi}_T^V(M_V^2) = 0, \quad \frac{d}{dq^2} \text{Re } \tilde{\Pi}_T^V(q^2) \Big|_{q^2=M_V^2} = 0, \quad (1.37)$$

which give

$$\delta M_V^2 = -\text{Re } \Pi_T^V(M_V^2), \quad \delta Z_V^{1/2} = \frac{1}{2} \frac{d}{dq^2} \text{Re } \Pi_T^V(q^2) \Big|_{q^2=M_V^2}. \quad (1.38)$$

In practical calculations, one has to calculate $\Pi^H(q^2)$, $K_1(q^2)$, $K_\gamma(q^2)$, $K_{5\gamma}(q^2)$ and $\Pi_T^V(q^2)$ as sums of various two-point functions. The full results in the SM can be found in [46, 47, 51].

1.3 Higgs Feynman Rules

In order to understand the phenomenology of Higgs production, it is important to write down the relevant Feynman rules.

The Feynman rules listed here are taken from [47]. Their Feynman rules derived from \mathcal{L}_{GSW} differs from the normal Feynman rules derived by using $i\mathcal{L}_{GSW}$ by a factor i ⁶. A particle at the endpoint *enters* the vertex. For instance, if a line is denoted as W^+ , then the line shows either the incoming W^+ or the outgoing W^- . The momentum assigned to a particle is defined as *inward*. The following Feynman rules are for the linear gauge.

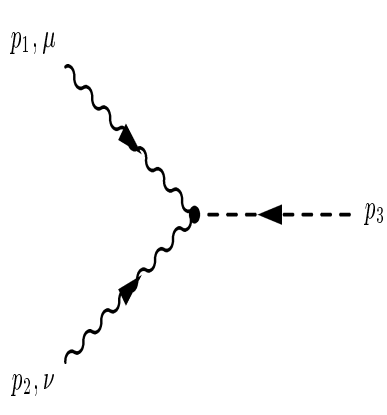
⁵In a general case, one should keep in mind that there is mixing between the photon and the Z boson.

⁶In the QCD section 1.1 we have adapted the same rules of this section.

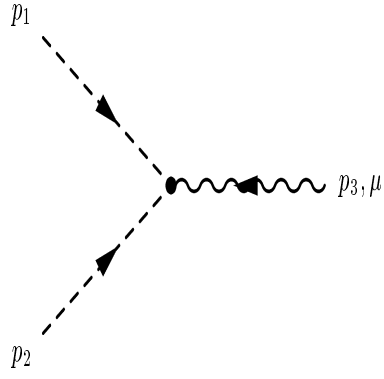
Propagators

W^\pm	$\frac{1}{k^2 - M_W^2} \left(g_{\mu\nu} - (1 - \xi_W) \frac{k_\mu k_\nu}{k^2 - \xi_W M_W^2} \right)$
Z	$\frac{1}{k^2 - M_Z^2} \left(g_{\mu\nu} - (1 - \xi_Z) \frac{k_\mu k_\nu}{k^2 - \xi_Z M_Z^2} \right)$
f	$\frac{-1}{\not{k} - m_f}$
H	$\frac{-1}{k^2 - M_H^2}$
χ^\pm	$\frac{-1}{k^2 - \xi_W M_W^2}$
χ_3	$\frac{-1}{k^2 - \xi_Z M_Z^2}$

Vector-Vector-Scalar

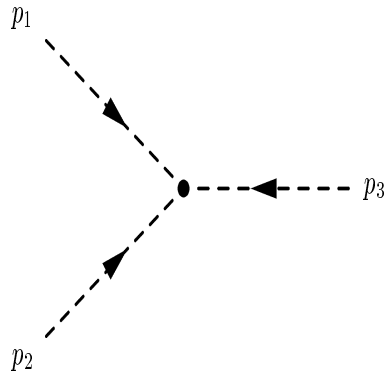
	$p_1 \ (\mu)$	$p_2 \ (\nu)$	p_3
	W^-	W^+	H
	$e \frac{1}{s_W} M_W g^{\mu\nu}$		
	Z	Z	H
	$e \frac{1}{s_W c_W^2} M_W g^{\mu\nu}$		

Scalar-Scalar-Vector

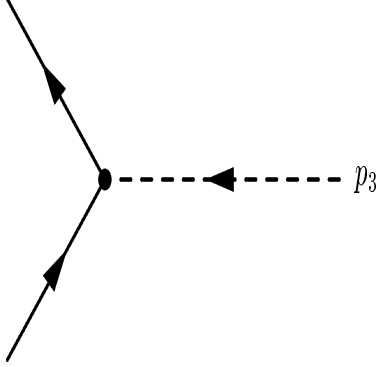


p_1	p_2	p_3	(μ)
H	χ^\mp	W^\pm	$ie\frac{1}{2s_W}(p_2^\mu - p_1^\mu)$
H	χ_3	Z	$ie\frac{1}{2s_W c_W}(p_2^\mu - p_1^\mu)$

Scalar-Scalar-Scalar



p_1	p_2	p_3	
H	H	H	$-e\frac{3}{2s_W M_W}M_H^2$
H	χ^-	χ^+	$-e\frac{M_H^2}{2s_W M_W}$
H	χ_3	χ_3	$-e\frac{M_H^2}{2s_W M_W}$

Fermion-Fermion-Scalar


p_1	p_2	p_3	
\bar{f}	f	H	$-e \frac{1}{2s_W} \frac{m_f}{M_W}$
\bar{U}/\bar{D}	U/D	χ_3	$(-/+)ie \frac{1}{2s_W} \frac{m_f}{M_W} \gamma_5$
\bar{U}	D	χ^+	$-ie \frac{1}{2\sqrt{2}s_W} \frac{1}{M_W} [(m_D - m_U) + (m_D + m_U)\gamma_5]$
\bar{D}	U	χ^-	$-ie \frac{1}{2\sqrt{2}s_W} \frac{1}{M_W} [(m_U - m_D) + (m_U + m_D)\gamma_5]$

We would like to make some connections between the underlying Feynman rules of the SM and the main calculation of this thesis, one-loop Yukawa corrections to the process $gg \rightarrow b\bar{b}H$. The relevant vertices will be "scalar-scalar-scalar" and "fermion-fermion-scalar". Of these, the vertex $\langle b\bar{b}\chi_3 \rangle$ will be excluded as it will result in Feynman diagrams proportional to $\lambda_{b\bar{b}H}^2$, which are neglected in our calculation.

1.4 Problems of the Standard Model

In spite of its great experimental success, the SM suffers from a conceptual problem known as the hierarchy problem⁷. This problem is related to the quantum corrections to the Higgs mass. In the calculation of one-loop corrections to the Higgs mass, we see that quadratic divergences appear. Of course, these UV-divergences have to be canceled by the corresponding counter terms. The leading correction is proportional to the largest mass squared, assumed to be m_t^2 . Since the value of $m_t \approx 174\text{GeV}$

⁷Indeed, there are other conceptual as well as phenomenological problems of the SM such as those related to gravity and dark matter. These discussions can be found in the recent review of Altarelli [45] and references therein. The discussion on the hierarchy problem can be found also in [58, 59].

is not so large, this correction is well under control in the SM. However, the SM is just an effective theory of a more general theory with heavy particles at some high energy scale, say the GUT scale $\Lambda_{GUT} \sim 2 \times 10^{16} \text{GeV}$ where the three gauge coupling constants unify. The masses of those heavy particles are at the order of Λ_{GUT} . Those heavy particles must couple to the SM Higgs boson and hence give enormous corrections to M_H . The fact the $M_H/\Lambda_{GUT} \sim 10^{-14}$ means that an extreme cancelation occurs among those huge corrections. This is known as the naturalness or fine-tuning problem. A related question, called the hierarchy problem, is why $\Lambda_{GUT} \gg M_Z$. These problems can be solved if there is a symmetry to explain that cancelation. There are a few options for such a symmetry, among them supersymmetry is the most promising candidate.

1.5 Minimal Supersymmetric Standard Model

The Minimal Supersymmetric Standard Model is a theory describing the interactions of all SM fundamental particles, their superpartners and some additional Higgs particles. None of these superpartners and new Higgs bosons has been seen in experiment. The fundamental superpartners arise as a consequence of the so-called supersymmetry (SUSY) imposed on the Lagrangian of the theory. The SUSY generator \mathcal{Q} transforms a fermion into a boson and vice versa:

$$\mathcal{Q}|\text{fermion}\rangle = |\text{boson}\rangle, \quad \mathcal{Q}|\text{boson}\rangle = |\text{fermion}\rangle. \quad (1.39)$$

It means that each SM particle has a corresponding superpartner. The superpartners of a fermion, a vector gauge boson, a scalar Higgs boson are called a sfermion, a gaugino, a higgsino respectively. SUSY requires that a superpartner has the same quantum numbers as its corresponding particle except for the spin. Sfermions are scalar while gauginos and higgsinos have spin 1/2. One notices immediately that some mixings among gauginos and higgsinos are allowed. The MSSM Lagrangian has three symmetries: Lorentz symmetry, SM gauge symmetry and SUSY.

The fact that we have never observed a fundamental scalar selectron with the same mass as the electron means that SUSY is broken. To date there is no completely satisfactory dynamical way to break SUSY. In the MSSM, SUSY is broken by introducing extra terms that explicitly break SUSY into the Lagrangian [60]. They are called soft-SUSY-breaking terms, all contained in \mathcal{L}_{soft} . The purpose of \mathcal{L}_{soft} is to give (quite heavy) masses to superpartners [59, 60, 61, 62].

The SM particles obtain masses by the Higgs mechanism. In the SM, we just need one Higgs doublet Φ (and $\tilde{\Phi} = i\sigma_2\Phi^*$) to generate masses for down quarks (up quarks). However, the same trick cannot be used for the MSSM since it will break SUSY. Thus one needs two complex Higgs doublets with opposite hypercharges

$$H_1 = \begin{pmatrix} H_1^0 \\ H_1^- \end{pmatrix} \quad \text{with } Y_{H_1} = -1/2; \quad H_2 = \begin{pmatrix} H_2^+ \\ H_2^0 \end{pmatrix} \quad \text{with } Y_{H_2} = 1/2, \quad (1.40)$$

to give masses for down fermions and up fermions respectively. Before symmetry breaking, these two Higgs doublets have 8 independent real fields. After symmetry breaking, 3 vector gauge bosons Z , W^\pm get masses by "eating" 3 Goldstone bosons, so five real fields remain. The MSSM therefore predicts the existence of 3 neutral Higgs bosons denoted H , h , A and 2 charged Higgs bosons denoted H^\pm .

In the unconstrained MSSM, \mathcal{L}_{soft} introduces a huge number (105) of unknown parameters (*e.g.* intergenerational mixing, complex phases), in addition to 19 parameters of the SM [59, 63]. This makes the phenomenology study of the MSSM extremely difficult if not impossible. There exists however the so-called constrained MSSMs with only a handful of parameters. Among them, mSUGRA is most well-known with the 5 following parameters [60, 61, 62, 64]

$$\tan\beta, \quad m_{1/2}, \quad m_0, \quad A_0, \quad \text{sign}(\mu). \quad (1.41)$$

This is achieved by imposing some conditions on the soft-SUSY-breaking parameters. These parameters are required to be real and satisfy a set of boundary conditions at the GUT scale ($\Lambda_{GUT} \sim 2 \times 10^{16} \text{GeV}$) where the three gauge coupling constants unify.

These boundary conditions say that: all gauginos have the same masses ($m_{1/2}$), all sfermions and Higgs bosons have the same mass (m_0) and all trilinear couplings in \mathcal{L}_{soft} are equal at the GUT scale.

1.5.1 The Higgs sector of the MSSM

The scalar Higgs potential V_H comes from three different sources [59, 58, 65]:

$$\begin{aligned} V_H &= V_D + V_F + V_{soft}, \\ V_D &= \frac{g^2}{8} \left[4|H_1^\dagger \cdot H_2|^2 - 2|H_1|^2|H_2|^2 + (|H_1|^2)^2 + (|H_2|^2)^2 \right] + \frac{g'^2}{8} (|H_2|^2 - |H_1|^2)^2, \\ V_F &= \mu^2 (|H_1|^2 + |H_2|^2), \\ V_{soft} &= m_{H_1}^2 H_1^\dagger H_1 + m_{H_2}^2 H_2^\dagger H_2 + B\mu (H_2 \cdot H_1 + h.c.), \end{aligned} \quad (1.42)$$

where g, g' are the usual two couplings of the groups $SU(2)$ and $U(1)$ respectively; μ and $B\mu$ are bilinear couplings; $|H_1|^2 = |H_1^0|^2 + |H_1^-|^2$ and the same definition for $|H_2|^2$. The first two terms of V_H are the so-called D- and F- terms. The last term V_{soft} is just a part of \mathcal{L}_{soft} discussed above. The MSSM Higgs potential contains the gauge couplings while the SM one given in Eq. (1.14) does not.

The neutral components of the two Higgs fields develop vacuum expectation values

$$\langle H_1^0 \rangle = \frac{v_1}{\sqrt{2}}, \quad \langle H_2^0 \rangle = \frac{v_2}{\sqrt{2}}. \quad (1.43)$$

One defines

$$\tan \beta = \frac{v_2}{v_1}. \quad (1.44)$$

Comparing to the SM we have

$$v_1^2 + v_2^2 = v^2. \quad (1.45)$$

We now develop the two doublet complex scalar fields H_1 and H_2 around the vacuum,

into real and imaginary parts

$$\begin{aligned} H_1 &= (H_1^0, H_1^-) = \frac{1}{\sqrt{2}} (v_1 + H_1^0 + iP_1^0, H_1^-) \\ H_2 &= (H_2^+, H_2^0) = \frac{1}{\sqrt{2}} (H_2^+, v_2 + H_2^0 + iP_2^0) \end{aligned} \quad (1.46)$$

where the real parts correspond to the CP-even Higgs bosons and the imaginary parts corresponds to the CP-odd Higgs and the Goldstone bosons. By looking at the Eq. 1.42, we see that those fields mix. After diagonalizing the mass matrices, one gets

$$\begin{aligned} \begin{pmatrix} \chi_3 \\ A \end{pmatrix} &= \begin{pmatrix} \cos \beta & \sin \beta \\ -\sin \beta & \cos \beta \end{pmatrix} \begin{pmatrix} P_1^0 \\ P_2^0 \end{pmatrix}, \\ \begin{pmatrix} \chi^\pm \\ H^\pm \end{pmatrix} &= \begin{pmatrix} \cos \beta & \sin \beta \\ -\sin \beta & \cos \beta \end{pmatrix} \begin{pmatrix} H_1^\pm \\ H_2^\pm \end{pmatrix}, \\ \begin{pmatrix} H \\ h \end{pmatrix} &= \begin{pmatrix} \cos \alpha & \sin \alpha \\ -\sin \alpha & \cos \alpha \end{pmatrix} \begin{pmatrix} H_1^0 \\ H_2^0 \end{pmatrix}, \end{aligned} \quad (1.47)$$

with the mixing angle α given by

$$\cos 2\alpha = -\cos 2\beta \frac{M_A^2 - M_Z^2}{M_H^2 - M_h^2}, \quad \sin 2\alpha = -\sin 2\beta \frac{M_H^2 + M_h^2}{M_H^2 - M_h^2}, \quad (1.48)$$

where χ_3, χ^\pm are massless Goldstone bosons to be eaten by the Z, W^\pm respectively; A, H^\pm, H and h are five physically massive Higgs bosons; the tree-level masses are given by

$$\begin{aligned} M_A^2 &= -B\mu(\tan \beta + \cot \beta) = -\frac{2B\mu}{\sin 2\beta}, \\ M_{H^\pm}^2 &= M_A^2 + M_W^2, \\ M_{h,H}^2 &= \frac{1}{2} \left[M_A^2 + M_Z^2 \mp \sqrt{(M_A^2 + M_Z^2)^2 - 4M_A^2 M_Z^2 \cos^2 2\beta} \right]. \end{aligned} \quad (1.49)$$

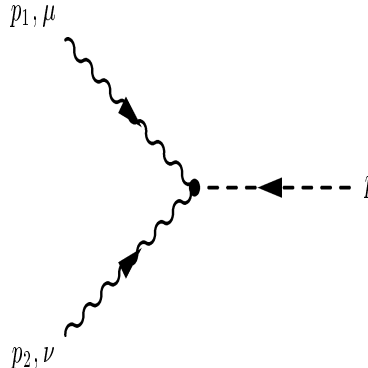
We remark that $M_h \leq M_Z$ at tree level. From Eqs. (1.48) and (1.49) we get

$$\cos^2(\beta - \alpha) = \frac{M_h^2(M_Z^2 - M_h^2)}{M_A^2(M_H^2 - M_h^2)}, \quad (1.50)$$

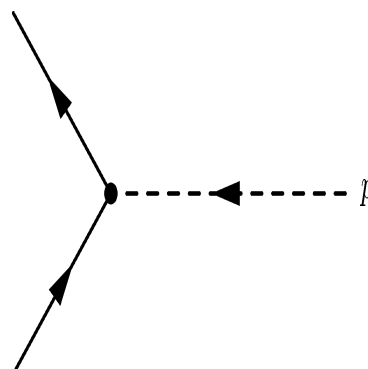
which will be useful later.

1.5.2 Higgs couplings to gauge bosons and heavy quarks

Like in the SM, the Higgs boson couplings to the gauge bosons are obtained from the kinetic terms with covariant derivatives of the Higgs fields H_1 and H_2 . The Yukawa Higgs boson couplings to the fermions are obtained from the Yukawa Lagrangian. We list here some relevant couplings needed in this thesis. For a full account of Higgs couplings in the MSSM, we refer to [59, 66, 67]. With λ_{WWH} , λ_{ZZH} , λ_{bbH} , λ_{ttH} are the SM couplings and using the same Feynman rules as in section 1.3, we have:



$p_1 (\mu)$	$p_2 (\nu)$	p_3	
W^-	W^+	H	$\lambda_{WWH} \cos(\beta - \alpha)$
W^-	W^+	h	$\lambda_{WWH} \sin(\beta - \alpha)$
Z	Z	H	$\lambda_{ZZH} \cos(\beta - \alpha)$
Z	Z	h	$\lambda_{ZZH} \sin(\beta - \alpha)$



p_1	p_2	p_3	
\bar{t}	t	H	$-\lambda_{ttH} [\cos(\beta - \alpha) - \cot \beta \sin(\beta - \alpha)]$
\bar{b}	b	H	$-\lambda_{bbH} [\cos(\beta - \alpha) - \tan \beta \sin(\beta - \alpha)]$
\bar{t}	t	h	$-\lambda_{ttH} [\sin(\beta - \alpha) + \cot \beta \cos(\beta - \alpha)]$
\bar{b}	b	h	$-\lambda_{bbH} [\sin(\beta - \alpha) - \tan \beta \cos(\beta - \alpha)]$

We remark that the $bb(tt)$ coupling of either the H or h boson is enhanced(suppressed) by a factor $\tan \beta$ with the enhancement(suppression) magnitude depending on the value of $\sin(\beta - \alpha)$ or $\cos(\beta - \alpha)$. Thus one can have very large value of bottom-Higgs Yukawa coupling, leading to a large cross section if $\tan \beta$ is large. In the decoupling limit where $M_A \rightarrow \infty$, *i.e.* $\cos(\beta - \alpha) \rightarrow 0$ (see Eq. (1.50)), the h is SM-like (the same couplings) while the H Yukawa coupling to $bb(tt)$ is exactly enhanced(suppressed) by a factor $\tan \beta$.

Chapter 2

Standard Model Higgs production at the LHC

2.1 The Large Hadron Collider

The Large Hadron Collider (LHC) is the world largest particle accelerator to date [10]. It collides two proton beams with the center-of-mass energy up to 14TeV. It is expected to start this year. It has four main experiments: ATLAS, CMS, LHCb and ALICE. ATLAS and CMS are general-purpose detectors. Their goals are to find the Higgs boson and discover new physics expected to be Supersymmetry. LHCb is for B-physics and CP violation. ALICE aim is to study the physics of strongly interacting matter at extreme energy densities, where the formation of a new phase of matter, the quark-gluon plasma, is expected. The number of events per second generated in the LHC collisions given by

$$N_{event} = L\sigma_{event}, \tag{2.1}$$

where σ_{event} is the cross section for the event under study and L the machine luminosity. The machine luminosity depends only on the beam parameters and can be

Table 2.1: LHC beam parameters relevant for the peak luminosity [68]

Number of particles per bunch (N_b)	1.15×10^{11}
Number of bunches per beam (n_b)	2808
Revolution frequency (f_{rev})	11245Hz
Relativistic gamma (γ_r)	7461 ($E = 7\text{TeV}$)
Normalized transverse emittance (ϵ_n)	$3.75 \times 10^{-4}\text{cm}$
Full crossing angle at the IP (θ_c) for ATLAS/CMS	$285\mu\text{rad} = 0.0163^\circ$
RMS bunch length (σ_z)	7.55cm
Transverse RMS beam size (σ^*) at ATLAS/CMS	$16.7\mu\text{m}$
Geometric luminosity reduction factor (F) at ATLAS/CMS	0.84
Optical beta function at ATLAS/CMS (β^*)	55cm

written for a Gaussian beam distribution as

$$L = \frac{N_b^2 n_b f_{rev} \gamma_r}{4\pi \epsilon_n \beta^*} F, \quad (2.2)$$

where N_b is the number of particles per bunch, n_b number of bunches per beam, f_{rev} the revolution frequency, γ_r the relativistic gamma factor, ϵ_n the normalized transverse beam emittance¹, β^* the optical beta function at the collision point² and F the geometric luminosity reduction factor due to the crossing angle at the interaction point (IP):

$$F = 1 / \sqrt{1 + \left(\frac{\theta_c \sigma_z}{2\sigma^*} \right)^2}, \quad (2.3)$$

where θ_c is the full crossing angle at the IP, σ_z the root-mean-square (RMS) bunch length and σ^* the transverse RMS beam size at the IP. Note that $F < 1$ since the angle between two beams at the collision point is greater than zero. The above expressions assumes equal beam parameters for both circulating beams. In order to calculate the

¹The beam emittance (ϵ), units of length, is the extent occupied by the particles of the beam in phase space. A low emittance particle beam is a beam where the particles are confined to a small distance and have nearly the same momentum. The normalized beam emittance $\epsilon_n = \gamma_r \beta_r \epsilon$.

²The optical beta function $\beta(s)$ appears in the amplitude of the solution of the equation of a harmonic oscillator $x''(s) + Kx(s) = 0$ describing the transverse beam dynamics (linear force in x and y , s is the beam direction).

peak luminosity, we need the LHC beam parameters given in Table 2.1. We then get the value of the peak luminosity at ATLAS/CMS $L = 10^{34}\text{cm}^{-2}\text{s}^{-1}$. Note that in luminosity formula (2.2) there are only two beam parameters β^* and F which depend on the collision point (experiment position), other beam parameters are the same for LHCb and ALICE. Other experiments LHCb and ALICE with $Pb-Pb$ collision have lower luminosity, $10^{32}\text{cm}^{-2}\text{s}^{-1}$ and $10^{27}\text{cm}^{-2}\text{s}^{-1}$ respectively. If the Higgs production cross section is 1pb then one has 10^{-2} events per second at ATLAS/CMS.

The luminosity in the LHC is not constant over a physics run but decays due to the degradation of intensities and emittances of the circulating beams. The LHC integrated luminosity ($L_{int} = \int_0^T L(t)dt$) expected per year is between 80fb^{-1} and 120fb^{-1} [68].

Despite of a number of enormous advantages: the high values of luminosity and center-of-mass energy, the dedicated detectors ATLAS and CMS designed to discover the Higgs boson and Supersymmetry particles; to get something out of a huge amount of data produced by the LHC is not easy. The main challenge for LHC physics is at the way one analyses data. Let us make it clear. The total cross section for inelastic scatterings which can be seen by LHC detectors is about 60mb [69]. It is translated to 6×10^8 events per second (event rate). To be optimistic and forget about the background, we say that the typical total cross section for Higgs production at the LHC is 60pb which corresponds to 6×10^{-1} event rate. Thus we have to know how to find out 6×10^{-1} events in 6×10^8 events per second. The task becomes much more complicated when backgrounds are taken into account. The only way to distinguish signal from backgrounds is to study various distributions.

2.2 SM Higgs production at the LHC

The SM Higgs profile is:

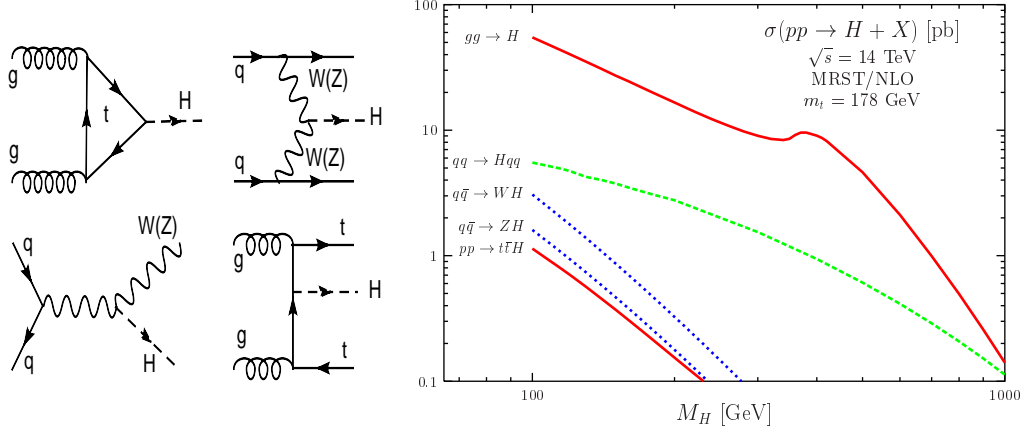


Figure 2.1: *Four mechanisms to produce the Higgs at the LHC. The right figure shows the cross sections as functions of M_H , which include the full NLO QCD corrections [11].*

- | | |
|------------------------------|-------------------------------------------------------------------------------------------------------------------------------------------------------------------------------------------------------------|
| (1) Electric charge: neutral | (5) Mass: $114\text{GeV} < M_H < 190\text{GeV}$ [9] |
| (2) Color charge: neutral | (6) Higgs couplings: $\lambda_{VVH} \propto M_V$, $\lambda_{ffH} \propto m_f/v$, $\lambda_{HHH} \propto \lambda v = \frac{M_H^2}{2v}$ with V is a massive gauge boson, f a fermion (see section 1.3). |
| (3) Spin: 0 | |
| (4) CP: even | |

In this section, we assume that the above Higgs profile is correct. The last property means that the Higgs boson couples mainly to heavy particles: W and Z gauge bosons, the top quark and, to lesser extent, the bottom quark. The four main mechanisms for single Higgs boson production are [11]:

1. gluon-gluon fusion: $gg \rightarrow H$
2. associated production with heavy quarks: $gg \rightarrow Q\bar{Q} + H$ with $Q = b, t$
3. vector boson fusion: $q\bar{q} \rightarrow V^*V^* \rightarrow q\bar{q} + H$ with q is a light quark
4. associated production with $W(Z)$: $qq(q\bar{q}) \rightarrow W(Z) + H$

We will use the item number to refer to the corresponding process. The Feynman diagrams and total cross sections are shown in Fig. 2.1. It is important to know that in the second mechanism, there is also a contribution from $q\bar{q}$ in the initial state. However, this contribution is very small compared to the gg contribution and can be neglected. There are two reasons for this. First, the quark density in the proton is very small compared to the gluon density. Second, $q\bar{q}$ contribution contains only S-channel diagrams strongly suppressed at high energy while gg contribution contains T and U channels.

From the plot of total cross sections as functions of M_H in Fig. 2.1 we see that for $M_H \in [114, 190]\text{GeV}$ the total cross section for gg fusion process is largest and almost 10 times bigger than the second one from vector boson fusion process. For $M_H = 120\text{GeV}$, the total cross sections for the four processes are about:

$$\begin{pmatrix} H & t\bar{t}H & q\bar{q}H & WH(ZH) \\ 40\text{pb} & 0.7\text{pb} & 5\text{pb} & 2(1)\text{pb} \end{pmatrix} \quad (2.4)$$

We can conclude that: for Higgs production, the LHC is just the gg collider. The Higgs discovery channel is clearly the gg fusion process.

The first important signal for a Higgs boson is a peak in the invariant mass distribution of its leptonic decay products ³. However, if we observe a new bump at around 120GeV in some production channel it is not necessarily the SM Higgs boson. All we can say is that it is new physics, a new particle with mass around 120GeV. Now we look back at the Higgs profile and assume that all the properties are confirmed except for the last one (the coupling property). We still cannot say that it is the SM Higgs boson. Remember that the Higgs originates from the Higgs potential defined by its self coupling (λ) and interacts with vector gauge bosons and heavy fermions in some special ways. The best way to check the SSB mechanism in the SM is to determine the three independent Higgs couplings: λ_{VVH} , λ_{ffH} and λ_{HHH} . If all these three couplings are consistent with the SM prediction then we can

³The Higgs hadronic decay products suffer from extreme QCD jet backgrounds.

definitely say that it is the SM Higgs boson. However, measuring accurately those three Higgs couplings is an extremely difficult task if not impossible at the LHC. The Higgs self-coupling is the most difficult one. For this, one can think of $gg \rightarrow HH$ but the total cross section is small and background is large. The two other couplings can be accessed at the LHC [11, 70].

2.3 Experimental signatures of the SM Higgs

The SM Higgs boson is a heavy particle and decays. Its decay branching ratios (Γ_i/Γ_H) and total width (Γ_H) are shown in Fig. 2.2. We first look at the plot for the Higgs decay branching ratios (BR) and impose the following conditions: $BR > 10^{-3}$, leptonic (photonic) decay product or heavy quarks in the decay product. These are the conditions for observing the Higgs in experiment. With the Higgs profile in hand ($M_H \in [114, 182]\text{GeV}$) we are left with 7 branching ratios: $b\bar{b}$, W^+W^- , ZZ , $\tau^+\tau^-$, $c\bar{c}$, $\gamma\gamma$, $Z\gamma$. Among these, $c\bar{c}$ and $Z\gamma$ can be discarded. For $c\bar{c}$ there are two reasons: $BR(c\bar{c})$ is 10 times smaller than $BR(b\bar{b})$ and it is more difficult to tag a charm-quark in experiment than a bottom-quark. For $Z\gamma$ there are also two reasons: $BR(Z\gamma)$ is at the same order as $BR(\gamma\gamma)$ and the Z is heavy and decays dominantly into hadrons and neutrinos and thus the combined branching ratio for this channel is very small. Thus we now have 5 potential Higgs signatures

$$\begin{pmatrix} b\bar{b} & \gamma\gamma & \tau^+\tau^- & W^+W^- & ZZ \\ 0.68 & 2.16 \times 10^{-3} & 6.78 \times 10^{-2} & 0.13 & 1.49 \times 10^{-2} \end{pmatrix} \quad (2.5)$$

where the second row are branching ratios for $M_H = 120\text{GeV}$. Of these $b\bar{b}$ and $\gamma\gamma$ can be observed "directly" in experiments. The three other decay modes cannot be directly seen in experiments and more branching ratios must be taken into account. $\gamma\gamma$ is the most beautiful signal in experiment but its branching ratio is smallest. This is unlikely to be a discovery channel. The $gg \rightarrow H \rightarrow b\bar{b}$ suffers from huge QCD

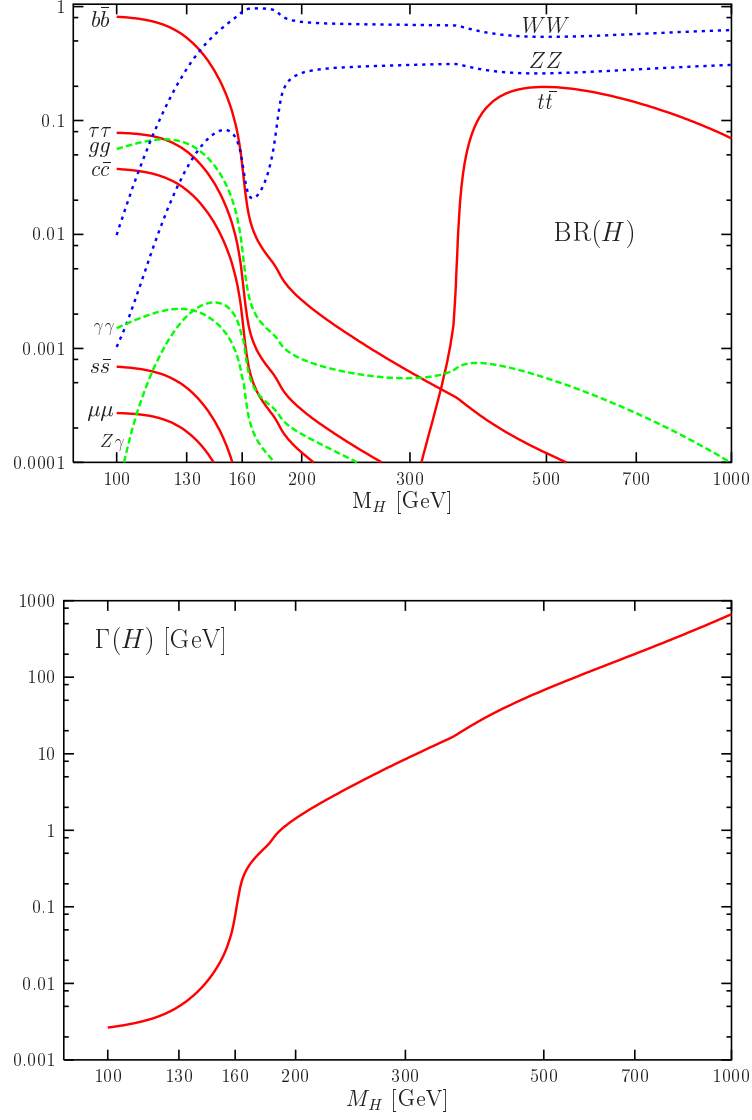


Figure 2.2: *Upper: The SM Higgs boson decay branching ratios as a function of M_H . Lower: The SM Higgs boson total decay width as a function of M_H . Ref. [11].*

backgrounds ⁴ [71] and cannot be realised in LHC experiments [11]. For $b\bar{b}$ signal, we have to use the mechanism of Higgs production associated with massive gauge bosons or heavy quarks. If we stick with the gg fusion mechanism then the Higgs discovery signal can be $\tau^+\tau^-$, W^+W^- or ZZ depending on the value of M_H . $\tau^+\tau^-$ signal is important for small Higgs mass. ZZ can give a beautiful 4-lepton signal but only for very large Higgs mass ($M_H > 2M_Z$). For the large range of M_H left, W^+W^- decay mode is the best signal to pursue.

The total Higgs decay width is shown in the Fig. 2.2. We first notice that $\Gamma_H \leq 0.63\text{GeV}$ for $M_H \leq 180\text{GeV}$. The SM Higgs boson is a heavy long-lived particle. This makes it easy to determine the Higgs mass accurately by using $H \rightarrow \gamma\gamma$ for small M_H and $H \rightarrow ZZ \rightarrow l^+l^-l^+l^-$ for large M_H [72, 73]. However, it will be difficult to measure Γ_H precisely.

2.4 Summary and outlook

If there exists only one Higgs boson in nature as predicted by the SM, it should be found at the LHC via the gluon-gluon fusion channel. However, if nature prefers having more than a unique Higgs boson, say five Higgs bosons as anticipated by the MSSM, then the situation of the SM-like Higgs (with the same Higgs profile given in section 2.2 except for the last coupling property) production at the LHC will be very different. From the results of subsection 1.5.2 we know that the SM-like Higgs coupling to the bottom quark can be strongly enhanced for large value of $\tan\beta$ while the same coupling with the top quark is much suppressed by the same factor. Thus the SM-like Higgs production associated with two bottom quarks can be the dominant mechanism at the LHC [59]. This channel with $H \rightarrow W^+W^-$ -signature is also very valuable for the determination of the bottom-Higgs Yukawa coupling. In order to identify those new physics characters or just to confirm the SM Higgs properties, the

⁴In a small window about the Higgs mass, the QCD background $pp \rightarrow b\bar{b}$ is still very large.

study of SM Higgs production associated with two bottom quarks at the LHC is very important. Indeed, it is the topic of the next chapter.

Chapter 3

Standard Model $b\bar{b}H$ production at the LHC

The content of this chapter is based on our publications [74, 75, 76].

3.1 Motivation

The study of the Higgs properties such as its self-couplings and couplings to the other particles of the standard model (SM) will be crucial in order to establish the nature of the scalar component of the model. In this respect most prominent couplings, in the SM, are the Higgs (λ_{HHH}), the top (λ_{tH}), and to a much lesser degree the bottom (λ_{bbH}), Yukawa couplings. The top Yukawa coupling is after all of the order of the strong QCD coupling and plays a crucial role in a variety of Higgs related issues. In our main calculation of EW corrections to $b\bar{b}H$, the leading contribution includes terms with largest powers of λ_{tH} .

The next-to-leading order (NLO) QCD correction to $pp \rightarrow b\bar{b}H$ has been calculated by different groups relying on different formalisms. In a nut-shell, in the five-flavour scheme (5FNS)[77, 78], use is made of the bottom distribution function

so that the process is approximated (at leading order, LO) by the fusion $b\bar{b} \rightarrow H$. This gives an approximation to the inclusive cross section dominated by the untagged low p_T outgoing b jets. If only one final b is tagged, the cross section is approximated by $gb \rightarrow bH$. The four flavour scheme (4FNS) has no b parton initiated process but is induced by gluon fusion $gg \rightarrow b\bar{b}H$, with a very small contribution from the light quark initiated process $q\bar{q} \rightarrow b\bar{b}H$ ¹. Here again the largest contribution is due to low p_T outgoing b 's which can be accounted for by gluon splitting into $b\bar{b}$. The latter needs to be resummed and hence one recovers most of the 5FNS calculation while retaining the full kinematics of the reaction. QCD NLO corrections have been performed in both schemes[78, 79, 80, 81] and one has now reached a quite good agreement[82]. The 5FNS approach, which at leading order is a two-to-one process has allowed the computation of the NNLO QCD correction[83, 84] and very recently the electroweak/SUSY (supersymmetry) correction[85] to $b\bar{b} \rightarrow \phi$, ϕ any of the neutral Higgs boson in the MSSM. SUSY QCD corrections have also been performed for $gg \rightarrow b\bar{b}h$ [86, 87] where h is the lightest Higgs in the MSSM as well as to $gb \rightarrow b\phi$ [88].

In order to exploit this production mechanism to study the Higgs couplings to b 's, one must identify the process and therefore one needs to tag both b 's, requiring somewhat large p_T b . This reduces the cross section but gives much better signal over background ratio. For large p_T outgoing quarks one needs to rely on the 4FNS to properly reproduce the high p_T b quarks. The aim of this and next chapters is to report on the calculation of the leading electroweak corrections to the exclusive $b\bar{b}H$ final state, meaning two b 's are detected. These leading electroweak corrections are triggered by top-charged Goldstone loops whereby, in effect, an external b quark turns into a top. This transition has a specific chiral structure whose dominant part is given by the top mass or, in terms of couplings, to the top Yukawa coupling. Considering that the latter is of the order of the QCD coupling constant, the corrections might be large. In fact, as we shall see, such type of transitions can trigger $gg \rightarrow b\bar{b}H$ even

¹In fact $q\bar{q} \rightarrow b\bar{b}H$ is dominated by $q\bar{q} \rightarrow HZ^* \rightarrow b\bar{b}H$ and does not vanish for vanishing bottom Yukawa coupling. However this contribution should be counted as ZH production and can be excluded by imposing an appropriate cut on the invariant mass of the $b\bar{b}$ pair.

with *vanishing* λ_{bbH} in which case the process is generated solely at one-loop. We will quantify the effect of such contributions.

3.2 General considerations

Before discussing the details of the calculation it is educative to expose some key features that appear when one considers the electroweak corrections at one-loop compared to the structure we have at tree-level or even the structure that emerges from QCD loop calculations. In particular the helicity structure is quite telling. So let us set our definition first. The process we consider is $g(p_1, \lambda_1) + g(p_2, \lambda_2) \rightarrow b(p_3, \lambda_3) + \bar{b}(p_4, \lambda_4) + H(p_5)$. $\lambda_i = \pm$ with $i = 1, 2, 3, 4$ are the helicities of the gluons, the bottom and anti-bottom while p_i are the momenta of particles². The corresponding helicity amplitude will be denoted by $\mathcal{A}(\lambda_1, \lambda_2; \lambda_3, \lambda_4)$.

3.2.1 Leading order considerations

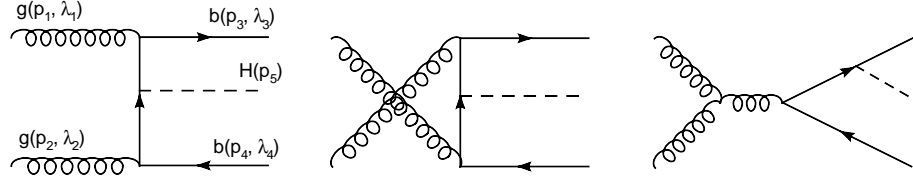


Figure 3.1: All the eight Feynman diagrams can be obtained by inserting the Higgs line to all possible positions in the bottom line.

At tree-level, see Fig. 3.1 for the contributing diagrams, the Higgs can only attach to the b -quark and therefore each diagram, and hence the total amplitude, is

²The cross section for $q\bar{q} \rightarrow g^* \rightarrow b\bar{b}H$ (with input parameters given in section 3.5 and $q = u, d, s$) is about 0.7% of the $\sigma(gg \rightarrow b\bar{b}H)$ and thus can be totally neglected. There are two reasons for this. First the density of gluon at the LHC is much bigger than the density of quarks. Second the $q\bar{q} \rightarrow b\bar{b}H$ which is S-channel is rather suppressed at high energy while the $gg \rightarrow b\bar{b}H$ contains also T and U channels which give the dominant contribution.

proportional to the Higgs coupling to $b\bar{b}$, λ_{bbH} . Compared to the gluon coupling this scalar coupling breaks chirality. These features remain unchanged when we consider QCD corrections. Moreover the QCD coupling and the Higgs coupling are parity conserving which allows to relate the state with helicities $(\lambda_1, \lambda_2; \lambda_3, \lambda_4)$ to the one with $(-\lambda_1, -\lambda_2; -\lambda_3, -\lambda_4)$ therefore cutting by half the number of helicity amplitudes to calculate. With our conventions for the definition of the helicity states, see Appendix A, parity conservation for the tree-level helicity amplitude gives

$$\mathcal{A}_0(-\lambda_1, -\lambda_2; -\lambda_3, -\lambda_4) = \lambda_3 \lambda_4 \mathcal{A}_0(\lambda_1, \lambda_2; \lambda_3, \lambda_4)^*. \quad (3.1)$$

This can be generalised at higher order in QCD with due care of possible absorptive parts in taking complex conjugation.

The number of contributing helicity amplitudes can be reduced even further at the leading order, in fact halved again, in the limit where one neglects the mass of the b -quark that originates from the b -quark spinors and therefore from the b quark propagators. We should in this case consider the λ_{bbH} as an independent coupling, intimately related to the model of symmetry breaking. In this case chirality and helicity arguments are the same, the b and \bar{b} must have opposite helicities for the leading order amplitudes and hence only $\mathcal{A}_0(\lambda_1, \lambda_2; \lambda, -\lambda)$ remain non zero. In this limit, this means that only a string containing an even number of Dirac γ matrices, which we will label in general as Γ^{even} as opposed to Γ^{odd} for a string with an odd number of γ 's, can contribute.

In the general case and reinstating the b mass, we may write the helicity amplitudes as

$$\begin{aligned} \mathcal{A}(\lambda_1, \lambda_2; \lambda_3, \lambda_4) &= \bar{u}(\lambda_3) (\Gamma_{\lambda_1, \lambda_2}^{even} + \Gamma_{\lambda_1, \lambda_2}^{odd}) v(\lambda_4) \\ &= \delta_{\lambda_3, -\lambda_4} \left(\mathcal{A}^{even} + m_b \tilde{\mathcal{A}}^{odd} \right) + \delta_{\lambda_3, \lambda_4} \left(\mathcal{A}^{odd} + m_b \tilde{\mathcal{A}}^{even} \right). \end{aligned} \quad (3.2)$$

The label even in \mathcal{A}^{even} and $\tilde{\mathcal{A}}^{even}$ are the contributions of Γ^{even} to the amplitude and likewise for odd . This way of writing shows that m_b originates from the mass

insertion coming from the massive spinors and are responsible for chirality flip. In the limit $m_b \rightarrow 0$, $\Gamma_{\lambda_1, \lambda_2}^{even}$ and $\Gamma_{\lambda_1, \lambda_2}^{odd}$ contribute to different independent helicity amplitudes. In general Γ^{even} and Γ^{odd} differ by a (fermion) mass insertion. In fact Γ^{odd} is proportional to a fermion mass insertion from a propagator. At leading order the mass insertion is naturally m_b , such that Γ^{odd} is $\mathcal{O}(m_b)$. This shows that at leading order, corrections from $m_b = 0$ to the total cross section are of order $\mathcal{O}(m_b^2)$. Of course there might be some enhancement of the $\mathcal{O}(m_b^2)$ terms if one remembers that the cross section can bring about terms of order $m_b^2/(p_T^b)^2$. However, in our calculation where we require the b 's to be observed hence requiring a p_T^b cut, the effect will be minimal. With $m_b = 4.62\text{GeV}$, the effect of neglecting m_b is that the cross section is increased by 3.7% for $|\mathbf{p}_T^{b, \bar{b}}| > 20\text{GeV}$ and 1.1% for $|\mathbf{p}_T^{b, \bar{b}}| > 50\text{GeV}$. At one-loop, the chiral structure of the weak interaction and the contribution of the top change many of the characteristics that we have just discussed for the tree-level.

3.2.2 Electroweak Yukawa-type contributions, novel characteristics

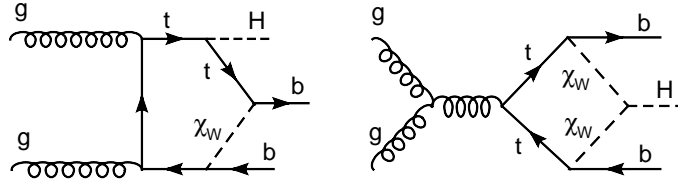


Figure 3.2: *Sample of one-loop diagrams related to the Yukawa interaction in the SM. χ_W represents the charged Goldstone boson.*

Indeed, look at the two contributions arising from the one loop electroweak corrections given in Fig. 3.2. Now the Higgs can attach to the top or to the W . Therefore these contributions do not vanish in the limit $\lambda_{bbH} = 0$. The mass insertion in what we called Γ^{odd} is proportional to the top mass and is not negligible. In fact the

diagrams in Fig. 3.2 show the charged Goldstone boson in the loop. The latter triggers a $t \rightarrow b\chi_W$ transition whose dominant coupling is proportional to the Yukawa coupling of the top. We will in fact be working in the approximation of keeping only the Yukawa couplings. This reduces the number of diagrams and if working in the Feynman gauge as we do in this computation, only the Goldstone contributions survive. The neutral Goldstone bosons can only contribute corrections of order λ_b^2 (see section 1.3 for the Feynman rules). We will neglect these $\mathcal{O}(\lambda_b^2)$ contributions at the amplitude level. However the order $\mathcal{O}(\lambda_b)$ corrections will be kept. All the corrections are then triggered by $t \rightarrow b\chi_W$ and apart from the QCD vertices, only the Yukawa vertices shown in Fig. 3.3 below are needed to build up the full set of electroweak corrections. Note that in the MSSM, the Higgs coupling to the fermion

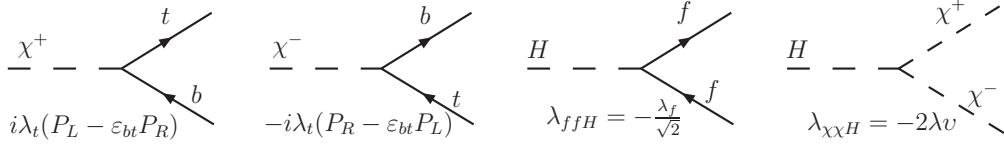


Figure 3.3: *Relevant vertices appearing at one loop.* $\varepsilon_{bt} = \lambda_b/\lambda_t$ and λ is the Higgs self-coupling, related to the Higgs mass in the Standard Model. The relations to the gauge couplings can be obtained by comparing to the SM Feynman rules given in section 1.3.

f , λ_{ffH} , can involve other parameters beside the corresponding Yukawa coupling λ_f , as shown in subsection 1.5.2. The Higgs coupling to the charged Goldstone involves the Higgs self-coupling or Yukawa coupling of the Higgs, $\lambda = M_H^2/2v^2$ proportional to the square of the Higgs mass. The latter can be large for large Higgs masses. These considerations allow to classify the contributions into three gauge invariant classes.

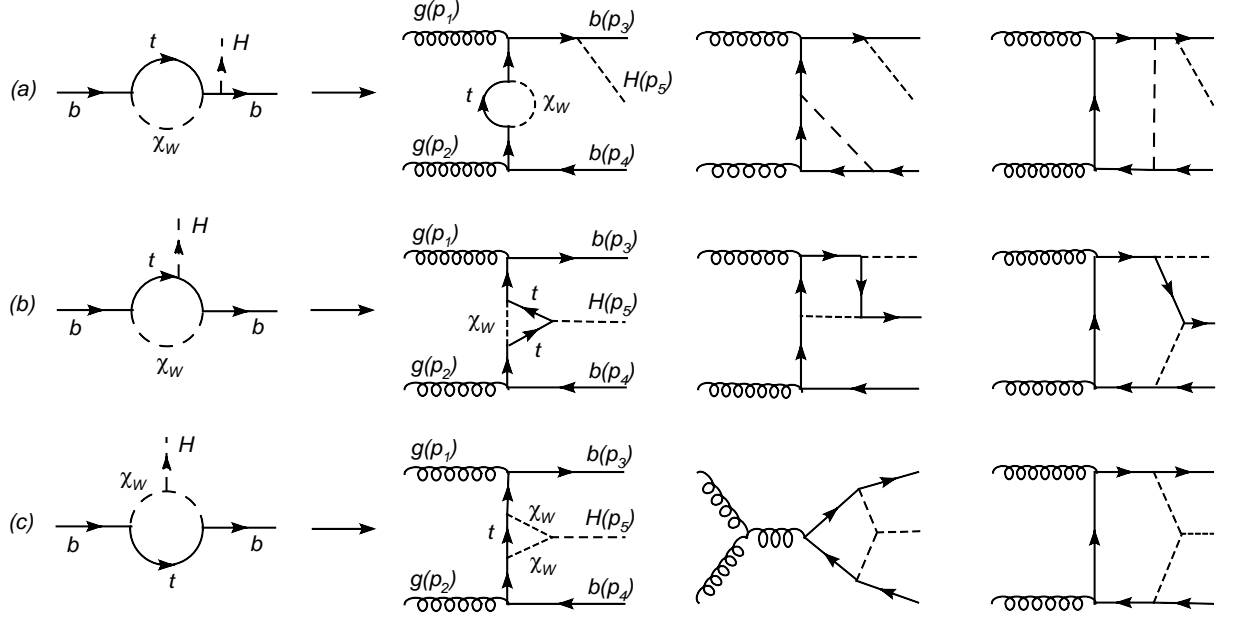


Figure 3.4: All the diagrams in each group can be obtained by inserting the two gluon lines or one triple gluon vertex (not shown) to all possible positions in the generic bottom line, which is the first diagram on the left. We have checked the number of diagrams through *Grace-loop*[47].

3.2.3 Three classes of diagrams and the chiral structure at one-loop

All the one-loop diagrams are classified into three gauge invariant groups as displayed in Fig. 3.4. The Higgs couples to the bottom quark in the first group (Fig. 3.4a), to the top quark in the second group (Fig. 3.4b) and to the charged Goldstone boson in the third group (Fig. 3.4c). As shown in Fig. 3.4 each class can be efficiently reconstructed from the one-loop vertex $b\bar{b}H$, depending on which leg one attaches the Higgs, by then grafting the gluons in all possible ways. We have also checked explicitly that each class with its counterterms, see below, constitutes a QCD gauge invariant subset. Note that these three contributions depend on different combinations of independent couplings and therefore constitute independent sets.

The chiral structure $t \rightarrow b\chi_W$ impacts directly on the structure of the helicity amplitudes at one-loop. The split of each contribution according to Γ^{even} and Γ^{odd} , see Eq. (3.2) will turn out to be useful and will indicate which helicity amplitude can be enhanced by which Yukawa coupling at one-loop. We show only one example in class (b) of Fig. 3.4. It is straight forward to carry the same analysis for all other diagrams. We choose the first diagram in group (b) in Fig. 3.4. For clarity we will here take $m_b = 0$, we have already shown how m_b insertions are taken into account, see Eq. (3.2). Leaving aside the colour part which can always be factorised out (see Appendix B) and the strong coupling constant, we write explicitly the contribution of this diagram as

$$\mathcal{A}_{b1}(\lambda_1, \lambda_2; \lambda_3, \lambda_4) = \lambda_{tH} \lambda_t^2 \bar{u}(\lambda_3, p_3) \not{\epsilon}(\lambda_1, p_1) \frac{\not{p}_{13}}{\bar{p}_{13}^2} C_{b1} \frac{\not{p}_{24}}{\bar{p}_{24}^2} \not{\epsilon}(\lambda_2, p_2) u(\lambda_4, p_4). \quad (3.3)$$

C_{b1} is the Yukawa vertex correction. In D -dimension, with q the integration variable, the momenta as defined in Fig. 3.1 with $p_{ij} = p_i + p_j$ and $\bar{p}_{ij} = p_j - p_i$ we have

$$C_{b1} = \int \frac{d^D q}{(2\pi)^D i} \frac{(P_R - \varepsilon_{bt} P_L)(m_t + \not{q} + \not{p}_{13})(m_t + \not{q} - \not{p}_{24})(P_L - \varepsilon_{bt} P_R)}{(M_W^2 - q^2)[m_t^2 - (q + \bar{p}_{13})^2][m_t^2 - (q - \bar{p}_{24})^2]}, \quad (3.4)$$

where $\varepsilon_{bt} = \lambda_b/\lambda_t$ as defined in Fig. 3.3. The numerator of the integrand of Eq. (3.4), neglecting terms of $\mathcal{O}(\lambda_b^2)$, can be re-arranged such as

$$\begin{aligned} \mathcal{A}_{b1}(\lambda_1, \lambda_2; \lambda_3, \lambda_4) &\xrightarrow{\text{numerator}} - \underbrace{\varepsilon_{bt} (m_t^2 + (\not{q} + \not{p}_{13})(\not{q} - \not{p}_{24}))}_{\Gamma^{even}} \\ &+ \underbrace{m_t P_R (2\not{q} + \not{p}_{13} - \not{p}_{24})}_{\Gamma^{odd}}. \end{aligned} \quad (3.5)$$

This shows explicitly that Γ^{odd} structures with a specific chirality, P_R , can indeed be generated. They do not vanish as $\lambda_{bbh} \rightarrow 0$. The even one-loop structures on the other hand are $\mathcal{O}(\lambda_b)$. The structure in class (c), Higgs radiation off the charged Goldstones, is the same. For class (a), radiation off the b -quark, the structure of the correction is different, the odd part is suppressed and receives an $\mathcal{O}(\lambda_b)$ correction. To summarise, with $m_b = 0$, making explicit the Yukawa couplings and the chiral structure if any, for example P_R , that characterise each class and comparing to the leading order, one has

	Γ^{even}	Γ^{odd}
tree-level	λ_{bbH}	0
(a)	$\lambda_t^2 \lambda_{bbH}$	$\lambda_b \lambda_t \lambda_{bbH}$
(b)	$\lambda_b \lambda_t \lambda_{ttH}$	$\lambda_t^2 \lambda_{ttH}, (P_R)$
(c)	$\lambda_b \lambda_t \lambda_{\chi\chi H}$	$\lambda_t^2 \lambda_{\chi\chi H}, (P_R)$

Despite the existence of the simple relation $\lambda_{ffH} = -\lambda_f/\sqrt{2}$ in the SM, we have kept λ_{ffH} and λ_f separate to distinguish their different origins (λ_f comes from the Goldstone couplings). As discussed in subsection 1.5.2, in the MSSM λ_{bbH} is enhanced by $\tan\beta$ but not λ_b . We clearly see that all one-loop Γ^{even} contributions vanish in the limit $\lambda_b = 0$ and $\lambda_{bbH} = 0$. On the other hand this is not the case for the one-loop Γ^{odd} contribution belonging to class (b) and (c). However for these contributions to interfere with the tree-level LO contribution requires a chirality flip through a m_b insertion. Therefore in the SM for example, the NLO cross section is necessarily of order m_b^2 , like the LO, with corrections proportional to the top Yukawa coupling for example. On the other hand, in the limit of $\lambda_{bbH} = 0$, the tree level vanishes but $gg \rightarrow b\bar{b}H$ still goes with an amplitude of order $g_s^2 \lambda_t^2 \lambda_{ttH}$ or $g_s^2 \lambda_t^2 \lambda_{\chi\chi H}$. For $\lambda_{bbH} \neq 0$ these contributions should be considered as part of the NNLO “corrections” however they do not vanish in the limit $m_b \rightarrow 0$ (or $\lambda_{bbH} = 0$) while the tree level does. These contributions can be important and we will therefore study their effects. For these contributions at the “NNLO” we can set $m_b = 0$.

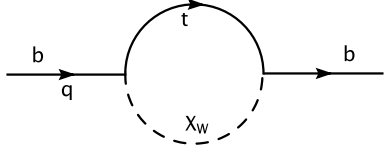
The classification in terms of structures as we have done makes clear also that the novel one-loop induced Γ^{odd} contributions must be ultraviolet finite. This is not necessarily the case of the Γ^{even} structures where counterterms to the tree-level structures are needed through renormalisation to which we now turn.

3.3 Renormalisation

We use an on-shell (OS) renormalisation scheme exactly along the lines described in subsection 1.2.6. Ultraviolet divergences are regularised through dimensional regularisation. In our approximation we only need to renormalise the vertices $b\bar{b}g$ and $b\bar{b}H$ as well as the bottom mass, m_b . For the $b\bar{b}g$ vertex, its counterterm reads

$$\delta_{bbg}^\mu = 2g_s\gamma^\mu(\delta Z_{b_L}^{1/2}P_L + \delta Z_{b_R}^{1/2}P_R). \quad (3.6)$$

$\delta Z_{b_{L,R}}^{1/2}$ are calculated by using Eq. (1.35). For this one needs to know the coefficients $K_{1,\gamma,5\gamma}$ which are very simple in our approximation:



$$\implies \Sigma(q^2) = K_1 + K_\gamma \not{q} + K_{5\gamma} \not{q} \gamma_5$$

We get

$$\begin{aligned} K_1(q^2) &= -\frac{\lambda_t^2}{16\pi^2} (C_{UV} - F_0(t, W)), \\ K_\gamma(q^2) &= -K_{5\gamma}(q^2) = \frac{\lambda_t^2}{64\pi^2} (C_{UV} - 2F_1(t, W)) \\ \text{with } C_{UV} &= \frac{1}{\epsilon} - \gamma_E + \ln 4\pi, D = 4 - 2\epsilon, \\ F_n(A, B) &= \int_0^1 dx x^n \ln \left((1-x)m_A^2 + xm_B^2 - x(1-x)q^2 \right). \end{aligned} \quad (3.7)$$

The reason we get $K_\gamma(q^2) = -K_{5\gamma}(q^2)$ is due to the particular chiral structure of the $t \rightarrow b\chi_W$ loop insertion. In particular for $m_b = 0$, one recovers that these corrections only contribute to $\delta Z_{b_L}^{1/2}$ and not $\delta Z_{b_R}^{1/2}$.

For the $b\bar{b}H$ vertex with the bare Lagrangian term $\mathcal{L}_{bbH} = -\frac{m_b}{v}\bar{\psi}_b\psi_b\varphi_H$, one needs to renormalise m_b , v , $\psi_{b_{L(R)}}$ and φ_H . With $v \rightarrow v(1 + \delta v)$ and the rules given in Eq. (1.26) we get the counterterm

$$\delta_{bbH} = \lambda_{bbH} \left[\frac{\delta m_b}{m_b} + \delta Z_{b_L}^{1/2} + \delta Z_{b_R}^{1/2} + (\delta Z_H^{1/2} - \delta v) \right]. \quad (3.8)$$

Again $\delta Z_{b_{L,R}}^{1/2}$ and δm_b are calculated by using Eqs. (1.35) and (3.7). $\delta Z_H^{1/2}$ is calculated through Eq. (1.31) where $\Pi^H(q^2)$ comes from the diagrams with heavy particles in the loop. As we are interested in the Yukawa corrections, these particles are the top quark, the Higgs boson, the W-Goldstone bosons and the Z-Goldstone boson. Indeed, those corrections include all the leading Higgs couplings: λ_{tH} and λ_{HHH} . We get

$$\begin{aligned}\Pi^H(q^2) &= \frac{M_H^4}{16\pi^2 v^2} \left[3C_{UV} - \frac{9}{2}F_0(H, H) - F_0(W, W) - \frac{1}{2}F_0(Z, Z) - 3(1 - \ln M_H^2) \right] \\ &+ \frac{3m_t^2}{8\pi^2 v^2} \{ q^2 [C_{UV} - F_0(t, t)] + 4[1 - \ln m_t^2 + F_0(t, t)] \}.\end{aligned}\quad (3.9)$$

From this and Eq. (1.31) we get

$$\begin{aligned}\delta Z_H^{1/2} &= -\frac{1}{8\pi^2} \text{Re} \left\{ \frac{3\lambda_t^2}{4} [C_{UV} - F_0(t, t) - M_H^2 G_0(t, t) + 4m_t^2 G_0(t, t)] \right. \\ &\quad \left. - \frac{\lambda}{4} [9G_0(H, H) + 2G_0(W, W) + G_0(Z, Z)] \right\} \Big|_{q^2=M_H^2}, \\ G_n(A, B) &= q^2 \frac{d}{dq^2} F_n(A, B) = q^2 \int_0^1 dx \frac{-x^n x(1-x)}{(1-x)m_A^2 + xm_B^2 - x(1-x)q^2}.\end{aligned}\quad (3.10)$$

For δv , we use the relation

$$v = \frac{2s_W M_W}{e}, \quad s_W = \sqrt{1 - \frac{M_W^2}{M_Z^2}} \quad (3.11)$$

to write δv in terms of δM_W^2 , δM_Z^2

$$\delta v = -\frac{c_W^2}{s_W^2} \left(\frac{\delta M_W^2}{2M_W^2} - \frac{\delta M_Z^2}{2M_Z^2} \right) + \frac{\delta M_W^2}{2M_W^2}. \quad (3.12)$$

We do not need to renormalise e since we are interested only in the Yukawa sector hence do not touch the photon. We now use Eq. (1.38) to calculate δM_W^2 and δM_Z^2 . Like in the case of Π^H , Π_T^W and Π_T^Z include all the leading contributions related to

the Goldstone bosons:

$$\begin{aligned}
\frac{\Pi_F^W(M_W^2)}{M_W^2} &= \frac{M_H^2}{8\pi^2 v^2} \left\{ [F_1(H, W) - F_0(H, W)] \Big|_{q^2=M_W^2} + \frac{\ln M_H^2}{2} \right\} \\
&+ \frac{m_t^2}{8\pi^2 v^2} [3C_{UV} - 6F_1(b, t)] \Big|_{q^2=M_W^2}, \\
\frac{\Pi_F^Z(M_Z^2)}{M_Z^2} &= \frac{M_H^2}{8\pi^2 v^2} \left\{ [F_1(H, Z) - F_0(H, Z)] \Big|_{q^2=M_Z^2} + \frac{\ln M_H^2}{2} \right\} \\
&+ \frac{m_t^2}{8\pi^2 v^2} [3C_{UV} - 3F_0(t, t)] \Big|_{q^2=M_Z^2}.
\end{aligned} \tag{3.13}$$

Then we get

$$\begin{aligned}
\delta v &= -\frac{1}{8\pi^2} \text{Re} \left\{ \frac{3\lambda_t^2}{4} [C_{UV} - 2F_1(b, t)] \Big|_{q^2=M_W^2} \right. \\
&- \lambda [F_0(H, W) - F_1(H, W) - \frac{1}{2} \ln M_H^2] \Big|_{q^2=M_W^2} \\
&- \frac{c_W^2}{s_W^2} \left[-\frac{3\lambda_t^2}{2} F_1(b, t) + \lambda (-F_0(H, W) + F_1(H, W)) \right] \Big|_{q^2=M_W^2} \\
&- \left. \frac{c_W^2}{s_W^2} \left[\frac{3\lambda_t^2}{4} F_0(t, t) + \lambda (F_0(H, Z) - F_1(H, Z)) \right] \Big|_{q^2=M_Z^2} \right\}.
\end{aligned} \tag{3.14}$$

From Eqs. (3.10) and (3.14), one clearly sees that $(\delta Z_H^{1/2} - \delta v)$ is UV-finite. Therefore, by looking at Eqs. (3.6) and (3.8), we conclude that to make all the contributions of diagrams in Fig. 3.4 UV-finite, it is sufficient to renormalise the mass and wave function of bottom-quark as done above. On the other hand $(\delta Z_H^{1/2} - \delta v)$ can be seen as a universal correction to Higgs production processes. We will include this correction as it has potentially large contributions scaling like λ_t^2 and λ which fall into the category of the corrections we are seeking.

In the actual calculation, the counter term δ_{bbg}^μ belongs to class (a) in the classification of Fig 3.4. This makes class (a) finite. The counterterm we associate to class (b) is the part of δ_{bbH} from the $t \rightarrow b\chi_W$ loops and therefore does not include what we termed the universal Higgs correction, *i.e* does not include the contribution $(\delta Z_H^{1/2} - \delta v)$. This is sufficient to make class (b) finite. In our approach (c) is finite without the addition of a counterterm. We will keep the $(\delta Z_H^{1/2} - \delta v)$ contribution

separate from the contributions in classes (a), (b), (c). We will of course include it in the final result.

3.4 Calculation details

We have written two independent codes. In the first one we set $m_b = 0$ in all propagators and other spinors that emerge from the helicity formalism we follow. In this limit, the helicity formalism is very much simplified and the expression quite compact. This code is in fact subdivided in two separate sub-codes. One sub-code is generated for the “even” part (constituted by the Γ^{even} contributions, see Eq. (3.2)) and the other by the “odd” part. We also generate a completely independent code for the case $m_b \neq 0$ where in particular we use the helicity formalism with massive fermions. Details of the helicity formalism that we use are given in Appendix A.

The steps that go into writing these codes are the following. In the first stage, we use FORM[89] to generate expressions for the tree level and one loop helicity amplitudes. Each helicity amplitude is written in terms of Lorentz invariants, scalar spinor functions $(A, B, C)_{\lambda_i \lambda_j}$ defined in Appendix A and the Passarino-Veltman[32] tensor functions T_M^N for a tensor of rank M for N -point function. We have also sought to write the contribution of each amplitude as a product of different structures or blocks that reappear for different graphs and contributions. For example colour factorisation is implemented, this further allows to rearrange the amplitude into an Abelian part and a non-Abelian part which will not interfere with each other at the matrix element squared level. The helicity information is contained in a set of basic blocks for further optimisation. Another set of blocks pertains to the loop integrals and other elements. The factorisation of the full amplitude in terms of independent building blocks is easily processed within FORM. These building blocks can still consist of long algebraic expressions which can be efficiently abbreviated into compact variables with the help of a Perl script which also allows to convert

the output of FORM into the Fortran code ready for a numerical evaluation. More details on the FORM code as well as the optimisation we implemented can be found in Appendix B.

3.4.1 Loop integrals, Gram determinants and phase space integrals

The highest rank M of the Passarino-Veltman tensor functions T_M^N with $M \leq N$ that we encounter in our calculation is $M = 4$ and is associated to a pentagon graph, $N = 5$. We use the library LoopTools[33, 35] to calculate all the tensorial one loop integrals as well as the scalar integrals, this means that we leave it completely to LoopTools to perform the reduction of the tensor integrals to the basis of the scalar integrals. In order to obtain the cross section one needs to perform the phase-space integration and convolution over the gluon distribution function (GDF), $g(x, Q)$ with Q representing the factorisation scale. We have

$$\begin{aligned} \sigma(pp \rightarrow b\bar{b}H) &= \frac{1}{256} \int_0^1 dx_1 g(x_1, Q) \int_0^1 dx_2 g(x_2, Q) \\ &\times \frac{1}{\hat{F}} \int \frac{d^3\mathbf{p}_3}{2e_3} \frac{d^3\mathbf{p}_4}{2e_4} \frac{d^3\mathbf{p}_5}{2e_5} |\mathcal{A}(gg \rightarrow b\bar{b}H)|^2 \delta^4(p_1 + p_2 - p_3 - p_4 - p_5), \end{aligned} \quad (3.15)$$

where $\frac{1}{256} = \frac{1}{4} \times \frac{1}{8} \times \frac{1}{8}$ is the spin and colour average factor and the flux factor is $1/\hat{F} = 1/(2\pi)^5 2\hat{s}$ with $\hat{s} = x_1 x_2 s \geq (2m_b + M_H)^2$.

The integration over the three body phase space and momentum fractions of the two initial gluons is done by using two “integrators”: BASES[37] and DADMUL[90]. BASES is a Monte Carlo that uses the importance sampling technique while DADMUL is based on the adaptive quadrature algorithm. The use of two different phase space integration routines helps control the accuracy of the results and helps detect possible instabilities. In fact some numerical instabilities in the phase space integration do occur when we use DADMUL but not when we use BASES which gives

very stable results with small integration error, typically 0.08% for 10^5 Monte Carlo points per iteration (see section C.2 for more details). For the range of Higgs masses we are studying in this chapter, the instabilities that are detected with DADMUL were identified as spurious singularities having to do with vanishing Gram determinants for the three and four point tensorial functions calculated in LoopTools by using the Passarino-Veltman reduction method³. Because this problem always happens at the boundary of phase space, we can avoid it by imposing appropriate kinematic cuts in the final state. In our calculation, almost all zero Gram determinants disappear when we apply the cuts on the transverse momenta of the bottom quarks relevant for our situation, see section 3.5.1 for the choice of cuts. The remaining zero Gram determinants occur when the two bottom quarks or one bottom quark and the Higgs are produced in the same direction. Our solution, once identified as spurious, was to discard these points by imposing some tiny cuts on the polar, θ , and relative azimuthal angles, ϕ of the outgoing b -quarks, the value of the cuts is $\theta_{cut}^{b,\bar{b}} = |\sin \phi^{\bar{b}}|_{cut} = 10^{-6}$. DADMUL then produces the same result as BASES within the integration error.

3.4.2 Checks on the results

i) Ultraviolet finiteness:

The final results must be ultraviolet (UV) finite. It means that they should be independent of the parameter C_{UV} defined in Eq. (3.7). In our code this parameter is treated as a variable. The cancellation of C_{UV} has been carefully checked in our code. Upon varying the value of the parameter C_{UV} from $C_{UV} = 0$ to $C_{UV} = 10^5$, the results are stable within more than 9 digits using double precision. This check makes sure that the divergent part of the calculation is correct. The correctness of the finite part is also well checked in our code by confirming that each helicity configuration is QCD gauge invariant.

³The reduction of the five point function using the method of Denner and Dittmaier [12, 34] which avoids the Gram determinant at this stage as implemented in LoopTools gives very stable results.

ii) QCD gauge invariance:

In the physical gauge we use, the QCD gauge invariance reflects the fact that the gluon is massless and has only two transverse polarisation components. In the helicity formalism that we use, the polarisation vector of the gluon of momentum p and helicity λ is constructed with the help of a reference vector q , see Appendix A for details. The polarisation vector is then labelled as $\epsilon^\mu(p, \lambda; q)$. A change of reference vector from q to q' amounts essentially to a gauge transformation (up to a phase)

$$\epsilon^\mu(p, \lambda; q') = e^{i\phi(q', q)} \epsilon^\mu(p, \lambda; q) + \beta(q', q) p^\mu. \quad (3.16)$$

QCD gauge invariance in our case amounts to independence of the cross section in the choice of the reference vector, q . We have carefully checked that the numerical result for the norm of each helicity amplitude at various points in phase space is independent of the reference vectors say $q_{1,2}$ for gluon 1 and 2, up to 12 digits using double precision. By default, our numerical evaluation is based on the use of $q_{1,2} = (p_2, p_1)$. For the checks in the case of massive b quarks the result with the default choice $q_{1,2} = (p_2, p_1)$ is compared with a random choice of $q_{1,2}$, keeping away from vectors with excessively too small or too large components, see Appendix A for more details.

iii) As stated earlier, the result based on the use of the massive quark helicity amplitude are checked against those with the independent code using the massless helicity amplitude by setting the mass of the b quark to zero. This is though just a consistency check.

iv) At the level of integration over phase space and density functions we have used two integration routines and made sure that we obtain the same result once we have properly dealt with the spurious Gram determinant as we explained in section 3.4.1.

v) Moreover, our tree level results have been successfully checked against the results of CalcHEP[91].

3.5 Results: $M_H < 2M_W$

3.5.1 Input parameters and kinematical cuts

Our input parameters are $\alpha(0) = 1/137.03599911$, $M_W = 80.3766\text{GeV}$, $M_Z = 91.1876\text{GeV}$, $\alpha_s(M_Z) = 0.118$, $m_b = 4.62\text{GeV}$, $m_t = 174.0\text{GeV}$ with $c_W \equiv M_W/M_Z$. The CKM parameter V_{tb} is set to be 1. We consider the case at the LHC where the center of mass energy of the two initial protons is $\sqrt{s} = 14\text{TeV}$. Neglecting the small light quark initiated contribution, we use CTEQ6L[92, 93, 94, 95] for the gluon distribution function (GDF) in the proton. The factorisation scale for the GDF and energy scale for the strong coupling constant are chosen to be $Q = M_Z$ for simplicity.

As has been done in previous analyses [80, 96], for the exclusive $b\bar{b}H$ final state, we require the outgoing b and \bar{b} to have high transverse momenta $|\mathbf{p}_T^{b,\bar{b}}| \geq 20\text{GeV}$ and pseudo-rapidity $|\eta^{b,\bar{b}}| < 2.5$. These kinematical cuts reduce the total rate of the signal but also greatly reduce the QCD background. As pointed in [79] these cuts also stabilise the scale dependence of the QCD NLO corrections compared to the case where no cut is applied. In the following, these kinematical cuts are always applied unless otherwise stated.

Talking of the NLO QCD scale uncertainty and before presenting our results, let us remind the reader of the size of the QCD corrections. Taking a renormalisation/factorisation scale as we take here at M_Z , the QCD corrections in a scheme where the bottom Yukawa coupling is taken on-shell amount to $\sim -22\%$ for a Higgs mass of 120GeV .

3.5.2 NLO EW correction with $\lambda_{bbH} \neq 0$

The cross sections with two high- p_T bottom quarks at LO and NLO at the LHC are displayed in Fig. 3.5 as a function of the Higgs mass. The NLO EW correction reduces the cross section by about 4% to 5% as the Higgs mass is varied from 110GeV

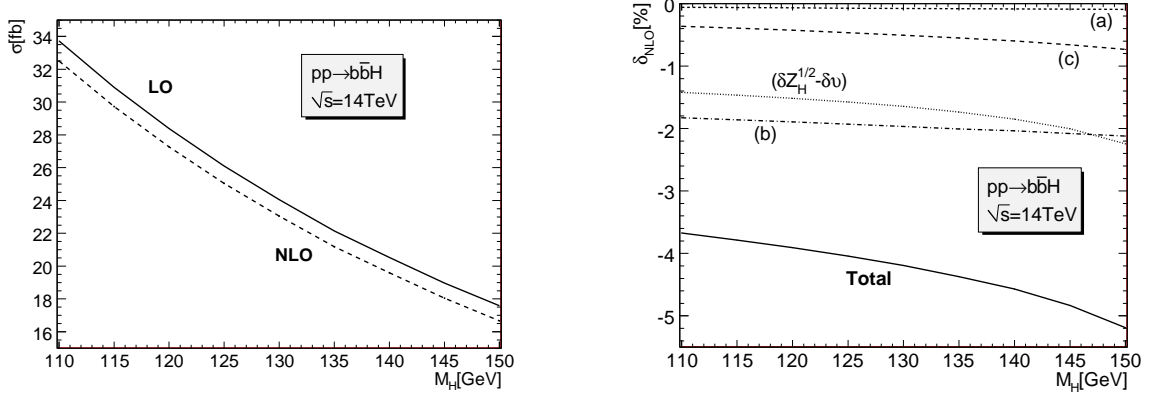


Figure 3.5: *Left: the LO and NLO cross sections as functions of M_H . Right: the relative NLO EW correction normalized to tree level σ_{LO} . (a), (b), (c) correspond to the three classes of diagrams as displayed in Fig. 3.4 to which counterterms are added (see section 3.3). $(\delta Z_H^{1/2} - \delta v)$ is the correction due to the universal correction contained in the renormalisation of the $b\bar{b}H$ vertex. “Total” refers to the total electroweak correction, of Yukawa type, at one-loop.*

to 150 GeV. The first conclusion to draw is that this correction is small if we compare it to the QCD correction or even to the QCD scale uncertainty. Considering that we have pointed to the fact that the contributions could be grouped into three gauge invariant classes that reflect the strengths of the Higgs coupling to the b , the t or its self-coupling, one can ask whether this is the result of some cancellation. It turns out not to be the case. All contributions are below 3%, see Fig. 3.5. Class (a) with a Higgs radiated from the bottom line is totally negligible ranging from -0.09% to -0.06% . We have failed in finding a good reason for the smallness of this contribution compared to the others. Those due to the Higgs self-coupling are below 1%. Radiation from the top contributes about -2% and is of the same order as the contribution of the universal correction. We had argued that the Yukawa corrections brought about by the top might be large. It seems that the mass of the top introduces also a large scale which can not be neglected compared to the effective energy of the hard process even for LHC energies.

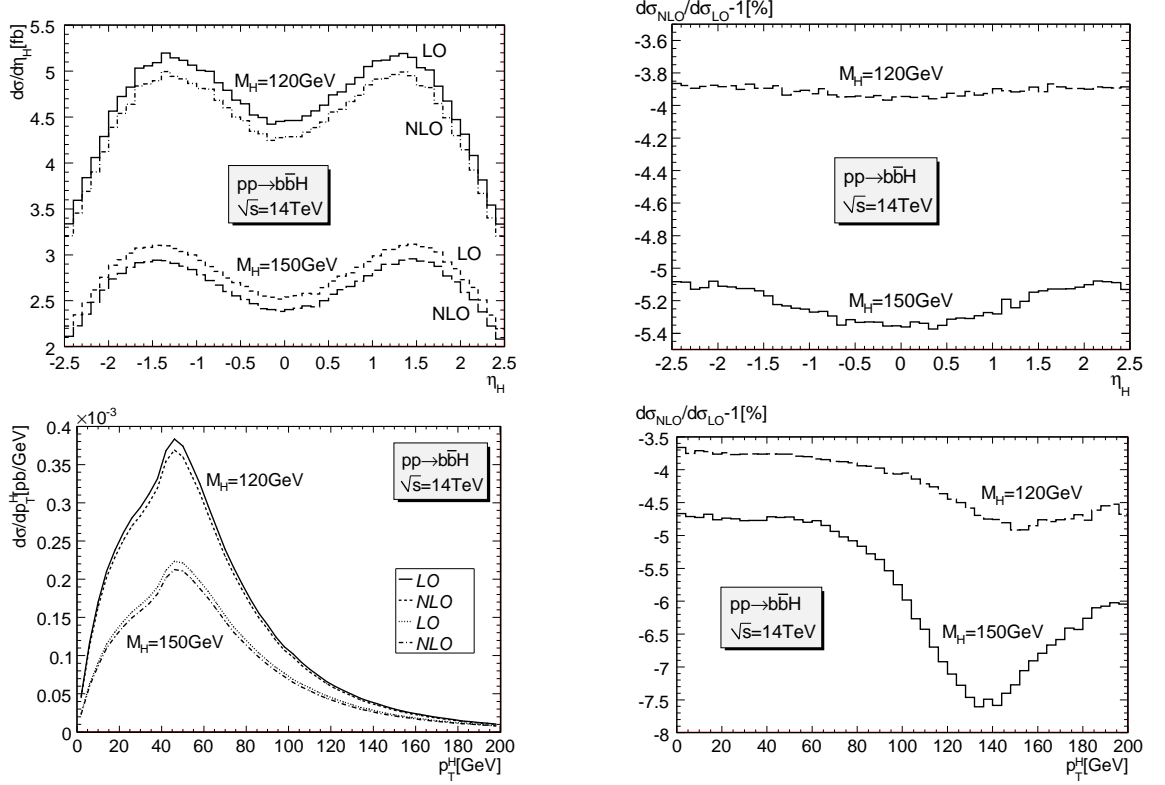


Figure 3.6: *Effect of the NLO electroweak corrections on the pseudo-rapidity and transverse momentum distributions of the Higgs for $M_H = 120, 150$ GeV. The relative corrections $d\sigma_{\text{NLO}}/d\sigma_{\text{LO}} - 1$ is also shown.*

The NLO corrections are spread rather uniformly on all the distributions we have looked at. We have chosen to show in Fig. 3.6 the effect on pseudo-rapidity and transverse momentum distributions of the Higgs for two cases $M_H = 120$ GeV and $M_H = 150$ GeV. As Fig. 3.6 shows the relative change in these two distributions is sensibly constant especially for $M_H = 120$ GeV. For $M_H = 150$ GeV, the corrections are largest for p_T^H around 140 GeV, however this is where the cross section is very small. A similar pattern, *i.e.* a constant change in the distributions, is observed for the bottom variables.

3.5.3 EW correction in the limit of vanishing λ_{bbH}

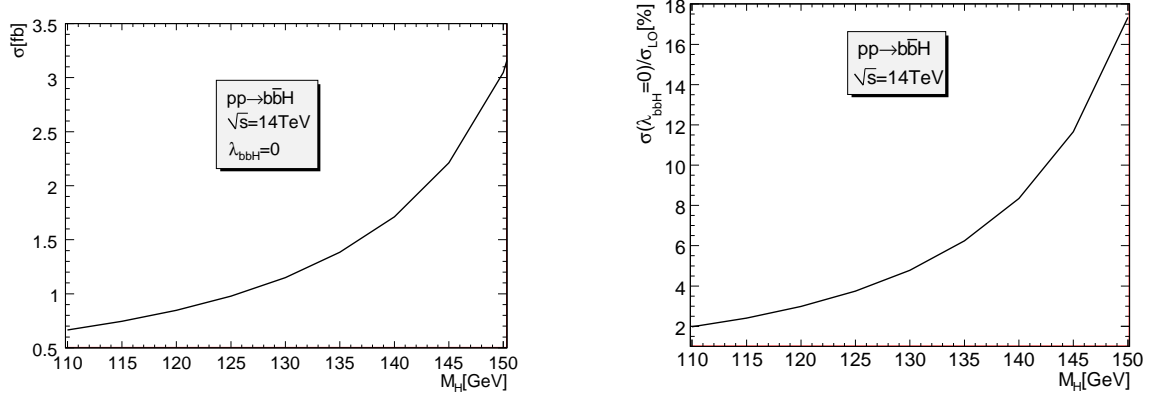


Figure 3.7: The one-loop induced cross section as a function of M_H in the limit of vanishing bottom-Higgs Yukawa coupling. The right panel shows the percentage contribution of this contribution relative to the tree level cross section calculated with $\lambda_{bbH} \neq 0$.

The cross section for $\lambda_{bbH} = 0$ can be induced at one-loop through the top loop. This “NNLO” contribution rises rather quickly as the Higgs mass increases even in the narrow range $M_H = 110 - 150\text{GeV}$ as can be seen in Fig. 5.11. Indeed relative to the tree level, the cross section with $M_H = 120\text{GeV}$ amounts to 3% while for $M_H = 150\text{GeV}$ it has increased to as much as 17%. Going past $M_H \geq 2M_W$ we encounter a Landau singularity[30] (a pinch singularity in the loop integral) from diagrams like the one depicted in Fig. 3.2 (right) with the Higgs being attached to the W ’s or their Goldstone counterpart. It corresponds to a situation where all particles in the loop are resonating and can be interpreted as the production and decay of the tops into (longitudinal) W ’s with the later fusing to produce the Higgs. This leading Landau singularity is not integrable, at the level of the loop amplitude squared and must be regulated by the introduction of a width for the unstable particles. This issue together with a general discussion of Landau singularities will be considered in the next chapters. Fig. 3.8 shows the pseudo-rapidity and transverse momentum

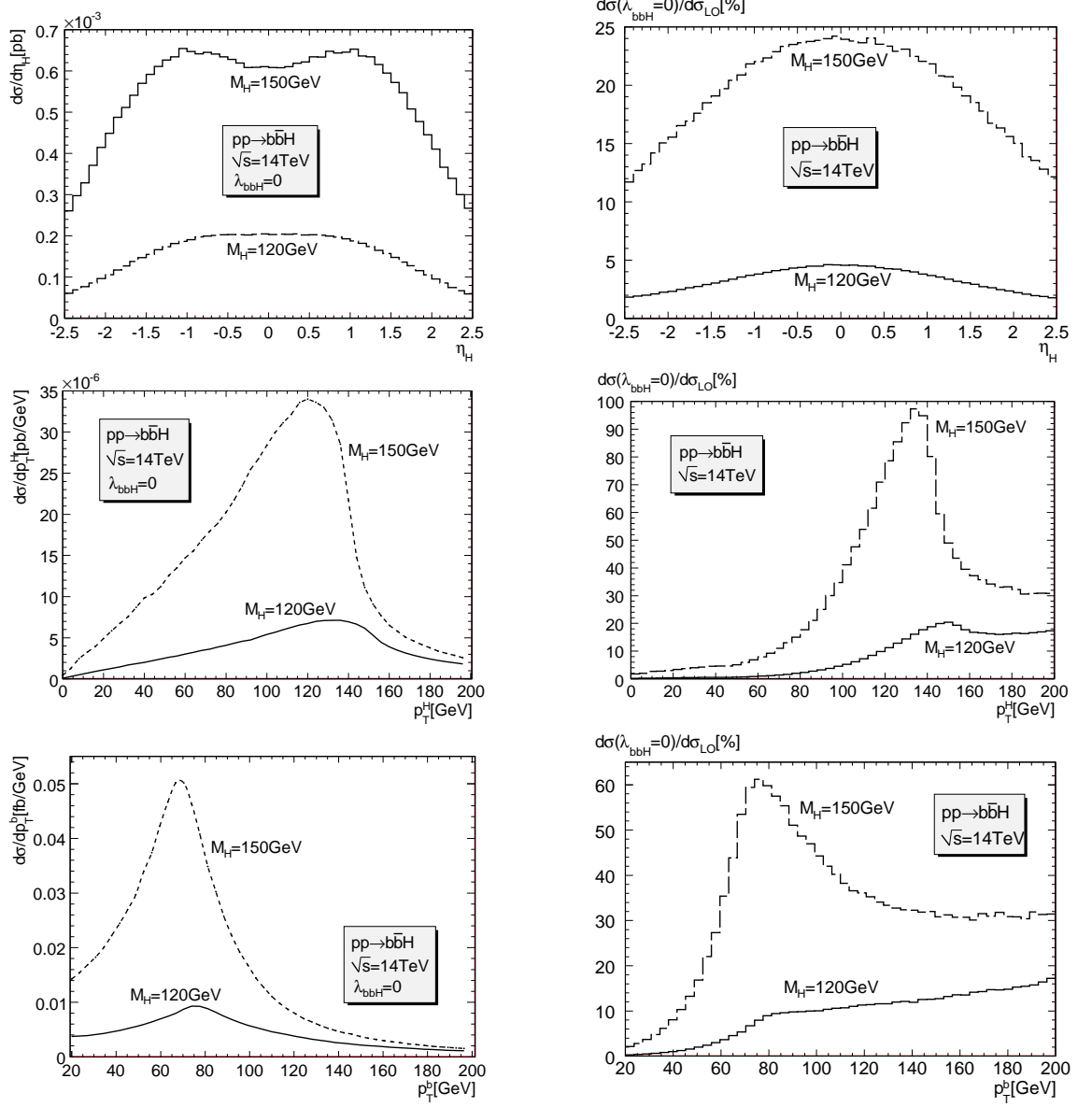


Figure 3.8: The pseudo-rapidity of the Higgs and transverse momentum distributions of the Higgs and the bottom for $M_H = 120, 150 \text{ GeV}$ arising from the purely one-loop contribution in the limit of vanishing LO ($\lambda_{bbH} = 0$). Its relative percentage contribution $d\sigma(\lambda_{bbH} = 0)/d\sigma_{LO}$ is also shown

distributions of the Higgs as well as the the p_T of the bottom for two cases $M_H = 120\text{GeV}$ and $M_H = 150\text{GeV}$ in the limit of vanishing bottom-Higgs Yukawa coupling. These distributions are significantly different from the ones we observed at tree-level (and with the electroweak NLO corrections), see Fig. 3.6. The Higgs prefers being produced at high value of transverse momentum, about 130GeV . In the case of a Higgs with $M_H = 150\text{GeV}$ this contribution can significantly distort the shape of the p_T^H distribution for high p_T^H with a "correction" of more than 70% over a rather large range. The distribution in the p_T of the bottom is also very telling. The new contributions do not produce the bottom preferentially with low p_T^b as the case of the LO contribution.

3.6 Summary

We have calculated the EW radiative corrections triggered by the Yukawa coupling of the top to the process $pp \rightarrow b\bar{b}H$ at the LHC through gluon fusion in the Standard Model. This process is triggered through Higgs radiation of the bottom quark with a small coupling proportional to the mass of the bottom. Yet in order to analyse this coupling, precision calculations that include both the QCD and electroweak corrections are needed. In this perspective, to identify the process one needs to tag both b -jets. Our calculation is therefore conducted in this kinematical configuration.

Inserting a top quark loop with a Yukawa transition of the type $t \rightarrow b\chi_W$, χ_W is the charged Goldstone, allows now the Higgs to be radiated from the top or from the Goldstone boson. The latter coupling represents the Higgs self-coupling and increases with the Higgs mass. The former, the top Yukawa coupling, is also large. As a consequence, the one-loop amplitude $gg \rightarrow b\bar{b}H$ no longer vanishes as the Higgs coupling to b 's does, like what occurs at leading order.

We find that in the limit of vanishing λ_{bbH} , the one-loop induced electroweak process should be taken into account for Higgs masses larger than 140GeV or so. Indeed,

though this contribution is quite modest for a Higgs mass of 110GeV it increases quite rapidly as the Higgs mass increases, reaching about 17% of the leading order value, calculated with $m_b = 4.62\text{GeV}$, for $M_H = 150\text{GeV}$. For these new corrections to interfere with the leading order requires helicity flip. Therefore at next-to-leading order in the Yukawa electroweak corrections, all corrections involve either a bottom mass insertion or a bottom Yukawa coupling. At the end the total Yukawa electroweak NLO contribution brings in a correction which is within the range -4% to -5% for Higgs masses in the range $110\text{GeV} < M_H < 150\text{GeV}$. They are therefore negligible compared to the NLO QCD correction and even the remaining QCD scale uncertainty. This modest effect translates also as an uniform rescaling of the distributions in the most interesting kinematical variables we have looked at (pseudo-rapidities and p_T of both b -quarks and the Higgs). This is not the case of the one-loop induced contributions which survive in the limit of $m_b \rightarrow 0$ (and $\lambda_{bbH} \rightarrow 0$). Here the distributions for the Higgs masses where the corrections for the total cross section is large are drastically different from the LO distributions. A summary for the corrections including the NLO with $\lambda_{bbH} \neq 0$ and the part of the NNLO counted as loop induced in the limit $\lambda_{bbH} \rightarrow 0$ is shown in Fig. 3.9.

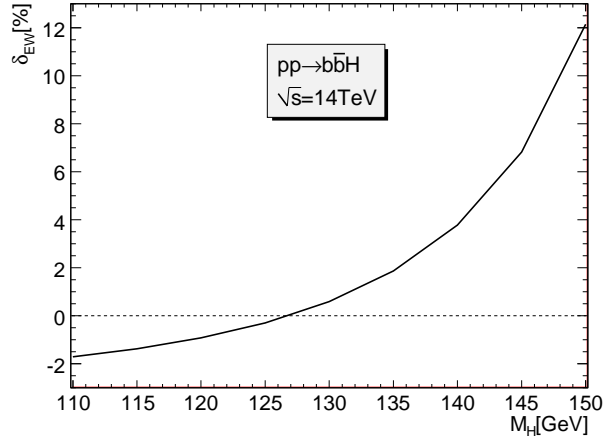


Figure 3.9: $\delta_{EW} = \delta_{NLO} + \frac{\sigma(\lambda_{bbH}=0)}{\sigma_0}$ as a function of M_H .

The analysis we have performed in this chapter does not cover Higgs masses over 150 GeV and rests within the range of Higgs masses preferred by indirect precision measurements. In fact as the threshold for $H \rightarrow WW$ opens up, important phenomena take place. Foremost Landau singularities, or pinch singularities in some loop integrals, develop. This important issue will be addressed in the next two chapters.

There is another contribution which does not vanish for vanishing λ_{bbH} and which contributes to $gg \rightarrow b\bar{b}H$ through a closed top quark loop. This contribution represents $gg \rightarrow Hg^* \rightarrow Hb\bar{b}$. We have not included this contribution in the present work as we do not consider it to be a *genuine* $b\bar{b}H$ final state. This correction can be counted as belonging to the *inclusive* $gg \rightarrow H$ process. The same line of reasoning has been argued in [82]. Nonetheless from the experimental point of view it would be interesting to include all these effects together with the NLO QCD corrections and the electroweak corrections that we have studied here.

Chapter 4

Landau singularities

Let us start this chapter by quoting a paragraph in p.30 of the important book *The Analytic S-matrix* written by Eden, Landshoff, Olive and Polkinghorne (1966) [29]:

For an individual Feynman integral, the singularities, and hence the analytic structure of the integral, arise from singularities in the integrand. Those that arise from ultraviolet divergences are removed by renormalisation and will not concern us. The singularities that do concern us come from zeros of the denominator factors. These denominator factors are the same for scalar particles as they are for particles with spin, namely of the general form

$$p^2 - m_r^2 + i\epsilon \tag{4.1}$$

for mass m_r and four-momentum p .

The issue of loop-integral singularities is also discussed in other text books [97, 98, 99], see also the recent lecture notes of Denner for a practical review [100].

In this chapter we will restrict ourselves to *one-loop* Feynman integrals. To set the mathematical background, we first consider the case of some general complex integrals.

4.1 Singularities of complex integrals

We would like to consider two simple examples taken from [29].

(i) With w complex

$$f(w) = \int_a^b \frac{dz}{z - w} = \ln(b - w) - \ln(a - w). \quad (4.2)$$

(ii) With w, a complex and real x

$$\begin{aligned} f(w) &= \int_0^1 \frac{dx}{(x - w)(x - a)} \\ &= \frac{[\ln(1 - w) - \ln(1 - a)] - [\ln(-w) - \ln(-a)]}{w - a}. \end{aligned} \quad (4.3)$$

In the first example we see that the integrand $1/(z - w)$ is singular at the end-points a, b if $w = a, b$, corresponding to the singularity of the logarithm at these points. We see clearly that $f(w)$ is always singular if $w = a, b$ whatever the integration contour is. $w = a, b$ are called end-point singularities. We notice also that if w lies somewhere on the integration contour but not at the end points then we can always use Cauchy's integral theorem to deform the contour to avoid the pole.

The second example is more interesting. Again we see that $w = 0, 1$ are end-point singularities. One notices also that there may be a problem when $w = a$. In order to see the point, we consider the case where $a = a - i\epsilon$ with ϵ is infinitesimal positive and $w = w - i\rho$ with ρ is also infinitesimal but can be positive or negative. a and w now should be considered as real numbers. We distinguish the three following cases:

1. For $0 < a < 1$ and $w \rightarrow a$ we have $\ln(-a + i\epsilon) = \ln(a) + i\pi$, $\ln(-w + i\rho) = \ln(w) + i\pi \operatorname{sign}(\rho)$ and

$$f(w \rightarrow a) = -\frac{1}{1 - a} - \frac{1}{a} - i\pi[\operatorname{sign}(\rho) - 1] \lim_{w \rightarrow a} \frac{1}{w - a}. \quad (4.4)$$

2. For $a < 0$ then all logarithmic arguments in Eq. (4.3) are strictly positive. We then can forget about ϵ and ρ to get

$$f(w \rightarrow a) = -\frac{1}{1-a} - \frac{1}{a}. \quad (4.5)$$

3. For $a > 1$ then all logarithmic arguments in Eq. (4.3) are negative. We have

$$\begin{aligned} f(w \rightarrow a) &= -\frac{1}{1-a} - \frac{1}{a} + \{i\pi[\text{sign}(\rho) - 1] - i\pi[\text{sign}(\rho) - 1]\} \lim_{w \rightarrow a} \frac{1}{w-a} \\ &= -\frac{1}{1-a} - \frac{1}{a}. \end{aligned} \quad (4.6)$$

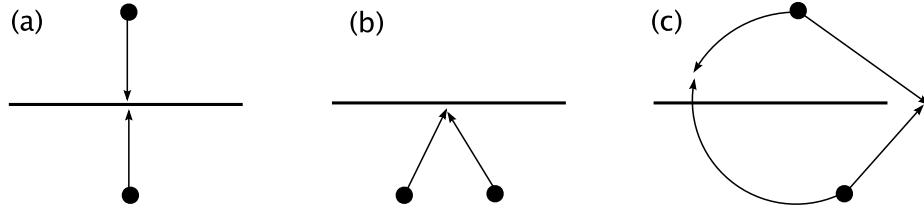


Figure 4.1: (a) Two singularities in the complex plane coming together and pinching the contour of integration, $[0, 1]$ along the real axis. (b) and (c) Examples of coincidence of two singularities that do not pinch the integration contour.

We remark immediately that $w = a$ is a singular point if and only if two conditions are satisfied:

$$0 < a < 1 \quad \text{and} \quad \text{sign}(\rho) = -1, \quad (4.7)$$

which simply mean that the real integration contour $[0, 1]$ is trapped when $w \rightarrow a$ (see Fig. 4.1a). This is a pinch singularity. We learn also from the first case that if $\text{sign}(\rho) = 1$, *i.e.* both w and a approach the real axis from the same side, then the contour is not trapped and there is no singularity (see Fig. 4.1b). In the second and third cases there is no singularity because w and a come together nowhere near the contour (see Fig. 4.1c). In this simple example, it is easy to find out the situation where the integration contour is trapped. However, in a general case with more

than one integration variables finding whether the contour is actually trapped is very difficult. The “ ϵ -prescription” and multivalued function play crucial roles in the second example. These two elements will appear again when one considers loop integrals ¹.

Those two examples will guide us all the way. For now they lead us to two important statements for simple complex integrals. For this we first define the context [29]. Let $g(w, z)$ be an analytic function of two complex variables and let C be some finite contour in the complex z -plane. Define a function $f(w)$ by

$$f(w) = \int_C g(w, z) dz. \quad (4.8)$$

It is supposed that the singularities of the integrand g are known and that their locations in the z -plane are

$$z = z_r(w), \quad r = 1, 2, \dots \quad (4.9)$$

$f(w)$ is analytic as long as C does not intersect with any $z_r(w)$ or can be deformed accordingly. From the above examples, we see that $f(w)$ can be singular at w_1 for one of two reasons:

- (i) End-point singularities: One of the singularities z_r reaches one of the end-points of the contour C when $w \rightarrow w_1$. No deformation of C can avoid them and w_1 is a singularity of $f(w)$.
- (ii) pinch singularities: If two (or more) singularities approach the contour from opposite sides and coincide, the contour C will be trapped between them and no deformation can avoid them. w_1 is a singularity of $f(w)$.

¹In fact, we will see later in this thesis that one way to deal with pinch singularities of loop integrals, named as Landau singularities, is to kill the ϵ -prescription by introducing the widths of internal unstable particles. The width moves the singularities away from the real axis, so they do not occur in the physical region (the real axis).

In order to deal with loop integrals, we have to generalise the above consideration to the case of multiple integrals. Consider

$$f(w) = \int_H \prod dz_i g(w, z_i), \quad (4.10)$$

where H is a hypercontour in the multi-dimensional complex z_i -space. The singularities of the integrand $g(w, z_i)$ are given by various equations

$$S_r(w, z_i) = 0, \quad r = 1, 2, \dots \quad (4.11)$$

The boundary of H is specified by

$$\tilde{S}_s(w, z_i) = 0, \quad s = 1, 2, \dots \quad (4.12)$$

Singularities occur when a surface of singularity meets a boundary surface or when the hypercontour H is pinched between two or more surfaces of singularities. More precisely, it may be shown that a necessary condition of singularity is that there exists a set of complex parameters $\alpha_r, \tilde{\alpha}_s$ not all equal to zero such that [29, 97]

$$\alpha_r S_r = 0, \quad \text{for each } r,$$

(so that either α_r or $S_r = 0$),

$$\tilde{\alpha}_s \tilde{S}_s = 0, \quad \text{for each } s,$$

and, for each integration variable z_i ,

$$\frac{\partial}{\partial z_i} \left[\sum_r \alpha_r S_r + \sum_s \tilde{\alpha}_s \tilde{S}_s \right] = 0. \quad (4.13)$$

The last condition expresses that the hypersurfaces are tangent. This is only a necessary condition and does not guarantee that the hypercontour H is pinched. This is easy to understand if we look back at the example two. If the hypersurfaces come to be tangent from one side of the hypercontour or they are tangent at nowhere on the hypercontour then they are harmless.

To find necessary and sufficient conditions for a pinch singularity of multiple integrals is very difficult and requires homology theory. This is obviously beyond the scope of this thesis and we refer to [101, 102] for more study.

4.2 Landau equations for one-loop integrals

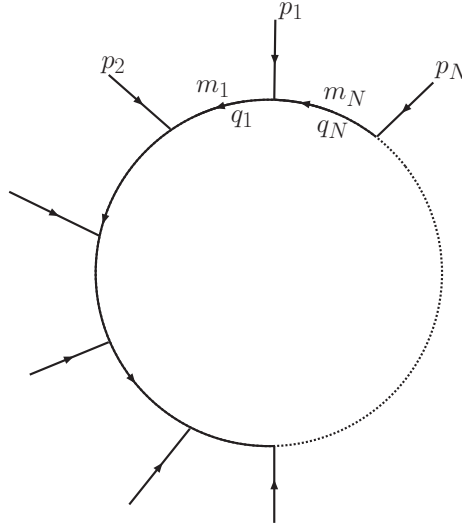


Figure 4.2: *One-loop Feynman diagram with N external particles.*

We would like to clarify the important terminology used in this and the next chapters. The terminology "phase space" means the kinematical allowed region obtained by using the energy-momentum conservation on external momenta. The terminology "physical region" means the physical integration contour of the one-loop integral defined in Eq. (4.20). It means $\{x_i = x_i^*, x_i \geq 0, q_i = q_i^*\}$ where x_i are Feynman parameters and q_i are loop momenta. The real condition on x_i and q_i accords with the $i\epsilon$ prescription.

We are now in the position to apply the previous analysis for one-loop Feynman integrals. Consider the one-loop process $F_1(p_1) + F_2(p_2) + \dots F_N(p_N) \rightarrow 0$, where F_i stands for either a scalar, fermion or vector field with momentum p_i as in the figure opposite. The internal momentum for each propagator is q_i with $i = 1, \dots, N$. The scalar one-loop integral reads

- In momentum space

$$T_0^N \equiv \int \frac{d^D q}{(2\pi)^{D_i}} \frac{1}{\prod_{i=1}^N D_i},$$

$$D_i = q_i^2 - m_i^2 + i\epsilon, \quad q_i = q + r_i, \quad r_i = \sum_{j=1}^i p_j, \quad (4.14)$$

where m_i are the masses of internal particles, all the external particle are outgoing, $p_i = q_{i+1} - q_i$ are the external momenta.

- Introducing Feynman parameters and integrating over q one gets

$$T_0^N = \frac{(-1)^N \Gamma(N - D/2)}{(4\pi)^{D/2}} \int_0^\infty dx_1 \cdots dx_N \frac{\delta(\sum_{i=1}^N x_i - 1)}{\Delta^{N-D/2}} \quad (4.15)$$

with

$$\Delta = \frac{1}{2} \sum_{i,j=1}^N x_i x_j Q_{ij} - i\epsilon, \quad Q_{ij} = m_i^2 + m_j^2 - (r_i - r_j)^2. \quad (4.16)$$

In representation (4.14) the *physical* hypercontour is $[-\infty, \infty]^D$ along the *real* axes, by definition. Each factor in the denominator is protected from zero by $i\epsilon$ with $\epsilon > 0$. Thus the integral can be singular only when $\epsilon \rightarrow 0$. However, even in the case when $\epsilon \rightarrow 0$ and the singularities of the integrand reach the real hypercontour one can deform the real hypercontour to be complex to avoid the singularities. Indeed, the generalised definition of Feynman integral is Eq. (4.14) and its analytical continuation². As already pointed out in the second example of the previous subsection, a singularity arises when the real hypercontour is pinched and therefore cannot be deformed. The pinch singularity of a Feynman integral is called Landau singularity. Necessary condition for this singularity is that equations (4.13) have solution with *real* q . The boundaries are at infinity so we can set all $\tilde{\alpha}_s = 0$. With $S_i = q_i^2 - m_i^2$

²Based on this definition, a method called contour deformation technique to calculate Feynman integrals numerically has been realised in practice [103, 104]. This method works as long as the contour can be deformed to avoid singularities, *i.e.* when the singularities approach the contour from the same side like in Fig. 4.1b.

equations (4.13) become

$$\begin{cases} \forall i \quad \alpha_i(q_i^2 - m_i^2) = 0, \\ \sum_{i=1}^N \alpha_i q_i = 0. \end{cases} \quad (4.17)$$

These are the Landau equations corresponding to representation (4.14). If equations (4.17) have a solution with some complex $\alpha_i \neq 0$ and *real* q_i then one can say that integral (4.14) may have a Landau singularity.

The drawback of this representation is that there are not any constraints on the range of α_i . By introducing Feynman parameters and requiring them to be real (this is the purpose of $i\epsilon$ prescription), one imposes more constraint on the physical region. It will be clear later on that for Landau singularities to be in that physical region, α_i must be real and positive.

For representation (4.15), the *physical* hypercontour is $[0, \infty]^N$ along the *real* axes by definition ³. Thus the boundaries are $\tilde{S}_i = x_i = 0$ for all i . The hypersurface of singularities of the integrand is $S = \Delta = 0$. One might think that the hypercontour cannot be pinched now because there is only one hypersurface of singularities and the singularities are just end-point singularities if they occur. Indeed, a hypersurface can be very complicated and contains several sub-hypersurfaces which can trap the hypercontour. This is very difficult to imagine but the condition for that to happen is very simple, just like the extreme condition [29]:

$$S = 0 = \frac{\partial S}{\partial x_i}. \quad (4.18)$$

Other way to get the condition is to use equations (4.13). We can set $\alpha = 1$ since there is only one singular hypersurface. One gets

$$\begin{cases} \Delta = 0, \\ \forall i \quad x_i \frac{\partial \Delta}{\partial x_i} = 0. \end{cases} \quad (4.19)$$

The first condition comes from the second equation of (4.13). The second condition comes from the first and third equations of (4.13). If one picks up the solution $x_i = 0$

³One might think that the hypercontour should be $[0, 1]^N$. However, it can be expanded to infinity because of the Dirac delta function in the integrand.

from the second condition of (4.19) then that is for end-point singularities. Otherwise, one has the condition for pinch singularities, which is the same as Eq. (4.18). So everything is consistent. Since Δ is a homogeneous function of x_i , the first equation in (4.19) is automatically satisfied when the second is. Necessary condition for integral (4.15) to have Landau singularities is that equations (4.19) have solution with some $x_i > 0$, x_i are *real*. The drawback of this representation is that equations (4.19) do not tell us anything about q_i .

There exists a representation which contains all the advantages of Eqs. (4.17) and (4.19). That is the mixed representation of Feynman integrals in the space of real momentum and real Feynman parameters ⁴:

$$T_0^N = \Gamma(N) \int_0^\infty dx_1 \cdots dx_N \delta\left(\sum_{i=1}^N x_i - 1\right) \int \frac{d^D q}{(2\pi)^{D_i}} \frac{1}{[\sum_{i=1}^N x_i (q_i^2 - m_i^2 + i\epsilon)]^N}. \quad (4.20)$$

The *physical* hypercontours are *real* $[-\infty, \infty]^D$ for q and *real* $[0, \infty]^N$ for x_i . The boundaries are $\tilde{S}_i = x_i = 0$ for all i . The hypersurface of singularities of the integrand is $S = \sum_{i=1}^N x_i (q_i^2 - m_i^2) = 0$. From Eq. (4.13) one gets

$$\begin{cases} \forall i \ x_i (q_i^2 - m_i^2) = 0, \\ \sum_{i=1}^N x_i q_i = 0, \end{cases} \quad (4.21)$$

together with

$$\begin{cases} x_i \geq 0, \\ q_i = q_i^*. \end{cases} \quad (4.22)$$

The first condition of (4.21) comes from the second equation and third equation (with $z_i = x_i$) of (4.13). The second condition of (4.21) comes from the third equation of (4.13) with $z_i = q$. One notices immediately that Eq. (4.21) can be obtained from Eq. (4.17) by replacing complex α_i with real x_i . Conditions (4.22) come from the definition of the physical hypercontours. The Landau singularities *may* occur in the physical region if equations (4.21) and (4.22) are satisfied. These are necessary

⁴Landau has used this representation to devise the condition for singularities [30].

conditions since we cannot be sure that the real hypercontours are pinched when $\epsilon \rightarrow 0$ (remember the second example of the previous subsection).

If all x_i are strictly positive then we have a leading Landau singularity (LLS). Otherwise one has conditions for sub-leading Landau singularities (sub-LLS).

4.3 Necessary and sufficient conditions for Landau singularities

It may be shown that if Landau matrix Q_{ij} (defined in Eq. (4.16), see also Eq. (4.25)) has *only one* zero eigenvalue then the necessary and sufficient conditions for the appearance of a singularity in the physical region are equations (4.21) and (4.22).

This important conclusion has been pointed out in the paper of Coleman and Norton [31]⁵. The proof is very simple and will be given in the next subsection (after equation (4.43)). It is based on the underlying fact that the Landau matrix Q_{ij} is real and symmetric hence can be diagonalized by a real orthogonal co-ordinate transformation. It means that for unstable particles with complex masses the argument fails and the conditions based on Landau equations are no longer sufficient.

We seek conditions for Eq. (4.21) to have a solution $x_i = 0$ for $i = M + 1, \dots, N$ with $1 \leq M \leq N$ and $x_i > 0$ for every $i \in \{1, \dots, M\}$. The Eq. (4.21) becomes

$$\begin{cases} x_i = 0 & \text{for } i = M + 1, \dots, N, \\ q_i^2 = m_i^2 & \text{for } i = 1, \dots, M, \\ \sum_{i=1}^M x_i q_i = 0. \end{cases} \quad (4.23)$$

For $M = N$ one has a leading singularity, otherwise if $M < N$ this is a sub-leading singularity. Multiplying the third equation in (4.23) by q_j leads to a system of M

⁵See also Itzykson and Zuber [97] in p.306.

equations

$$\begin{cases} Q_{11}x_1 + Q_{12}x_2 + \cdots Q_{1M}x_M &= 0, \\ Q_{21}x_1 + Q_{22}x_2 + \cdots Q_{2M}x_M &= 0, \\ \vdots & \\ Q_{M1}x_1 + Q_{M2}x_2 + \cdots Q_{MM}x_M &= 0, \end{cases} \quad (4.24)$$

where the Q matrix is defined as

$$Q_{ij} = 2q_i \cdot q_j = m_i^2 + m_j^2 - (q_i - q_j)^2 = m_i^2 + m_j^2 - (r_i - r_j)^2, \quad i, j = 1, \dots, M, \quad (4.25)$$

which agrees with Eq. (4.16). The necessary and sufficient conditions for the appearance of a singularity in the physical region now become

$$\begin{cases} \det(Q) = 0 \\ x_i > 0 \\ q_i^2 = m_i^2 \\ q_i = q_i^* \end{cases} \quad (4.26)$$

for $i = 1, \dots, M$.

The condition $\det(Q) = 0$ defines a singular surface or a Landau curve.

If some internal (external) particles are massless like in the case of six photon scattering, then some Q_{ij} are zero, the above conditions can be easily checked. However, if the internal particles are massive then it is difficult to check the second condition explicitly, especially if M is large. In this case, we can rewrite the second condition as following

$$x_j = \det(\hat{Q}_{jM}) / \det(\hat{Q}_{MM}) > 0, \quad j = 1, \dots, M-1, \quad (4.27)$$

where \hat{Q}_{ij} is obtained from Q by discarding row i and column j from Q and $\det(\hat{Q}_{jM}) = d[\det(Q)]/(2dQ_{jM})$, $\det(\hat{Q}_{MM}) = d[\det(Q)]/dQ_{MM}$. The proof for Eq. (4.27) is the following. It is obvious that when the condition $\det(Q) = 0$ is satisfied one can set $x_M = 1$ and discard the last equation in (4.24). After moving the M -column from the

left hand side to the right hand side, one obtains a system of $M - 1$ equations with $M - 1$ variables. The solution of this is clearly equation (4.27). If $\det(\hat{Q}_{MM}) = 0$ then condition (4.27) becomes $\det(\hat{Q}_{jM}) = 0$ with $j = 1, \dots, M - 1$.

Conditions (4.21) and (4.22) admit a beautiful physical interpretation. This was discovered by Coleman and Norton [31]. Consider the case where all x_i are strictly positive. All the internal loop particles are therefore on-shell and have real momenta. An internal particle ⁶ has a real four-momentum: $q_i = m_i u_i$ (for each i) with u_i is a four-velocity. Each vertex can be regarded as a real space-time point. The space-time separation between two vertices reads

$$dX_i = d\tau_i u_i = \frac{d\tau_i}{m_i} q_i, \quad \text{for each } i, \quad (4.28)$$

where $d\tau_i$ is the proper time. Following a closed loop, one has $\sum_i dX_i = 0$. Comparing this to the second equation of (4.21) we get the correspondence: $d\tau_i = m_i x_i > 0$ for each i . It means that the loop particle is moving forward in time. dX_i can be positive or negative depending on the sign of q_i . If one chooses a reference frame where vertices are ordered in time, *i.e.* $dX_i^0 > 0$, then $q_i^0 > 0$ in that frame. This information can be very useful in practice. Let us illustrate this point. Consider two important Feynman diagrams in Fig. 4.3. We choose a reference frame where the arrows of the

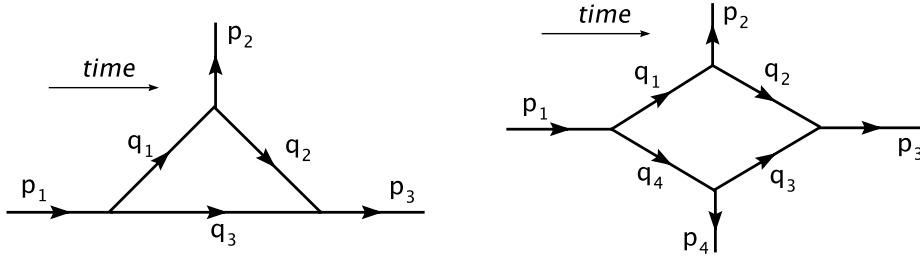


Figure 4.3: Typical triangle and box Feynman diagrams.

internal lines follow the time direction. We look at vertex 2 (connected to p_2) of the

⁶One can regard different particles running in a loop as different states of one particle. Each vertex is associated with an external "force".

triangle diagram and choose a co-ordinate system such that $q_1 = (m_1, 0, 0, 0)$, $q_2 = (e_2, q_{2x}, 0, 0)$. With $p_i^2 = M_i^2$, from the energy-momentum conservation $p_2 = q_1 - q_2$ we get

$$\begin{aligned} e_2 &= \frac{m_1^2 + m_2^2 - M_2^2}{2m_1}, \\ q_{2x}^2 &= \frac{\lambda(M_2^2, m_1^2, m_2^2)}{4m_1^2} = \frac{[M_2^2 - (m_1 - m_2)^2][M_2^2 - (m_1 + m_2)^2]}{2m_1}. \end{aligned} \quad (4.29)$$

From the conditions $q_2 = q_2^*$ and $e_2 > 0$ we get

$$M_2^2 \leq (m_1 - m_2)^2. \quad (4.30)$$

Similarly, for other vertices of the triangle diagram we have

$$M_1^2 \geq (m_1 + m_4)^2, \quad M_3^2 \geq (m_2 + m_3)^2. \quad (4.31)$$

By using the same trick one can easily see that necessary conditions to have a leading Landau singularity in the box diagram are

$$\begin{cases} M_1^2 \geq (m_1 + m_4)^2, & M_3^2 \geq (m_2 + m_3)^2 \\ M_2^2 \leq (m_1 - m_2)^2, & M_4^2 \leq (m_3 - m_4)^2. \end{cases} \quad (4.32)$$

Similarly, with $t = (p_2 + p_3)^2$ and $u = (p_3 + p_4)^2$ and using the energy-momentum conservation, we get the constraint

$$t \geq (m_1 + m_3)^2 \quad \text{and} \quad u \geq (m_2 + m_4)^2. \quad (4.33)$$

Thus a necessary condition for any diagram to have a leading Landau singularity is that it has at least two cuts which can produce physical on-shell particles ⁷. Other external particle which does not correspond to those cuts must have mass smaller than the difference of the two internal masses associated with it.

⁷In the case of two-point function, the two cuts coincide due to energy-momentum conservation.

4.4 Nature of Landau singularities

4.4.1 Nature of leading Landau singularities

Our purpose is to extract the LLS by using Feynman parameter representation (4.15). The matrix Q which appears in the denominator is real and symmetric hence can be diagonalized by a real orthogonal co-ordinate transformation. In general, Q has N real eigenvalues called $\lambda_1, \dots, \lambda_N$. The characteristic equation of Q is given by

$$\begin{aligned} f(\lambda) &= \lambda^N + (-1)a_{N-1}\lambda^{N-1} + (-1)^2a_{N-2}\lambda^{N-2} - \dots (-1)^{N-1}a_1\lambda + (-1)^Na_0 \\ &= (\lambda - \lambda_1)(\lambda - \lambda_2)\dots(\lambda - \lambda_n) = 0. \end{aligned} \quad (4.34)$$

For the case $N = 4$ we have

$$\begin{aligned} a_0 &= \lambda_1\lambda_2\lambda_3\lambda_4 = \det(Q_4), \\ a_1 &= \lambda_1\lambda_2\lambda_3 + \lambda_1\lambda_2\lambda_4 + \lambda_1\lambda_3\lambda_4 + \lambda_2\lambda_3\lambda_4, \\ a_2 &= \lambda_1\lambda_2 + \lambda_1\lambda_3 + \lambda_1\lambda_4 + \lambda_2\lambda_3 + \lambda_2\lambda_4 + \lambda_3\lambda_4 = \frac{1}{2}[\text{Tr}(Q_4)^2 - \text{Tr}(Q_4^2)], \\ a_3 &= \lambda_1 + \lambda_2 + \lambda_3 + \lambda_4 = \text{Tr}(Q_4), \end{aligned} \quad (4.35)$$

Consider the case where Q has only one very small eigenvalue $\lambda_N \ll 1$. Then, to leading order

$$\lambda_N = \frac{a_0}{a_1}, \quad a_1 = \lambda_1\lambda_2\dots\lambda_{N-1} \neq 0. \quad (4.36)$$

Let $V = \{x_1^0, x_2^0, \dots, x_N^0\}$ be the eigenvector corresponding to λ_N . V is normalised to

$$\sum_{i=1}^N x_i^0 = 1. \quad (4.37)$$

For later use, we define

$$v^2 = V.V. \quad (4.38)$$

The expansion of Δ around V reads

$$\begin{aligned}\Delta &= \frac{1}{2} \sum_{i,j=1}^N Q_{ij} y_i y_j + \lambda_N \sum_{i=1}^N x_i^0 y_i + \frac{1}{2} \lambda_N v^2 - i\epsilon, \\ &\approx \frac{1}{2} \sum_{i,j=1}^N Q_{ij} y_i y_j + \frac{1}{2} \lambda_N v^2 - i\epsilon,\end{aligned}\tag{4.39}$$

where $y_i = x_i - x_i^0$. For the leading part of the singularity it is sufficient to neglect the linear terms. The Q -matrix can be diagonalised by rotating the y -vector

$$y_i = \sum_{j=1}^N A_{ij} z_j,\tag{4.40}$$

where A is an orthogonal matrix whose columns are the normalised eigenvectors of Q . Thus we have

$$\begin{aligned}\det(A) &= 1, \quad \sum_{j=1}^N A_{Nj} = \frac{\sum_{i=1}^N x_i^0}{\sqrt{V \cdot V}} = \frac{1}{v}, \\ \Delta &= \frac{1}{2} \sum_{i=1}^{N-1} \lambda_i z_i^2 + \frac{1}{2} \lambda_N v^2 - i\epsilon.\end{aligned}\tag{4.41}$$

Note that the term $\lambda_N z_N^2$ in the rhs has been neglected as this term would give a contribution of the order $\mathcal{O}(\lambda_N^2)$ to the final result. Equation (4.15) can now be re-written in the form

$$T_0^N = \frac{(-1)^N \Gamma(N - D/2)}{\pi^{D/2} 2^{3D/2 - N}} \int_{-\infty}^{+\infty} dz_1 \cdots dz_N \frac{\delta(\sum_{i,j=1}^N A_{ij} z_j)}{(\sum_{i=1}^{N-1} \lambda_i z_i^2 + \lambda_N v^2 - i\epsilon)^{N-D/2}}.\tag{4.42}$$

Although the original integration contour is some segment around the singular point $z_i = 0$ with $i = 1, \dots, N$, the singular part will not be changed if we extend the integration contour to infinity, provided the power $(N - D/2)$ of the denominator in Eq. (4.42) is sufficiently large. Integrating over z_N gives

$$T_0^N = \frac{(-1)^N \Gamma(N - D/2) v}{\pi^{D/2} 2^{3D/2 - N}} \int_{-\infty}^{+\infty} dz_1 \cdots dz_{N-1} \frac{1}{(\sum_{i=1}^{N-1} \lambda_i z_i^2 + \lambda_N v^2 - i\epsilon)^{N-D/2}},\tag{4.43}$$

where the factor v comes from the δ -function. One sees clearly that each integration contour is pinched when $\epsilon \rightarrow 0$ if all $\lambda_i \neq 0$ with $i = 1, \dots, N - 1$.

Assuming that $\lambda_i > 0$ for $i = 1, \dots, K$ and $\lambda_j < 0$ for $j = K + 1, \dots, N - 1$ with $0 \leq K \leq N - 1$. We then change the integration variables as follows

$$\begin{cases} t_i = \sqrt{\lambda_i} z_i & \text{for } i = 1, \dots, K, \\ t_j = \sqrt{-\lambda_j} z_j & \text{for } j = K + 1, \dots, N - 1. \end{cases} \quad (4.44)$$

This makes sure that all t_i are real. We get

$$\begin{aligned} T_0^N &= \frac{(-1)^N \Gamma(N - D/2) v}{\pi^{D/2} 2^{3D/2 - N} \sqrt{(-1)^{N-K-1} a_1}} \\ &\times \int_{-\infty}^{+\infty} dt_1 \cdots dt_K \int_{-\infty}^{+\infty} dt_{K+1} \cdots dt_{N-1} \frac{1}{(-\sum_{i=K+1}^{N-1} t_i^2 + b^2)^{N-D/2}}, \end{aligned} \quad (4.45)$$

where

$$b^2 = \sum_{i=1}^K t_i^2 + \lambda_N v^2 - i\epsilon, \quad \text{Re}(b^2) > 0. \quad (4.46)$$

Changing to spherical coordinates by using formulae (D.18) we get

$$\begin{aligned} T_0^N &= \frac{(-1)^N \Gamma(N - D/2) v}{\pi^{D/2} 2^{3D/2 - N} \sqrt{(-1)^{N-K-1} a_1}} \frac{2\pi^{(N-K-1)/2}}{\Gamma((N-K-1)/2)} \\ &\times \int_{-\infty}^{+\infty} dt_1 \cdots dt_K \int_0^\infty dr \frac{r^{N-K-2}}{(b^2 - r^2)^{N-D/2}}. \end{aligned} \quad (4.47)$$

Note that $(b^2 - r^2)^{N-D/2} = e^{-i\pi(N-D/2)}(r^2 - b^2)^{N-D/2}$ due to the fact that $\epsilon > 0$.

Then by using formula (D.19) we have

$$\begin{aligned} T_0^N &= \frac{(-1)^N e^{i\pi(N-K-1)/2} v}{\pi^{D/2} 2^{3D/2 - N} \sqrt{(-1)^{N-K-1} a_1}} \pi^{(N-K-1)/2} \Gamma((N-D+K+1)/2) \\ &\times \int_{-\infty}^{+\infty} dt_1 \cdots dt_K \frac{1}{(\sum_{i=1}^K t_i^2 + \lambda_N v^2 - i\epsilon)^{(N-D+K+1)/2}}. \end{aligned} \quad (4.48)$$

Repeat the above steps to get

$$T_0^N = \frac{(-1)^N e^{i\pi(N-K-1)/2} v}{2^{(3+N)/2} \pi \sqrt{(-1)^{N-K-1} a_1}} \frac{(4\pi)^{(N-D+1)/2} \Gamma((N-D+1)/2)}{\left(\frac{\lambda_N v^2}{2} - i\epsilon\right)^{(N-D+1)/2}}. \quad (4.49)$$

This result holds provided

$$a_1 \neq 0 \quad \text{and} \quad N - D + 1 > 0. \quad (4.50)$$

In the case where $N - D + 1 \leq 0$ one can write $D = 4 - 2\varepsilon$ ($\varepsilon > 0$) and do the expansion in ε . Apart from a divergent term of the form $1/\varepsilon$ related to the artificial infinite boundary, the other terms give the nature of singularities.

A similar result for the nature of the singularity has been derived in [105] in the general case of a multi-loop diagram including the behaviour of the sub-LLS. The extraction of the overall, regular, factor which is the K -dependent part in Eq. (4.49) (see also Eq. (4.72) for the sub-LLS) is more transparent in our derivation.

For $N = 4$, $D = 4$

$$\begin{aligned} (T_0^4)_{div} &= e^{i\pi(3-K)/2} \frac{1}{4\sqrt{(-1)^{3-K}a_1}} \frac{1}{\sqrt{\lambda_4 - i\epsilon}} \\ &= e^{i\pi(3-K)/2} \frac{1}{4\sqrt{(-1)^{3-K}a_0 - i\epsilon}}. \end{aligned} \quad (4.51)$$

For $N = 3$, $D = 4 - 2\varepsilon$, we use $\Gamma(\varepsilon) = (1/\varepsilon) - \gamma_E$ to get

$$(T_0^3)_{div} = \frac{e^{i\pi(2-K)/2} v}{8\pi\sqrt{(-1)^{2-K}\lambda_1\lambda_2}} \ln(\lambda_3 v^2 - i\epsilon). \quad (4.52)$$

For $N = 2$, $D = 4 - 2\varepsilon$, we use $\Gamma(-1/2) = -2\sqrt{\pi}$ to get

$$(T_0^2)_{div} = -\frac{v}{8\pi\sqrt{\lambda_1}} (\lambda_2 v^2 - i\epsilon)^{1/2}. \quad (4.53)$$

For $N = 1$, $D = 4 - 2\varepsilon$, we have

$$\begin{aligned} T_0^1 &= \frac{-\Gamma(-1+\varepsilon)(4\pi)^\varepsilon}{16\pi^2\lambda_1^\varepsilon} \lambda_1 \\ &= \frac{\lambda_1}{16\pi^2} \left(\frac{1}{\varepsilon} - \gamma_E + \ln(4\pi) - \ln(\lambda_1) \right), \end{aligned} \quad (4.54)$$

with $\lambda_1 = m^2$.

Remarks: The leading Landau singularity appears when $\lambda_N \rightarrow 0$. The nature of the leading singularities for the scalar one-, two-, three-, four- functions are 1, $1/2$, \log , $-1/2$ respectively. One remarks that in the case $N = 4, 3$ the LLS is divergent, *i.e.* becomes infinite. The LLS is finite but singular, *i.e.* the derivative is divergent at the singular point, in the case $N = 2$ and is regular in the case $N = 1$. The

scalar three-point function and its square are integrable at the LLS point. The scalar four-point function is also integrable at the LLS point but its square is not.

One may wonder if we can use the general result in Eq. (4.49) for the case $N \geq 5$. The answer is YES as long as $a_1 \neq 0$. As will be proved in the next subsection, a_1 is proportional to the Gram determinant $\det(G)$ at the singular point. Since $\det(G) = 0$ for $N \geq 6$ in four dimensional space, we conclude that Eq. (4.49) cannot be used for the case $N \geq 6$. However, the LLS can occur for $N = 5$. If this happens, we will have five on-shell equations $q_i^2 = m_i^2$ with $i = 1, \dots, 5$ to solve for q^μ . We just need four equations to find q^μ , the rest is a δ -function to give some constraint on the internal masses and external momenta. Thus the nature of 5-point function LLS is a pole [29]. Indeed, it is highly nontrivial to find a physical process which contains a 5-point function LLS.

4.4.2 Nature of sub-LLS

In order to understand the nature of sub-leading Landau singularities, one should integrate over x_N from Eq. (4.15). This gives

$$T_0^N = \frac{(-1)^N \Gamma(N - D/2)}{(4\pi)^{D/2}} \int_0^1 dx_1 \cdots dx_{N-1} \frac{\eta(1 - \sum_{i=1}^{N-1} x_i)}{[\hat{\Delta}(x_1, \dots, x_{N-1})]^{N-D/2}}, \quad (4.55)$$

where η is Heaviside step function and

$$\begin{aligned} \hat{\Delta}(x_1, \dots, x_{N-1}) &\equiv \Delta(x_1, \dots, x_{N-1}, 1 - x_1 - \dots - x_{N-1}) \\ &= \frac{1}{2} \sum_{i,j=1}^{N-1} x_i x_j G_{ij} - \sum_{i=1}^{N-1} x_i \beta_i + \frac{1}{2} Q_{NN} - i\epsilon, \end{aligned} \quad (4.56)$$

where

$$G_{ij} = Q_{ij} - Q_{iN} - Q_{jN} + Q_{NN} = 2r_i \cdot r_j, \quad \beta_i = Q_{NN} - Q_{iN} = m_N^2 - m_i^2 + r_i^2. \quad (4.57)$$

Thus $\det(G)$ is just the Gram determinant. From Eq. (4.57) we get

$$\det(Q) = Q_{NN} \det(G) - \sum_{i,j=1}^{N-1} \beta_i \beta_j \hat{G}_{ij}. \quad (4.58)$$

The Landau equations for representation (4.55) are⁸

$$\begin{cases} \hat{\Delta} = 0, \\ x_i = 0, \quad i = 1, 2, \dots, \nu, \\ \frac{\partial \hat{\Delta}}{\partial x_i} = 0, \quad i = \nu + 1, \dots, N - 1. \end{cases} \quad (4.59)$$

The third equation of (4.59) gives

$$\sum_{j=\nu+1}^{N-1} G_{ij} x_j = \beta_i, \quad i = \nu + 1, \dots, N - 1. \quad (4.60)$$

If $\det(G) \neq 0$ then the solution reads

$$\bar{x}_i = \sum_{j=\nu+1}^{N-1} \beta_j G_{ij}^{-1} = \frac{1}{\det(G)} \sum_{j=\nu+1}^{N-1} \beta_j \hat{G}_{ij}, \quad i = \nu + 1, \dots, N - 1. \quad (4.61)$$

Thus the solution of the second and third equations of (4.59) is $x_i = \bar{x}_i$ with

$$\bar{x} = (\underbrace{0, \dots, 0}_{\nu}, \bar{x}_{\nu+1}, \dots, \bar{x}_{N-1}). \quad (4.62)$$

The first equation of (4.59) gives the equation of the surface of singularity [106]

$$\begin{aligned} \hat{\Delta}(\bar{x}) &= \frac{Q_{NN}}{2} - \frac{1}{2} \sum_{i=\nu+1}^{N-1} \bar{x}_i \beta_i \\ &= \frac{1 \det(Q)}{2 \det(G)} = 0, \end{aligned} \quad (4.63)$$

where we have used Eqs. (4.61) and (4.58). Not surprisingly, one obtains again $\det(Q) = 0$. In the case $\det(G) = 0$, the condition for the second and third equations of (4.59) to have solution is $\sum_{j=\nu+1}^{N-1} \beta_j \hat{G}_{ij} = 0$ (see Eq. (4.61)). This together with Eq. (4.58) give $\det(Q) = 0$.

⁸It is important to notice that when one performs the x_N -integration the boundaries become: $x_i = 0$ for $i = 1, \dots, N - 1$ and $1 - \sum_{i=1}^{N-1} x_i = 0$. In the mean time $\hat{\Delta}$ becomes inhomogeneous, so that the first equation of (4.59) is not automatically satisfied when the others are.

In the neighbourhood of a point \bar{x} that lies on the surface of singularity, we expand $\hat{\Delta}$, keeping only the lowest terms:

$$\begin{aligned}\hat{\Delta}(x) &= \hat{\Delta}(\bar{x}) + \sum_{i=1}^{\nu} x_i \frac{\partial \hat{\Delta}}{\partial x_i} \Big|_{x=\bar{x}} + \frac{1}{2} \sum_{i,j=\nu+1}^{N-1} (x_i - \bar{x}_i)(x_j - \bar{x}_j) \frac{\partial^2 \hat{\Delta}}{\partial x_i \partial x_j} \Big|_{x=\bar{x}} \\ &= \frac{1}{2} \left[C(x_i) + \sum_{i,j=\nu+1}^{N-1} y_i y_j G_{ij} \right],\end{aligned}\quad (4.64)$$

with

$$\begin{aligned}C(x_i) &= 2\hat{\Delta}(\bar{x}) + 2 \sum_{i=1}^{\nu} x_i \frac{\partial \hat{\Delta}}{\partial x_i} \Big|_{x=\bar{x}} - i\epsilon, \\ y_i &= x_i - \bar{x}_i, \quad i = \nu + 1, \dots, N-1.\end{aligned}\quad (4.65)$$

Integral (4.55) becomes

$$\begin{aligned}T_0^N &= \frac{(-1)^N \Gamma(N - D/2)}{\pi^{D/2} 2^{3D/2-N}} \int_0^1 \prod_{i=1}^{\nu} dx_i \\ &\times \int_{-\infty}^{+\infty} \prod_{i=\nu+1}^{N-1} dy_i \frac{1}{[\sum_{i,j=\nu+1}^{N-1} y_i y_j G_{ij} + C(x_i)]^{N-D/2}},\end{aligned}\quad (4.66)$$

where, similar to the calculation in the previous subsection, we have let each y_i -integration contour run from $-\infty$ to $+\infty$, provided the power $(N - D/2)$ of the denominator is sufficiently large. To understand the difference between the LLS and sub-LLS we should compare Eq. (4.39) to Eq. (4.64). One remarks that the linear terms only appear in the case of sub-LLS. The y_i -integration is exactly the same for the two cases. G_{ij} is a real symmetric matrix hence can be diagonalized by a real orthogonal co-ordinate transformation. Using the same method described in the previous subsection we integrate over y_i to get

$$\begin{aligned}T_0^N &= \frac{(-1)^N e^{i\pi(N-\nu-K-1)}}{2^{3D/2-N} \sqrt{(-1)^{N-\nu-1-K} \det(G)}} \pi^{(N-D-\nu-1)/2} \\ &\times \Gamma((N - D + \nu + 1)/2) \int_0^1 \prod_{i=1}^{\nu} dx_i [C(x_i)]^{-(N-D+\nu+1)/2},\end{aligned}\quad (4.67)$$

where K is the number of positive eigenvalues of Gram matrix G_{ij} . Of course, one can recover Eq. (4.49) by setting $\nu = 0$. Assuming that $b_i = \left. \frac{\partial \hat{\Delta}}{\partial x_i} \right|_{x=\bar{x}} \neq 0$, for the leading part of the singularity occurred when $x_i \rightarrow 0^+$ we have

$$\begin{aligned} \int_0^1 \prod_{i=1}^{\nu} dx_i [C(x_i)]^{\alpha} &= 2^{\alpha} \int_0^1 \prod_{i=1}^{\nu} dx_i [b_i x_i + \hat{\Delta}(\bar{x})]^{\alpha}, \\ &\sim 2^{\alpha} \frac{(-1)^{\nu}}{\prod_{i=1}^{\nu} b_i} \frac{\Gamma(\alpha+1)}{\Gamma(\alpha+\nu+1)} [\hat{\Delta}(\bar{x}) - i\epsilon]^{\alpha+\nu}. \end{aligned} \quad (4.68)$$

where $\alpha = -(N - D + \nu + 1)/2$. With $\gamma = -\alpha - \nu = (N - \nu - D + 1)/2$ we get

$$\begin{aligned} (T_0^N)_{div} &= \frac{(-1)^N e^{i\pi(N-\nu-K-1)}}{2^{3D/2-N} \sqrt{(-1)^{N-\nu-1-K} \det(G)}} \pi^{(N-D-\nu-1)/2} \\ &\times \frac{2^{-\nu}}{\prod_{i=1}^{\nu} b_i} \frac{(-1)^{\nu} \Gamma(\gamma+\nu) \Gamma(-\gamma-\nu+1)}{\Gamma(-\gamma+1)} [2\hat{\Delta}(\bar{x}) - i\epsilon]^{-\gamma}. \end{aligned} \quad (4.69)$$

We then make use of the following identity

$$\Gamma(1-z)\Gamma(z) = \frac{\pi}{\sin(z\pi)} \quad (4.70)$$

to get

$$\frac{(-1)^{\nu} \Gamma(\gamma+\nu) \Gamma(-\gamma-\nu+1)}{\Gamma(-\gamma+1)} = \Gamma(\gamma). \quad (4.71)$$

The final result reads⁹

$$(T_0^N)_{div} = \frac{(-1)^N e^{i\pi(N-\nu-K-1)}}{2^{(3+N-\nu)/2} \pi \sqrt{(-1)^{N-\nu-K-1} \det(G)}} \frac{(4\pi)^{\gamma} \Gamma(\gamma)}{\prod_{i=1}^{\nu} b_i} \left[\frac{\det(Q)}{2 \det(G)} - i\epsilon \right]^{-\gamma} \quad (4.72)$$

which holds provided

$$\det(G) \neq 0, \quad b_i = \left. \frac{\partial \hat{\Delta}}{\partial x_i} \right|_{x=\bar{x}} \neq 0 \quad \text{and} \quad \gamma = (N - \nu - D + 1)/2 > 0. \quad (4.73)$$

If some $b_i = 0$ then expansion (4.64) must be modified to take into account the higher order terms $x_i(x_j - \bar{x}_j) \left. \frac{\partial^2 \hat{\Delta}}{\partial x_i \partial x_j} \right|_{x=\bar{x}}$ with $i = 1, \dots, \nu$. If $\gamma \leq 0$ one can write $D = 4 - 2\epsilon$ ($\epsilon > 0$) and do the expansion in ϵ to get the divergent term independent of ϵ as in

⁹Similar result has been obtained by Polkinghorne and Sreaton [105].

the case of LLS.

Comparing Eq. (4.49) to Eq. (4.72) we see that, apart from the finite factor related to b_i , the nature of the singularities given by the latter can be obtained from the former by simply replacing N by $N - \nu$ which are the number of on-shell internal particles. We remark also that there must be some relation between a_1 and $\det(G)$ at the singular point, namely $\det(G) \propto a_1$ when $\det(Q) = 0$. As a consequence, if $a_1 = \det(Q) = 0$ (Landau matrix Q has at least two zero-eigenvalues) then $\det(G) = 0$ (Gram matrix G has at least one zero eigenvalue). There is a beautiful way to prove this mathematically ¹⁰. Let $V_a = \{x_i^{(a)}\}$ with $a = 1, 2$ and $i = 1, N$ be two linearly independent vectors of the degenerate zero-eigenvalue ¹¹. We can always normalise V_a such that

$$\sum_{i=1}^N x_i^{(a)} = 1, \quad a = 1, 2. \quad (4.74)$$

One has

$$\begin{aligned} 0 &= \sum_{j=1}^N Q_{ij} x_j^{(a)} = \sum_{j=1}^{N-1} Q_{ij} x_j^{(a)} + Q_{iN} \left(1 - \sum_{j=1}^{N-1} x_j^{(a)}\right) \\ &= \sum_{j=1}^{N-1} (Q_{ij} - Q_{iN}) x_j^{(a)} + Q_{iN} \\ &= \sum_{j=1}^{N-1} (Q_{ij} - Q_{iN} - Q_{jN} + Q_{NN}) x_j^{(a)} + \sum_{j=1}^{N-1} Q_{Nj} x_j^{(a)} - Q_{NN} \sum_{j=1}^{N-1} x_j^{(a)} + Q_{iN} \\ &= \sum_{j=1}^{N-1} G_{ij} x_j^{(a)} - \beta_i, \end{aligned} \quad (4.75)$$

where relations (4.57) have been used. Thus one gets

$$\sum_{j=1}^{N-1} G_{ij} x_j^{(a)} = \beta_i, \quad a = 1, 2. \quad (4.76)$$

¹⁰We have learnt this trick from Eric Pilon, many thanks!

¹¹In the case of the real symmetric matrix Q , the degree of degeneracy of one zero-eigenvalue is equal to the number of zero-eigenvalues.

With $V_0 = V_1 - V_2 \neq 0$ this gives

$$G.V_0 = 0. \quad (4.77)$$

This means that the Gram matrix has at least one zero-eigenvalue hence $\det(G) = 0$.

4.5 Conditions for leading Landau singularities to terminate

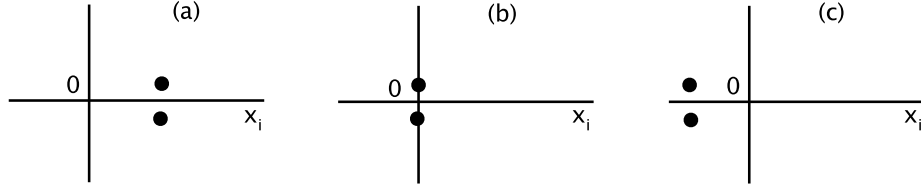


Figure 4.4: *Mechanism for termination of LLS in x_i -plane.*

This section concerns the termination of LLS as we vary the external parameters denoted by M_i (without any loss of generality, we assume that the internal masses are fixed for the sake of simplicity).

It is obvious that the position of LLS and its properties depend on the values of M_i . If we vary M_i continuously, while maintaining the pinch conditions, the only mechanism for the termination of a LLS is the following¹². The LLS moves to the end of the integration contour ($x_i = 0$). Thus the LLS will coincide with a sub-LLS and move off the physical region afterwards [107, 108, 109]. This is illustrated in Fig. 4.4.

The following remark will be useful later. The 4-point LLS terminates when it coincides with a 3-point sub-LLS which in turn will terminate when coinciding with

¹²In the case of more than one loop, there is another mechanism. The LLS can terminate if two pinches meet on the integration contour. If this happens, the singularity may somehow leave the physical region [107, 108].

a normal threshold. The normal threshold coincides with itself, *i.e.* it occurs at one point.

A good question to ask is "How does a LLS terminate?" This is a mathematically complicated question and we do not attempt to give a complete answer. What we understand is as follows. When moving from Fig. 4.4a to Fig. 4.4b, the leading Landau curve ($\det(Q_N) = 0$) changes continuously until it makes an *effective intersection* with a sub-leading Landau curve ($\det(Q_{N-1}) = 0$) [107, 109, 108]. At the point of contact, both curves have the same slope and both corresponding Landau equations have the same solution of x_i [107, 108]. At effective intersections the nature of the Landau singularity may change [109, 108]. In Fig. 4.4a we have a N -point LLS whose nature is given by

$$T_a(M_i) = A_a(M_i) + B_a(M_i)f_a(\det Q_N), \quad (4.78)$$

where the functions A and B are analytic in a neighborhood of the singular point M_i , the function $f_a(\det Q_N)$ is singular at this point. $f_a(z)$ can be $z^{1/2}$, $\ln z$ or $z^{-1/2}$ if N is 2, 3 or 4 respectively. For Fig. 4.4c we have a similar equation

$$T_c(M_i) = A_c(M_i) + B_c(M_i)f_c(\det Q_{N-1}), \quad (4.79)$$

where we have assumed that Fig. 4.4c has a $(N - 1)$ -point Landau singularity. The nature of the coincident singularity in Fig. 4.4b is a product of two factors which are similar to T_a and T_c [109]. Thus, we have

$$T_b(M_i) = A + Bf_a(\det Q_N) + Cf_c(\det Q_{N-1}) + Df_a(\det Q_N)f_c(\det Q_{N-1}). \quad (4.80)$$

If $D \neq 0$ then the leading singularity is given by the last term which means that the Landau singularity can be enhanced at termination point. This kind of enhancement can be somehow understood if we look at some formulae in this thesis: from Eq. (4.72) we see that if a leading N -point singularity coincides with a sub-LLS then $b_i = \left. \frac{\partial \hat{\Delta}}{\partial x_i} \right|_{x=\bar{x}} = 0$ leading to an enhancement from the prefactor; from Eq. (4.101) we observe a product of two singularities (a leading Landau singularity and a collinear

divergence); from Eq. (E.15) we see the possibility that a product of two singularities can occur if the integrals related to 3-point functions develop a pinch singularity at the same position where the prefactor related to the leading Landau determinant ($1/\det(Q_4)$) vanishes.

If a four-point LLS coincides with a three-point sub-LLS, the nature of this singularity can be $z^{-1/2} \ln z$ which is integrable but its square is not.

4.6 Special solutions of Landau equations

4.6.1 Infrared and collinear divergences

In this section, we will show that infrared and collinear singularities are solutions of Landau equations. However, in order for them to become divergent additional conditions must be satisfied. As one might anticipate from Eq. (4.72) sub-leading Landau singularities can be enhanced by various factors.

Infrared divergence

We consider the case of a sub-LLS where $x_1 = \dots = x_{N-1} = 0$ and $x_N > 0$. The Landau equations become

$$q_N^2 = m_N^2 \quad \text{and} \quad q_N = 0. \quad (4.81)$$

We get $m_N = 0$. As remarked in subsection 4.4, for the case $N = 1, 2$ the Landau singularities are finite hence there is no infrared divergence in those cases. We thus consider the case $N = 3$. With $\nu = 2$, equation (4.66) becomes

$$T_0^3 \sim \int_{0^+} dx_1 dx_2 \frac{1}{C(x_i)}, \quad (4.82)$$

with

$$C(x_i) = 2m_3^2 + 2 \sum_{i=1}^2 x_i \beta_i + \sum_{i,j=1}^2 G_{ij} x_i x_j - i\epsilon. \quad (4.83)$$

If $\beta_i = m_3^2 - m_i^2 + r_i^2 \neq 0$ then one can neglect the quadratic terms in $C(x_i)$ to get

$$(T_0^3)_{div} \sim \int_{0^+} dx_1 dx_2 \frac{1}{2m_3^2 + 2(\beta_1 x_1 + \beta_2 x_2)} \sim \frac{1}{\beta_1 \beta_2} m_3^2 \rightarrow 0. \quad (4.84)$$

If $\beta_i = m_3^2 - m_i^2 + r_i^2 = 0$ then we get

$$(T_0^3)_{div} \sim \int_{0^+} dx_1 dx_2 \frac{1}{2m_3^2 + \sum_{i,j=1}^2 G_{ij} x_i x_j} \sim \ln(m_3^2) \rightarrow \infty. \quad (4.85)$$

The nature of Landau singularity is m_3^2 if $\beta_i \neq 0$ and is enhanced to $\ln(m_3^2)$ if $\beta_1 = \beta_2 = 0$. The conditions to have an infrared divergence for the case of three-point function therefore are

$$m_3 = 0, \quad m_1^2 = r_1^2 = p_1^2, \quad m_2^2 = r_2^2 = p_2^2. \quad (4.86)$$

For the cases $N > 3$ we can always reduce them to three-point functions hence we get the same conclusion. Physically, one sees that conditions (4.86) can be satisfied only by the photon or gluon. For the electroweak theory, if we take the limit $M_W \rightarrow 0$ then the one-loop diagrams involving the W-gauge boson as an internal particle have no infrared divergence since it couples to particles with different masses.

Collinear divergence

For $M = 2$, i.e. $x_{1,2} > 0$ and $x_3 = \dots = x_N = 0$ equations (4.23) become

$$\begin{cases} x_{1,2} > 0, \\ q_1^2 = m_1^2, \quad q_2 = m_2^2, \\ x_1 q_1 + x_2 q_2 = 0. \end{cases} \quad (4.87)$$

One gets $x_1 m_1 = x_2 m_2$. If $m_{1,2} \neq 0$ then $x_1(q_1 + \frac{m_1}{m_2} q_2) = 0$ whose solution corresponds to the normal threshold $p^2 = (q_1 - q_2)^2 = (m_1 + m_2)^2$. If $m_{1,2} = 0$ one gets

$$x_1 m_1^2 + x_2 (q_1 \cdot q_2) = 0, \quad (4.88)$$

which gives $q_1 \cdot q_2 = 0$ or $p^2 = (q_1 - q_2)^2 = 0$. This solution corresponds to a collinear divergence whose nature is also logarithmic [110]. Clearly, this collinear divergence cannot occur if $N = 1$.

It is important to remark that the solutions for infrared and collinear divergences appear in the limit of massless internal particles. These solutions require no constraint on relevant Feynman parameters, even the positive condition is not necessary.

4.6.2 Double parton scattering singularity

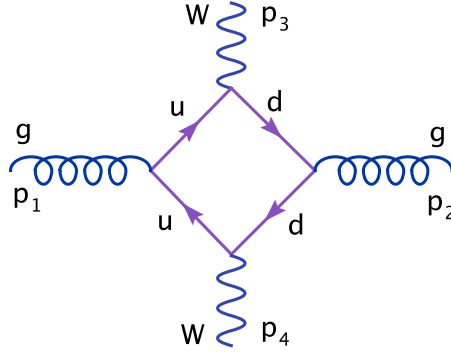


Figure 4.5: A typical box Feynman diagram which has a double parton scattering singularity.

There exists a special case of Landau singularity called double parton scattering (DPS) singularity [103, 22] which appears also in the massless limit. Unlike the sub-leading infrared and collinear divergences, the DPS singularity is a LLS and its solution requires some sort of constraint on relevant Feynman parameters (the positive sign condition is important).

Let us consider the case of $g(p_1)g(p_2) \rightarrow W(p_3)W(p_4)$ box diagram displayed in Fig. 4.5. The internal particles u -quark and d -quark are massless. The Q -matrix is given by

$$Q_4 = \begin{pmatrix} 0 & 0 & -t & -M_W^2 \\ 0 & 0 & -M_W^2 & -u \\ -t & -M_W^2 & 0 & 0 \\ -M_W^2 & -u & 0 & 0 \end{pmatrix} \quad (4.89)$$

where $t = (p_1 - p_3)^2$, $u = (p_2 - p_3)^2$. The Landau determinant, characteristic polynomial and Gram determinant read

$$\begin{aligned}\det(Q_4) &= (tu - M_W^4)^2 = 0, \\ f(\lambda) &= \lambda^4 - (t^2 + u^2 + 2M_W^4)\lambda^2 + \det(Q_4), \\ \det(G_3) &= 2s(tu - M_W^4),\end{aligned}\tag{4.90}$$

with $s = (p_1 + p_2)^2$. One sees that $a_1 = 0$ and $\det(Q_4) = \det(G_3) = 0$ at the boundary of phase space where the Landau matrix has two zero-eigenvalues. The phase space is defined as

$$s \geq 4M_W^2, \quad tu - M_W^4 \geq 0 \quad \text{with} \quad t + u = 2M_W^2 - s \leq -2M_W^2.\tag{4.91}$$

In this special case where the Landau matrix has two zero-eigenvalues at the singular point, the conditions given in subsection 4.3 (see Eq. (4.26)) are necessary but no longer sufficient. One should keep in mind that this box diagram always has a collinear divergence associated with the reduced two-point functions as discussed in the previous subsection. The necessary conditions for a LLS read

$$\begin{cases} tu = M_W^4, \\ t < 0, \quad u < 0, \end{cases}\tag{4.92}$$

which are compatible with Eq. (4.91). We now have two questions to be answered: whether they are sufficient conditions for a pinch singularity? If Yes then what is the nature of the singularity?

For these questions, we come back to equation (4.15) and perform the following nonlinear change of variables [106, 103]

$$x_1 = \sigma\alpha, \quad x_2 = \sigma(1 - \alpha), \quad x_3 = \tau\beta, \quad x_4 = \tau(1 - \beta).\tag{4.93}$$

The inverse solution gives us the range of new variables

$$0 \leq \sigma, \tau < \infty; \quad 0 \leq \alpha, \beta \leq 1.\tag{4.94}$$

The Jacobian is simply $\sigma\tau$. With $D = 4 + 2\varepsilon$ ($\varepsilon > 0$) equation (4.15) factorizes

$$T_0^4 = \frac{1}{(4\pi)^2} \int_0^\infty d\sigma d\tau \frac{\delta(\sigma + \tau - 1)}{(\sigma\tau)^{1-\varepsilon}} \times \int_0^1 d\alpha d\beta \frac{1}{[s\alpha\beta + (u - M_W^2)(\alpha + \beta) - u - i\epsilon]^{2-\varepsilon}}. \quad (4.95)$$

The first integral is just the Beta function $B(\varepsilon, \varepsilon)$ producing a collinear divergence.

We use

$$B(\varepsilon, \varepsilon) = \frac{\Gamma(\varepsilon)\Gamma(\varepsilon)}{\Gamma(2\varepsilon)} = \frac{2}{\varepsilon} + \mathcal{O}(\varepsilon) \quad (4.96)$$

to get

$$T_0^4 = \frac{1}{8\pi^2\varepsilon} \int_0^1 d\alpha d\beta \frac{1}{[s\alpha\beta + (u - M_W^2)(\alpha + \beta) - u - i\epsilon]^2} + \frac{1}{8\pi^2} \int_0^1 d\alpha d\beta \frac{\ln[s\alpha\beta + (u - M_W^2)(\alpha + \beta) - u]}{[s\alpha\beta + (u - M_W^2)(\alpha + \beta) - u - i\epsilon]^2}. \quad (4.97)$$

We are interested in the collinear divergent term. The relevant integral reads

$$I_1 = -\frac{1}{(M_W^2 - t)(M_W^2 - u)} \int_0^1 d\alpha \frac{1}{(\alpha - w)(\alpha - a)}, \quad (4.98)$$

where we have integrated over β and

$$a = \frac{M_W^2}{M_W^2 - t} - i\epsilon_a, \quad \epsilon_a = \frac{\epsilon}{M_W^2 - t}, \\ w = \frac{-u}{M_W^2 - u} + i\epsilon_w, \quad \epsilon_w = \frac{\epsilon}{M_W^2 - u}. \quad (4.99)$$

This is nothing but the second example (4.3). From Eq. (4.7) we have the necessary and sufficient conditions for a pinch singularity:

$$0 < w = a < 1 \quad \text{and} \quad (M_W^2 - t)(M_W^2 - u) > 0, \quad (4.100)$$

which are completely equivalent to Eq. (4.92). From Eq. (4.4) we get the following result at the singular point $tu = M_W^4$

$$(I_1)_{div} = \frac{1}{M_W^4} + \frac{2\pi i}{M_W^4 - tu}, \\ (T_0^4)_{div} = \frac{i}{4\pi(M_W^4 - tu)} \frac{1}{\varepsilon} + \dots = -\frac{i}{4\pi\sqrt{\det(Q_4)}} \frac{1}{\varepsilon} + \dots \quad (4.101)$$

We conclude that in this special case where the Landau matrix has two zero-eigenvalues, conditions (4.92) given by the Landau equations are necessary and sufficient for the appearance of a LLS. The nature of this singularity is $1/\sqrt{\det(Q_4)}$ which is consistent with Eq. (4.49). The LLS goes together with the collinear divergence (see also section 4.4). This LLS is called double parton scattering singularity first pointed out in [103].

We notice that Eq. (4.101) disagrees with the result of Ellis and Zanderighi given in Eq. (4.21) of [111]¹³ where they claimed that, apart from the collinear divergence, a finite result can be obtained by doing an expansion around the LLS point $tu = M_W^4$.

This DPS singularity is not integrable. In a practical calculation, the cross section must be finite. This singularity must somehow disappear order by order. For the process $gg \rightarrow WW$ there is no tree level diagram hence there is no real radiation at the leading order. One infers that the numerator must vanish at the singular point. The actual calculations [112, 113] have confirmed this. We have conjectured it as a consequence of the gauge dynamics [22]. To understand this dynamical cancellation, a physical investigation is necessary. The same phenomenon of DPS singularity happens in the case of six photon scattering whose numerical analysis around the singular point is given in [22].

¹³Many thanks to Denner for pointing out this reference to us.

Chapter 5

SM $b\bar{b}H$ production at the LHC:

$$M_H \geq 2M_W$$

The content of this chapter is based on our publications [114, 76].

An important notation used in this chapter should be clarified. The notation of center-of-mass energy, \sqrt{s} , can be used for the sub-process $gg \rightarrow b\bar{b}H$ or $pp \rightarrow b\bar{b}H$. Which use will depend on the context, as you will notice very easily.

5.1 Motivation

The aim of this chapter is to extend the study we made in chapter 3 to higher Higgs masses.

When trying to do so for the case $M_H \geq 2M_W$ we have encountered severe numerical instabilities for the cross section involving the one-loop amplitude squared. We have tried to understand this problem and found the following facts. At the level of NLO which involves the interference term between the tree-level and one-loop

amplitudes no instability was present. On close inspection it was found that the instabilities were only due to the box and pentagon diagrams of class (c) of Fig. 3.4. The contribution of various triangle diagrams does not show any numerical instabilities. At the partonic gluon-gluon level it was found that there is no instability for $\sqrt{s} < 2m_t$ and that independently of M_H and \sqrt{s} the result was completely stable for $m_t = M_W$. These threshold conditions were a sign for the possible existence of a leading Landau singularity for the box diagrams whose square is not integrable. The five point functions are reduced to four point functions hence should have the same problem. Indeed, some triangle diagrams of class (c) of Fig. 3.4 have also LLS whose nature is integrable. That's why they do not show any numerical instability.

In order to solve this problem of Landau singularities, we first have to understand them in detail by applying the general analysis of the previous chapter to the specific problem of $gg \rightarrow b\bar{b}H$.

5.2 Landau singularities in $gg \rightarrow b\bar{b}H$

In this section, we discuss all Landau singularities that occur in the Feynman diagrams of class (c) of Fig. 3.4. It is pedagogical to start with the three point function.

5.2.1 Three point function

As concluded in section 4.3, a necessary condition for a three point function to have a LLS is that it has two cuts which can produce physical on-shell particles. The other external particle which does not correspond to those cuts must have mass smaller than the difference of the two internal masses associated with it. The diagram in Fig. 5.1 satisfies those conditions. The scalar three point function of this diagram reads

$$T_0^3(s_2) = C_0(s_2, M_H^2, 0, m_t^2, M_W^2, M_W^2) \quad (5.1)$$

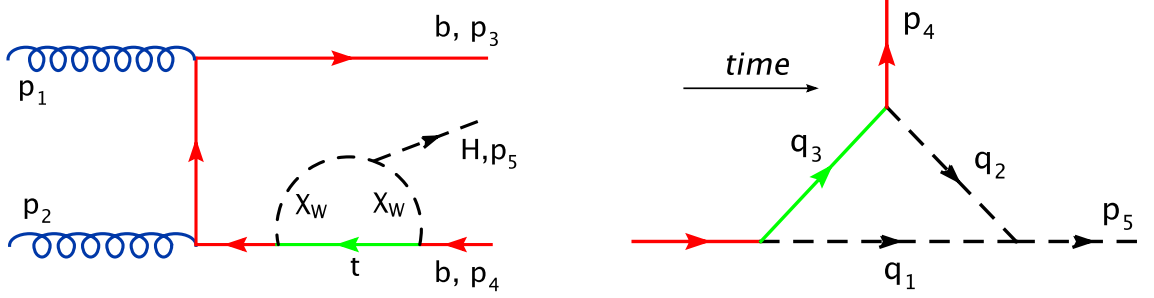


Figure 5.1: Left: A triangle diagram contributing to $gg \rightarrow b\bar{b}H$ that can develop a leading Landau singularity for $M_H \geq 2M_W$ and $\sqrt{s_2} \geq m_t + M_W$, i.e. all the three particles in the loop can be simultaneously on-shell. Right: the three point function of the left diagram where the arrows indicate momentum flow.

with $s_2 = (p_4 + p_5)^2$ and the bottom-quark mass has been neglected. Necessary conditions to have LLS are

$$M_H \geq 2M_W \quad \text{and} \quad \sqrt{s_2} \geq m_t + M_W. \quad (5.2)$$

The phase space is defined by

$$M_H^2 \leq s_2 \leq s. \quad (5.3)$$

The characteristic equation writes

$$-\lambda^3 + a_2\lambda^2 - a_1\lambda + a_0 = 0 \quad (5.4)$$

with

$$\begin{aligned} a_0 &= \det(Q_3) = -2M_W^2 s_2^2 + 2M_H^2 (m_t^2 + M_W^2) s_2 - 2M_H^2 [M_H^2 m_t^2 + (m_t^2 - M_W^2)^2], \\ a_1 &= -[M_H^2 (M_H^2 - 4M_W^2) + (s_2 - m_t^2 - M_W^2)^2 + m_t^4 + M_W^4 - 6m_t^2 M_W^2] \\ &\leq -[M_H^2 (M_H^2 - 4M_W^2) + (m_t^2 - M_W^2)^2] < 0, \\ a_2 &= 2(m_t^2 + 2M_W^2), \end{aligned} \quad (5.5)$$

where we have used conditions (5.2) to prove that a_1 is negative. The equation $\det(Q_3) = 0$ has two roots

$$s_2^\pm = \frac{1}{2M_W^2} \left[M_H^2 (M_W^2 + m_t^2) \pm (m_t^2 - M_W^2) M_H \sqrt{M_H^2 - 4M_W^2} \right]. \quad (5.6)$$

The sign condition ($x_i > 0$), Eq. (4.27), is very simple. For this, we need

$$\begin{aligned}\det(\hat{Q}_{33}) &= -M_H^2(M_H^2 - 4M_W^2) \leq 0, \\ \det(\hat{Q}_{13}) &= -M_H^2(m_t^2 + M_W^2) + 2s_2M_W^2 \leq 0, \\ \det(\hat{Q}_{23}) &= -M_H^2(m_t^2 + M_W^2) + s_2(M_H^2 - 2M_W^2) \leq 0,\end{aligned}\tag{5.7}$$

which together with Eq. (5.2) give

$$s_2 \leq \frac{M_W^2 + m_t^2}{M_H^2 - 2M_W^2} M_H^2 \leq 2(m_t^2 + M_W^2).\tag{5.8}$$

Only the minus solution given in Eq. (5.6) satisfies this, thus

$$s_2^{LLS} = s_2^- = \frac{1}{2M_W^2} \left[M_H^2(M_W^2 + m_t^2) - (m_t^2 - M_W^2)M_H \sqrt{M_H^2 - 4M_W^2} \right].\tag{5.9}$$

This result tells us many things. First, if $M_H < 2M_W$ there is no LLS. Second, if $M_H = 2M_W$ the LLS occurs at $s_2^{LLS} = 2(m_t^2 + M_W^2)$ which is the maximum value of s_2^{LLS} given by Eq. (5.8). If M_H increases then s_2^{LLS} becomes smaller and smaller. The maximum value of M_H is determined when s_2^{LLS} reaches the normal threshold (this condition for the termination of a LLS was discussed in section 4.4):

$$\begin{aligned}4M_W^2 \leq M_H^2 &\leq 4M_W^2 + \frac{M_W}{m_t}(m_t - M_W)^2, \\ (m_t + M_W)^2 &\leq s_2 \leq 2(m_t^2 + M_W^2).\end{aligned}\tag{5.10}$$

Numerically, we have

$$\begin{aligned}160.7532\text{GeV} &\leq M_H \leq 172.889\text{GeV}, \\ 254.3766\text{GeV} &\leq \sqrt{s_2} \leq 271.059\text{GeV}.\end{aligned}\tag{5.11}$$

If one keeps increasing $M_H > 172.889\text{GeV}$, s_2 will increase from its minimum value 254.3766GeV and become larger than the limit $\frac{M_W^2 + m_t^2}{M_H^2 - 2M_W^2} M_H^2$ (see Eq. (5.8)) required by the sign condition ($x_i > 0$) hence be outside the physical region. In the mean time, one should notice that the normal threshold is moving towards the left boundary of phase space as M_H increases. When $M_H = m_t + M_W = 254.3766\text{GeV}$, the normal

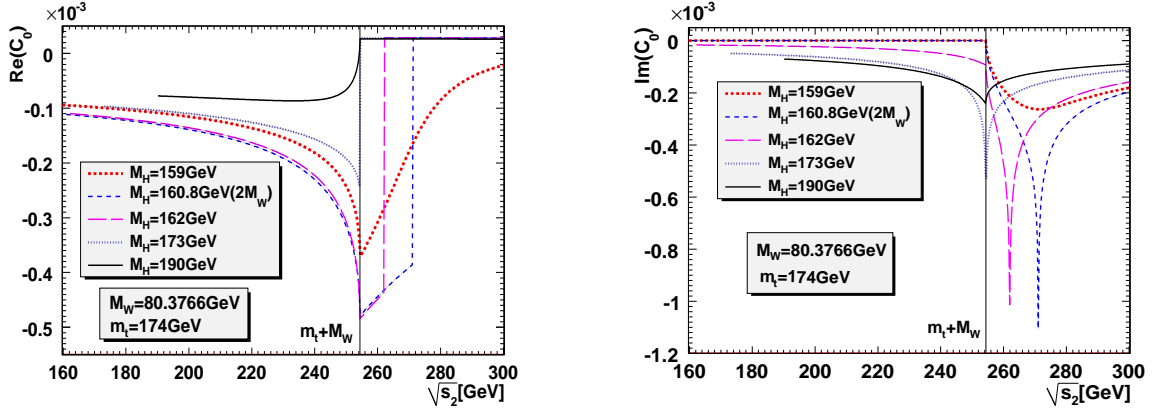


Figure 5.2: Left: the real part of C_0 as functions of $\sqrt{s_2}$ with various values of M_H . Right: the same plots for the imaginary part.

threshold is at the boundary and disappears if M_H passes that value. The function T_0^3 then has no structure. All this phenomenon is shown in Fig. 5.2.

We would like to explain the behaviour of the real and imaginary parts of C_0 at the LLS point. Since $\lambda_3 \rightarrow 0$, we have $\lambda_1 \lambda_2 = a_1 < 0$ as proved in Eq. (5.5). Thus there is one positive eigenvalue, *i.e.* $K = 1$. From Eq. (4.52) we get

$$(C_0)_{div} = \frac{iv}{8\pi\sqrt{|a_1|}} \ln(\lambda_3 v^2 - i\epsilon) = \frac{v}{8\pi\sqrt{|a_1|}} (i \ln |\lambda_3 v^2| + \pi). \quad (5.12)$$

Thus, one observes a positive jump in the real part and a logarithmic singularity in the imaginary part as described in Fig. 5.2. This singularity is integrable at the NLO as well as one-loop amplitude square level hence does not cause any numerical instability.

5.2.2 Four point function

The 5-point functions have no LLS but contain a sub-leading Landau singularity which is exactly the same as the LLS of the box diagram in Fig. 5.3. It is thus enough to study the singularity structure of this box diagram. With $s_1 = (p_3 + p_5)^2$, $s_2 =$

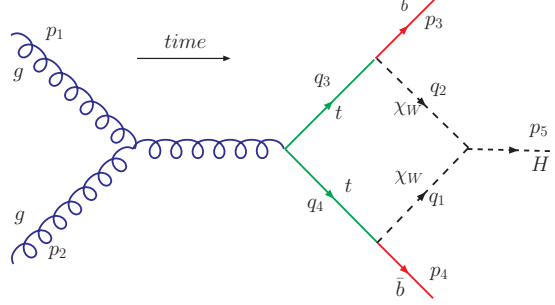


Figure 5.3: A box diagram contributing to $gg \rightarrow b\bar{b}H$ that can develop a Landau singularity for $M_H \geq 2M_W$ and $\sqrt{s} \geq 2m_t$, i.e. all the four particles in the loop can be simultaneously on-shell. The arrows indicate momentum flow. Internal momenta q_i are real, on-shell and have positive energies.

$(p_4 + p_5)^2$, and the on-shell conditions $p_1^2 = p_2^2 = 0$, $p_3^2 = p_4^2 = m_b^2 = 0$, $p_5^2 = M_H^2$, fixing s and M_H , the scalar box integral is a function of two variables $s_{1,2}$

$$T_0^4(s_1, s_2) = D_0(M_H^2, 0, s, 0, s_1, s_2, M_W^2, M_W^2, m_t^2, m_t^2). \quad (5.13)$$

The kinematically allowed region (phase space) is

$$M_H^2 \leq s_1 \leq s, \quad M_H^2 \frac{s}{s_1} \leq s_2 \leq M_H^2 + s - s_1, \quad (5.14)$$

where the latter is obtained by writing $s_2 = (p_4 + p_5)^2 = M_H^2 + 2e_4(e_5 - |\mathbf{p}_5| \cos \theta_{45})$ in the center-of-mass system of $(p_3 + p_5)$.

Conditions for the opening of normal thresholds

The condition $\sum x_i q_i = 0$ with $x_i > 0$ of Eq. (4.23) can be re-written in the form

$$x_2 q_2 + x_3 q_3 = x_1 q_1 + x_4 q_4 \quad (5.15)$$

with all $q_i^0 > 0$ as shown in Fig. 5.3. Indeed, there are other possibilities like $x_3 q_3 = x_1 q_1 + x_4 q_4 + x_2 q_2$ with all $q_i^0 > 0$ but this will require $m_b \geq (m_t + M_W)$ which is impossible in our case. Thus equation (5.15) is the unique possibility for a LLS. This

condition of positive energy together with the real and on-shell condition ($q_i = q_i^*$, $q_i^2 = m_i^2$) give a beautiful physical picture as shown in Fig. 5.3 where internal and external momenta share the same physical properties.

As already discussed in section 4.3, the above picture gives the following necessary conditions for the appearance of a LLS:

$$M_H \geq 2M_W \quad \text{and} \quad \sqrt{s} \geq 2m_t, \quad (5.16)$$

$$s_1 \geq (m_t + M_W)^2 \quad \text{and} \quad s_2 \geq (m_t + M_W)^2, \quad (5.17)$$

$$m_t > M_W, \quad (5.18)$$

where we have used the fact that the momenta of the bottom-quarks and the Higgs boson flow in the same positive direction to get the last constraint (if we consider the inverse process $H \rightarrow b\bar{b}gg$ where momenta of the bottom-quarks and the Higgs boson are in opposite directions then we get $M_W > m_t$ which cannot be satisfied by experimental data.). They are conditions for the opening of 4 normal thresholds.

Landau determinant

The reduced matrix, $S^{(4)}$, which is equivalent in this case to the Q matrix for studying the Landau singularity, is given by

$$S_4 = \begin{pmatrix} 1 & \frac{2M_W^2 - M_H^2}{2M_W^2} & \frac{m_t^2 + M_W^2 - s_1}{2M_W m_t} & \frac{M_W^2 + m_t^2}{2M_W m_t} \\ \frac{2M_W^2 - M_H^2}{2M_W^2} & 1 & \frac{M_W^2 + m_t^2}{2M_W m_t} & \frac{m_t^2 + M_W^2 - s_2}{2M_W m_t} \\ \frac{m_t^2 + M_W^2 - s_1}{2M_W m_t} & \frac{M_W^2 + m_t^2}{2M_W m_t} & 1 & \frac{2m_t^2 - s}{2m_t^2} \\ \frac{M_W^2 + m_t^2}{2M_W m_t} & \frac{m_t^2 + M_W^2 - s_2}{2M_W m_t} & \frac{2m_t^2 - s}{2m_t^2} & 1 \end{pmatrix}, \quad S_4^{ij} = \frac{Q_4^{ij}}{2m_i m_j}. \quad (5.19)$$

The determinant reads

$$\begin{aligned}
\det(Q_4) &= 16M_W^4 m_t^4 \det(S_4) = as_2^2 + bs_2 + c, \\
a &= \lambda(s_1, m_t^2, M_W^2) = [s_1 - (m_t + M_W)^2][s_1 - (m_t - M_W)^2], \\
b &= 2 \left\{ -s_1^2(m_t^2 + M_W^2) + s_1[(m_t^2 + M_W^2)^2 - (s - 2m_t^2)(M_H^2 - 2M_W^2)] \right. \\
&\quad \left. + sM_H^2(m_t^2 + M_W^2) \right\}, \\
c &= s_1^2(m_t^2 - M_W^2)^2 + 2M_H^2 s(m_t^2 + M_W^2)s_1 \\
&\quad + sM_H^2[(s - 4m_t^2)(M_H^2 - 4M_W^2) - 4(m_t^2 + M_W^2)^2].
\end{aligned} \tag{5.20}$$

We remark that $a = 0$ corresponds to a normal threshold and defines the asymptotes of the Landau curve.

The Landau determinant can be written in the following beautiful form

$$\begin{aligned}
\det(Q_4) &= a(s_2 - s'_2)^2 - \frac{\Delta}{4a}, \quad s'_2 = -\frac{b}{2a}, \\
\Delta &= \det Q_3(s, s_1) \det Q_3(M_H^2, s_1), \\
\frac{\det Q_3(M_H^2, s_1)}{2M_W^2} &= - \left[(s_1 - \frac{m_t^2 + M_W^2}{2M_W^2} M_H^2)^2 - \frac{M_H^2(M_H^2 - 4M_W^2)(m_t^2 - M_W^2)^2}{4M_W^4} \right], \\
\frac{\det Q_3(s, s_1)}{2m_t^2} &= - \left[(s_1 - \frac{m_t^2 + M_W^2}{2m_t^2} s)^2 - \frac{s(s - 4m_t^2)(m_t^2 - M_W^2)^2}{4m_t^4} \right],
\end{aligned} \tag{5.21}$$

which is very useful when one knows that the LLS coincides with a three-point sub-LLS. If that happens the Eq. $\det(Q_4) = 0$ has only one root $s_2 = s'_2$. The fact that the discriminant of a Landau determinant can be written as a product of lower-order Landau determinants is known as the Jacobi ratio theorem for determinants [109, 115].

Discussion of singular structure

We would like to understand the singular structure of the scalar 4-point function defined in Eq. (5.13). Namely, we will look at the behaviour of its real and imaginary parts as functions of s_1 and s_2 while other parameters are fixed. We take $m_t = 174$ GeV, $M_W = 80.3766$ GeV, $\sqrt{s} = 353$ GeV and $M_H = 165$ GeV.

The behaviour of the Landau determinant, the real and imaginary parts of the 4–point function T_0^4 are displayed in Fig. 5.4 as function of s_1, s_2 within the phase space defined by Eq. (5.14). We clearly see that the Landau determinant vanishes inside the phase space and leads to regions of severe instability in both the real and imaginary parts of the scalar integral. We notice that this region of Landau singularities is localised at the center of phase space. The boundary of singular region will be explained later, see Eqs. (5.35) and (5.36).

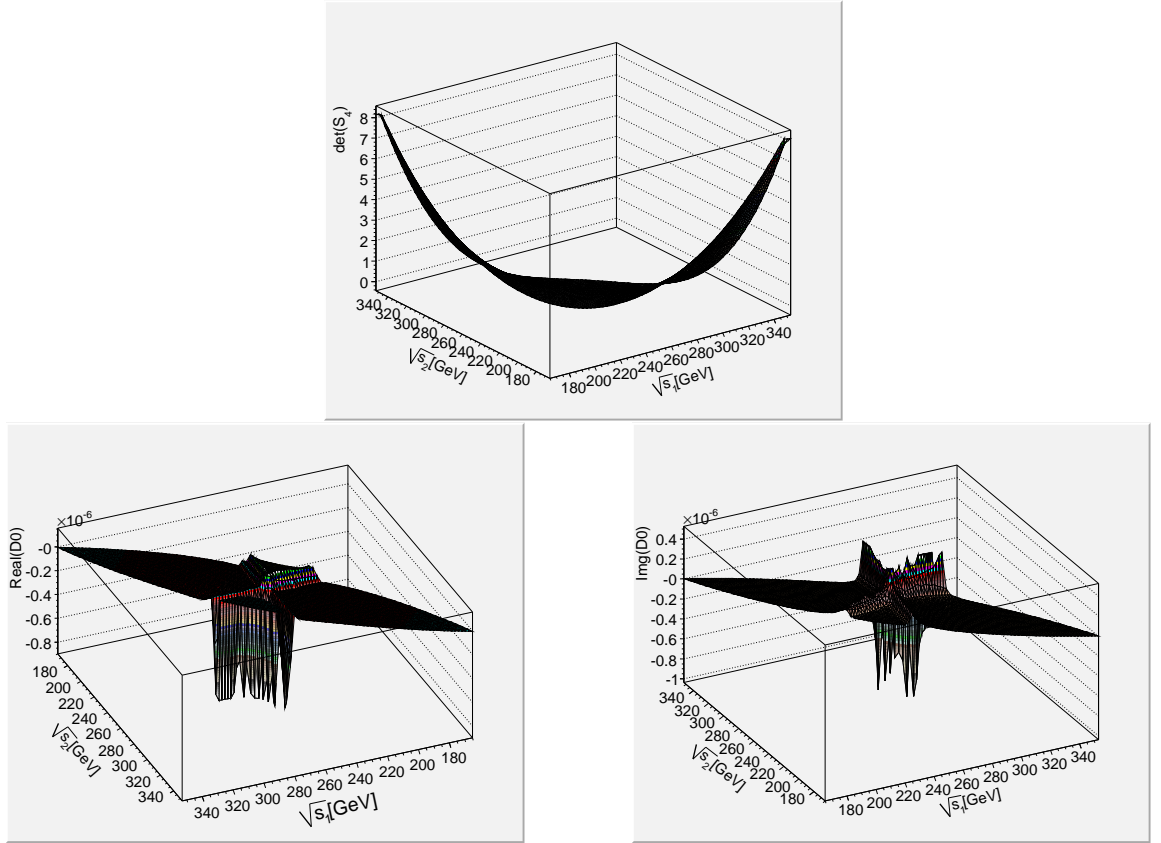


Figure 5.4: The Landau determinant as a function of s_1 and s_2 (upper figure). The real and imaginary parts of D_0 as a function of s_1 and s_2 .

To investigate the structure of the singularities in more detail let us fix $\sqrt{s_1} =$

$\sqrt{2(m_t^2 + M_W^2)} \approx 271.06$ GeV, so that the properties are studied for the single variable s_2 . In order to do so, we have to find all the reduced diagrams containing s_2 as an external momentum squared. There are 3 diagrams shown in Fig. 5.5: one self-energy and two triangle diagrams. The plots for the real and imaginary parts are shown in

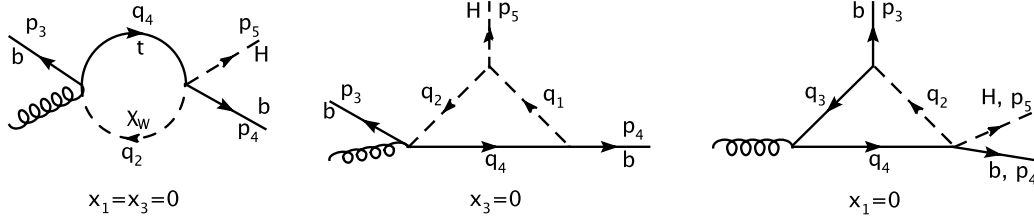


Figure 5.5: Three reduced diagrams of the box diagram in Fig. 5.3, that contain s_2 as an external momentum squared. The self-energy diagram has a normal threshold. The two triangle diagrams contain anomalous thresholds. We refer to subsection 5.2.1 for a detailed account of the 3-point Landau singularity.

Fig. 5.6. This figure is very educative. We see that there are four discontinuities in the function representing the real part of the scalar integral in the variable $\sqrt{s_2}$:

- As s_2 increases we first encounter a discontinuity at the normal threshold $\sqrt{s_2} = m_t + M_W = 254.38$ GeV, representing $Hb \rightarrow Wt$. This corresponds to the solution (for the Feynman parameters) $x_{1,3} = 0$ and $x_{2,4} > 0$ of the Landau equations (see Fig. 5.5-left).
- The second discontinuity occurs at the anomalous threshold $\sqrt{s_2} = 257.09$ GeV of a reduced triangle diagram. This corresponds to the solution $x_3 = 0$ and $x_{1,2,4} > 0$ of the Landau equations (see Fig. 5.5-middle). As discussed in subsection 5.2.1, the singular position is given by

$$s_2^H = \frac{1}{2M_W^2} \left(M_H^2(m_t^2 + M_W^2) - M_H \sqrt{M_H^2 - 4M_W^2(m_t^2 - M_W^2)} \right) \quad (5.22)$$

which gives $\sqrt{s_2} = 257.09$ GeV.

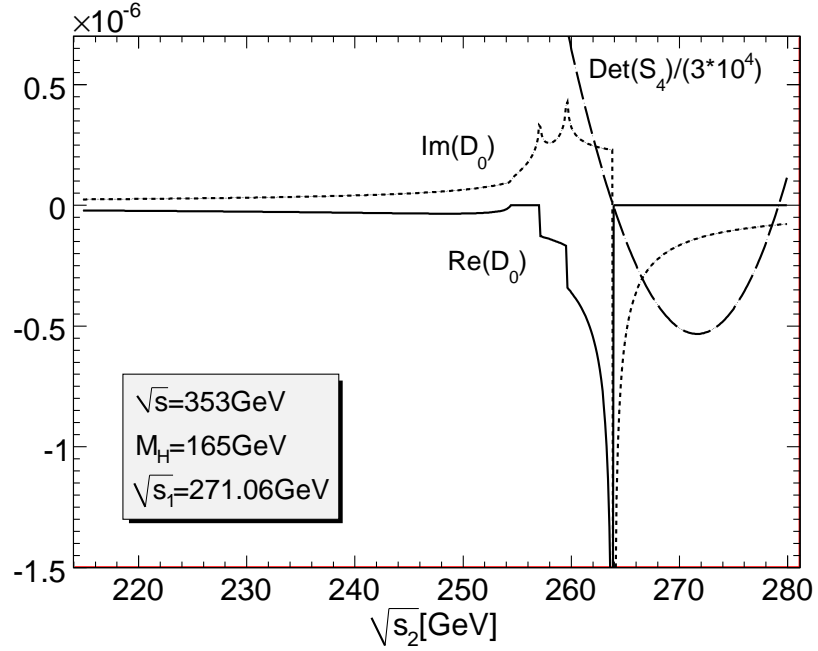


Figure 5.6: The imaginary, real parts of D_0 and the Landau determinant as functions of $\sqrt{s_2}$.

- The third discontinuity corresponds to the diagram of Fig. 5.5-right. The position of this Landau singularity is given by

$$s_2^s = \frac{1}{2m_t^2} \left(s(m_t^2 + M_W^2) - \sqrt{s} \sqrt{s - 4m_t^2} (m_t^2 - M_W^2) \right), \quad (5.23)$$

which gives $\sqrt{s_2} = 259.58$ GeV.

- The last singular discontinuity is the leading Landau singularity. The condition $\det(S_4) = 0$ for the box has two solutions which numerically correspond to $\sqrt{s_2} = 263.88$ GeV or $\sqrt{s_2} = 279.18$ GeV. Both values are inside the phase space, see Fig. 5.6. However after inspection of the corresponding sign condition, only $\sqrt{s_2} = 263.88$ GeV (with $x_1 \approx 0.53, x_2 \approx 0.75, x_3 \approx 0.77$) qualifies as a leading Landau singularity. $\sqrt{s_2} = 279.18$ GeV has $x_1 \approx -0.74, x_2 \approx -0.75, x_3 \approx 1.07$ and is outside the physical region.

The nature of the LLS in Fig. 5.6 can be extracted by using general formula (4.51). With the input parameters given above, the Landau matrix has only one positive eigenvalue at the leading singular point, *i.e.* $K = 1$. The leading singularity behaves as

$$D_0^{div} = -\frac{1}{16M_W^2 m_t^2 \sqrt{\det(S_4) - i\epsilon}}. \quad (5.24)$$

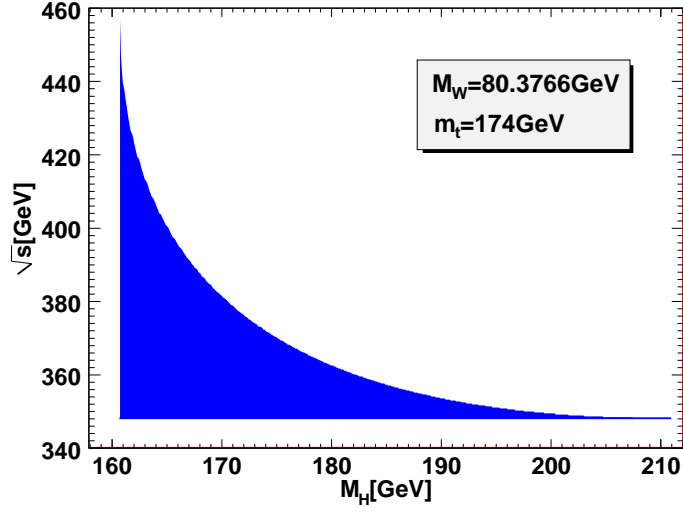
When approaching the singularity from the left, $\det(S_4) > 0$, the real part turns singular. When we cross the leading singularity from the right, $\det(S_4) < 0$, the imaginary part of the singularity switches on, while the real part vanishes. In this example, both the real and imaginary parts are singular because $\det(S_4)$ changes sign when the leading singular point is crossed.

At the position of the two 3-point sub-LLSs, the imaginary part shows logarithmic divergences while the real part has two finite negative jumps. This is similar to that shown in Fig. 5.2 whose explanation is given in Eq. (5.12). However, there is an important difference between Fig. 5.6 and Fig. 5.2 in the sign of the singularities. This is because the sign of the 3-point LLS is $(-1)^3$ (see Eq. (4.49) for $N = 3$) while the sign of the 3-point sub-LLS is $(-1)^4$ (see Eq. (4.72) for $N = 4$).

5.2.3 Conditions on external parameters to have LLS

The conditions for the opening of normal thresholds give the lower bounds on external parameters M_H^2 , s , $s_{1,2}$ as given in Eqs. (5.16) and (5.17). However, we have learnt from section 4.4 that the LLS can terminate as those external parameters increase. The conditions for the termination of LLS define the upper bounds of those parameters, as illustrated in subsection 5.2.1 for the case of 3-point function.

However, the situation becomes much more complicated in the case of 4-point function since there are 4 variables (M_H , s , s_1 , s_2) and 2 parameters (M_W , m_t) involved. We will show that there are two ways to find out the upper bounds by using numerical and analytical methods.

Figure 5.7: *The region of leading landau singularity.*

We first explain the numerical method to find the upper bounds of M_H^2 and s . This is done by a very simple Fortran code which includes the following steps. For each M_H^2 , what is the condition on s to have a LLS in the phase space? The Landau determinant takes the form $\det(Q_4) = as_2^2 + bs_2 + c$ as given in Eq. (5.20). If $\Delta = b^2 - 4ac < 0$ then there is no LLS. If $\Delta = b^2 - 4ac \geq 0$ then the Landau determinant can vanish at 2 points

$$s_2^\mp = \frac{-b \mp \sqrt{\Delta}}{2a}. \quad (5.25)$$

If s_2^\mp are not in the phase space defined by Eq. (5.14) then there is no LLS. If at least one root is in the phase space then we have to check condition (4.27). If this condition is satisfied then there is a LLS. The result is shown in Fig. 5.7. We conclude that the LLS occurs when $2M_W \leq M_H < 211\text{GeV}$ and $2m_t \leq \sqrt{s} < 457\text{GeV}$. The range of LLS region depends on M_W and m_t . If $m_t/M_W \leq 1$ then the first two conditions in Eq. (4.26) can never be satisfied. In particular, if $m_t/M_W = 1$ then the Landau determinant can vanish but the sign condition cannot be realised. When $M_H > 211\text{GeV}$ or $\sqrt{s} > 457\text{GeV}$ the Landau determinant $\det(Q_4)$ can vanish inside

the phase space but the sign condition $x_i > 0$ cannot be fulfilled.

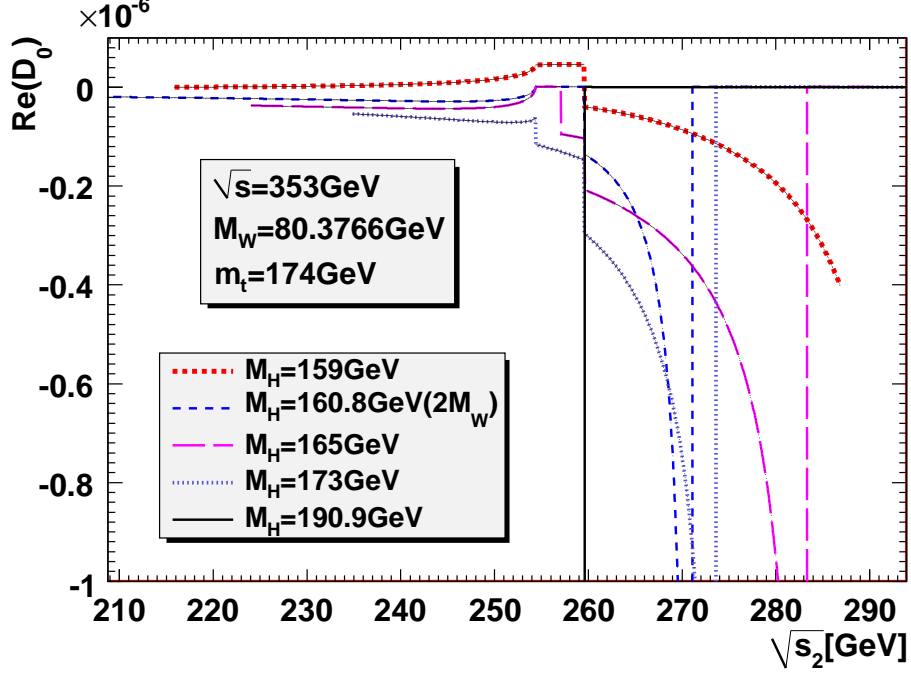


Figure 5.8: The real part of D_0 as a function of $\sqrt{s_2}$ for various values of M_H . For $M_H = 2M_W$ we have taken $s_1 = 2(m_t^2 + M_W^2)$. For the other cases, we take $s_1 = 260 \text{ GeV}$.

Before explaining the analytical method, we would like to show pictorially how the LLS moves and terminates as M_H increases. We fix $\sqrt{s} = 353 \text{ GeV}$ as in Fig. 5.6. We will increase M_H and look at the behaviour of the scalar 4-point function D_0 as a function of s_2 . We will explain what value of s_1 should be chosen. The result is shown in Fig. 5.8 which is just an extension of Fig. 5.6. The key points to understand this picture are as follows. At most, there are four discontinuities in the real part as a function of s_2 as already explained (see Fig. 5.6). When we fix s and increase M_H , two of them are fixed and the other two move. The normal threshold is fixed at $\sqrt{s_2^{tW}} = m_t + M_W = 254.3766 \text{ GeV}$, one 3-point sub-LLS is fixed at $\sqrt{s_2^s} = 259.576 \text{ GeV}$ as given in Eq. (5.23). The position of the other 3-point sub-LLS depends only on

M_H as given in Eq. (5.22). The position of LLS depends on M_H and s_1 as given in Eq. (5.25). As M_H increases, the Fig. 5.8 shows:

- For $M_H = 159\text{GeV} < 2M_W$, only the normal threshold and the three-point sub-LLS $\sqrt{s_2^s}$ show up.
- For $M_H = 2M_W$ the second three-point sub-LLS appears at $\sqrt{s_2^H} = 271.059\text{GeV}$. One has to change s_1 in the range defined by Eq. (5.14) with the condition $s_1 \geq (m_t + M_W)^2$ to make a LLS appeared. It is easy to find out that the LLS only occurs when $\sqrt{s_1} = \sqrt{2(m_t^2 + M_W^2)} = 271.059\text{GeV}$ and the LLS position coincides with the position of the three-point singularity $\sqrt{s_2^H}$. At this LLS point, the sign condition has the form $x_i = 0/0$ for $i = 1, 2, 3$. We have the ordering $\sqrt{s_2^{tW}} < \sqrt{s_2^s} < \sqrt{s_2^H} = \sqrt{s_2^{LLS}}$.
- For $M_H = 165\text{GeV}$ then $\sqrt{s_2^H} = 257.088\text{GeV}$ and we see that the LLS starts showing up at $\sqrt{s_2} \approx 283.5\text{GeV}$ when $\sqrt{s_1} \approx 260\text{GeV}$ (before this value there is no LLS) and moves to the left as $\sqrt{s_1}$ increases. We have the ordering $\sqrt{s_2^{tW}} < \sqrt{s_2^H} < \sqrt{s_2^s} < \sqrt{s_2^{LLS}}$.
- For $M_H \approx 173\text{GeV}$ then $\sqrt{s_2^H} = 254.3766\text{GeV}$ coinciding with the normal threshold and we see that the LLS starts showing up at $\sqrt{s_2} \approx 274\text{GeV}$ when $\sqrt{s_1} \approx 260\text{GeV}$ and moves to the left as $\sqrt{s_1}$ increases. After this value of M_H , the $\sqrt{s_2^H}$ -three-point singularity disappears from the physical region and the LLS continues moving to the left as M_H increases. We have the ordering $\sqrt{s_2^{tW}} = \sqrt{s_2^H} < \sqrt{s_2^s} < \sqrt{s_2^{LLS}}$.
- For the special value $M_H = 190.877\text{GeV}$, the LLS starts showing up and coincides with the fixed three-point singularity at $\sqrt{s_2} = \sqrt{s_2^s} = 259.576\text{GeV}$ when $\sqrt{s_1} \approx 260\text{GeV} \approx \sqrt{s_2^s}$ and moves off the physical region as $\sqrt{s_1}$ increases. If $M_H > 190.877\text{GeV}$ then the LLS disappears from the physical region.

We conclude that for $\sqrt{s} = 353\text{GeV}$, the upper bound of M_H to have a LLS is 190.877GeV which is consistent with Fig. 5.7. The above picture also leads to the

conclusion that the upper bound is determined when the LLS coincides with a sub-LLS. This important remark agrees with the explanation on the termination of LLS given in section 4.4.

We now are in the position to explain the equation of the upper bounds of M_H and \sqrt{s} , which is shown in Fig. 5.7, by using analytical method. The key points are as follows. The termination of LLS occurs when *all* LLSs coincides with a three-point sub-LLS. One should keep in mind that for each value of (M_H, \sqrt{s}) there may be a lot of LLSs corresponding to different values of (s_1, s_2) which make a $s_{1,2}$ -LLS-range. At the termination of LLS, this $s_{1,2}$ -LLS-range must become a point in order to coincide with a three-point sub-LLS.

If we express $\det(Q_4)$ as a quadratic polynomial of s_2 , there are 2 three-point sub-LLSs whose positions are given in Eqs. (5.22) and (5.23). Without losing any generality, we assume that the former coincides with the LLS. Thus, at the termination point we have

$$s_2 = s_2^H \quad \text{and} \quad \det(Q_4) = 0. \quad (5.26)$$

However, since our problem is completely symmetric under exchange of s_1 and s_2 , one should observe the same thing when expressing $\det(Q_4)$ as a quadratic polynomial of s_1 . The LLS therefore coincides with the s_2^H three-point sub-LLS when

$$s_1 = s_2^H \quad \text{and} \quad \det(Q_4) = 0. \quad (5.27)$$

We conclude that the LLS terminates when $s_1 = s_2$. With this information, the Eq. $\det(Q_4) = 0$ gives¹

$$s_1 = s_2 = 2(m_t^2 + M_W^2) - \sqrt{(s - 4m_t^2)(M_H^2 - 4M_W^2)}. \quad (5.28)$$

Equating the Eq. (5.28) with Eq. (5.22), we get

$$\sqrt{(s - 4m_t^2)} = \frac{1}{2M_W^2} \left(M_H(m_t^2 - M_W^2) - (m_t^2 + M_W^2)\sqrt{(M_H^2 - 4M_W^2)} \right). \quad (5.29)$$

¹Other roots do not satisfy the positive sign condition of the three-point sub-LLS.

We observe that this equation shows, in a very transparent way, that all thresholds:

$$m_t > M_W, M_H \geq 2M_W, \sqrt{s} \geq 2m_t$$

need to be open simultaneously. We can invert Eq. (5.29) to write the solution in terms of M_H . To arrive at the same result, it is more judicious however to go through exactly the same steps but choosing s_2^s instead of s_2^H . We derive

$$\sqrt{(M_H^2 - 4M_W^2)} = \frac{1}{2m_t^2} \left(\sqrt{s}(m_t^2 - M_W^2) - (m_t^2 + M_W^2)\sqrt{(s - 4m_t^2)} \right). \quad (5.30)$$

The maximum value of M_H (\sqrt{s}) is obtained by setting $\sqrt{s} = 2m_t$ ($M_H = 2M_W$), *i.e.* when the LLS, the two 3-point sub-LLSs and the normal threshold coincide. We have

$$\begin{aligned} 4M_W^2 &\leq M_H^2 \leq 4M_W^2 + \frac{(m_t^2 - M_W^2)^2}{m_t^2}, \\ 4m_t^2 &\leq s \leq 4m_t^2 + \frac{(m_t^2 - M_W^2)^2}{M_W^2}. \end{aligned} \quad (5.31)$$

Numerically, it means

$$348\text{GeV} \leq \sqrt{s} \leq 457.053\text{GeV} \quad \text{and} \quad 160.7532\text{GeV} \leq M_H \leq 211.129\text{GeV}. \quad (5.32)$$

Of course, those analytical formulae agree with the curve obtained by numerical method in Fig. 5.7.

There are many other ways to derive Eq. (5.29). Let us explain a very practical way. In order to obtain Eq. (5.29), we have assumed that $s_{1,2} = s_2^H$ as in Eq. (5.26). However, we can also equally assume that $s_{1,2} = s_2^s$ *i.e.* the LLS coincides with the other three-point sub-LLS. Of course, this assumption does lead to the same result². But this also means that, in order to have a unique result for the equation of upper bounds, at the termination of LLS one must have

$$s_2^s = s_2^H. \quad (5.33)$$

²This will fail if the equation of the upper bounds of s and M_H^2 (the maximum curve) is not analytic. If it happens, each assumption will give a part of the maximum curve.

Thus, a very practical way to quickly obtain the result Eq. (5.29) is equating two equations (5.22) and (5.23), without caring about Eq. $\det(Q_4) = 0$.

The same argument can be repeated for the two parameters $s_{1,2}$ to get their upper bounds. Namely, we express $\det(Q_4)$ as a quadratic polynomial of M_H^2 . The two 3-point singularities are found by considering the two reduced triangle diagrams containing p_5 as an external momentum. The equation of the upper bounds is obtained by requiring that $M_H^2(s_1) = M_H^2(s_2)$ (similar to Eq. (5.33)):

$$\begin{aligned} M_H^2 &= \frac{s_2(m_t^2 + M_W^2) - (m_t^2 - M_W^2)^2 - (m_t^2 - M_W^2)\sqrt{\lambda(s_2, m_t^2, M_W^2)}}{2m_t^2} \\ &= \frac{s_1(m_t^2 + M_W^2) - (m_t^2 - M_W^2)^2 - (m_t^2 - M_W^2)\sqrt{\lambda(s_1, m_t^2, M_W^2)}}{2m_t^2}, \end{aligned} \quad (5.34)$$

which is compatible with the sign condition $M_H^2 \leq [s_{1,2}(m_t^2 + M_W^2) - (m_t^2 - M_W^2)^2]/(2m_t^2)$ (the "plus" solution does not satisfies this); the equation writes

$$s_1 - s_2 = \frac{m_t^2 - M_W^2}{m_t^2 + M_W^2} \left[\sqrt{\lambda(s_1, m_t^2, M_W^2)} - \sqrt{\lambda(s_2, m_t^2, M_W^2)} \right]. \quad (5.35)$$

The maximum of s_2 is got from this equation by setting $s_1 = (m_t + M_W)^2$. We get

$$(m_t + M_W)^2 \leq s_{1,2} \leq (m_t + M_W)^2 + \frac{(m_t^2 - M_W^2)^2}{m_t M_W}, \quad (5.36)$$

which gives

$$254.3766\text{GeV} \leq \sqrt{s_{1,2}} \leq 324.442\text{GeV}. \quad (5.37)$$

From Eq. 5.35, one can make a very similar plot like the one in Fig. 5.7. We remark, by looking at Eqs. (5.31) and (5.36), that there is no LLS if $m_t = M_W$ (because $\sqrt{s} > M_H$).

A good question to ask is "What does the termination of the LLS mean physically?" The answer is very simple if one uses the physical interpretation of Coleman and Norton discussed in section 4.3. The relation between the Feynman parameter x_i and the proper time $d\tau_i = m_i x_i$ where $m_i = M_W, m_t$ means that at the termination of the LLS (when M_H or/and \sqrt{s} are large enough) at least one internal particle has zero proper time, *i.e.* it reaches the velocity of light.

5.3 The width as a regulator of Landau singularities

We will argue that the LLS which is not integrable at the level of one-loop amplitude squared can be tamed by introducing a width for unstable particles in the loops.

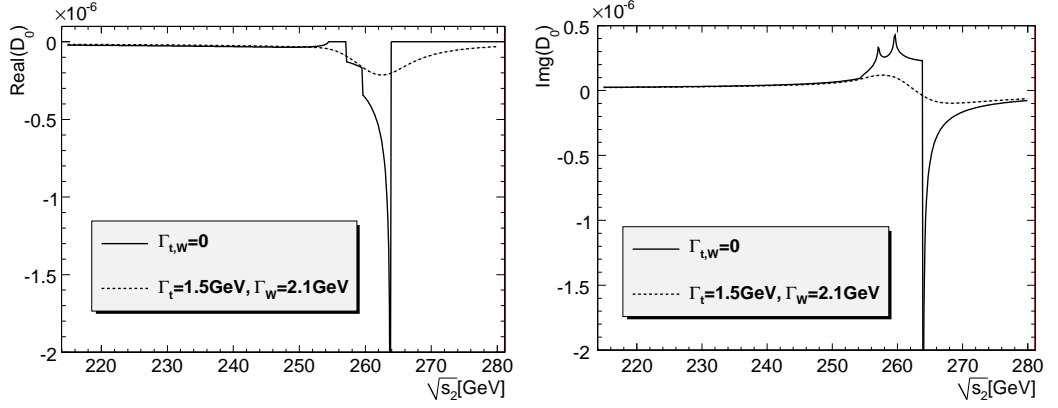


Figure 5.9: *Effect of the width of the W , Γ_W and the top, Γ_t , on the real and imaginary parts of the scalar four-point function.*

It is well-known that if internal unstable particles are on their mass shell, then one, in general, has to introduce a width for those particles. For example in the process $e^+e^- \rightarrow f\bar{f}$ at tree level, there is a pole in a S-channel diagram associated with the Z boson. It is obvious that one has to include the Z -width to solve this problem. On the other hand, there are several processes with unstable internal particles where the width effect is very small hence can be safely neglected. A famous example is a T-channel diagram. In that case, the internal particle is forced to be far away from the on-shell region.

In our case at hand, the LLS occurs when all loop internal particles (the top-quark and W Goldstone boson) are on-shell. Thus the width effect can be important. We take the simple prescription of a fixed width and make the substitution

$$m_t^2 \rightarrow m_t^2 - im_t\Gamma_t, \quad M_W^2 \rightarrow M_W^2 - iM_W\Gamma_W. \quad (5.38)$$

Mathematically, the width effect is to move Landau singularities into the complex plane, so they do not occur in the physical region (the real axis).

Applying rules (5.38) to the case of the scalar four-point function defined by Eq. (5.13) one sees in Fig. 5.9 that indeed the width regulates the LLS and gives a smooth result that nicely interpolates with the result at zero width away from the singularity. The normal threshold and the 3-point sub-leading singularity are also softened. The real part of the 4-point function still shows a smooth valley at the location of the LLS after regularisation. For the imaginary part we note that after introducing the width the LLS singularity is drastically reduced with a contribution of the order of the sub-leading singularity.

As we will explain in the next section and in more detail in Appendix E the introduction of the width in a four-point function requires careful extension of the usual 4-point function libraries.

In our calculation of Yukawa corrections where all the relevant couplings depend only on the top-quark mass and the vacuum expectation value v , we will keep m_t and v real while applying rules (5.38) to all the loop integrals³.

5.4 Calculation and checks

The one-loop calculation of this chapter is exactly the same as in the real mass case (see section 3.4) except the fact that we now have to consider the tensorial and scalar loop integrals with complex masses.

LoopTools [33] can handle the complex masses up to 3 point functions. The 5 point functions are reduced to 4 point functions [12, 34]. The tensorial 4 point functions

³In a general calculation of full electroweak correction and if one chooses the input parameters to be $\{\alpha(0), M_W, M_Z, m_t, \dots\}$ then rules (5.38) should be applied everywhere in the calculation so that the EW gauge invariance can be preserved. This idea of doing analytical continuation on gauge boson masses is the philosophy of the complex-mass scheme [116, 15]. For a practical discussion of methods to deal with unstable particles, see Denner's lecture notes at [117].

are reduced to the scalar 4 point function and 3 point functions. We therefore have to calculate only the scalar 4 point function. The analytical calculation of scalar 4-point function with complex masses in the most general case is practically intractable. The standard technique of 't Hooft and Veltman [118] has some restriction on the values of external momenta. In particular, the method works if at least one of the external momenta is lightlike. In that case, the result is written in terms of 72 Spence functions. In our present calculation, there are at least 2 lightlike external momenta in all boxes. If the positions of two lightlike momenta are opposite then we can write the result in terms of 32 Spence functions. If the two lightlike momenta are adjacent, the result contains 60 Spence functions. The detailed derivation and results are given in the Appendix E. We have implemented those analytical formulae for the case of two massless external momenta into a code and added this into LoopTools⁴. All the five point functions which have problem with Landau singularities in our calculation have 4 external massless momenta (two gluon and two bottom quarks). Thus they can always be reduced to a set of 4- point functions with at least 2 massless external momenta.

Checks on the loop integrals with complex internal masses: for all the tensorial and scalar loop integrals (4- and 5- point functions), we have performed a consistency check where we have made sure that the results with complex internal masses become asymptotic to the ones with real internal masses in the limit $widths \rightarrow 0^+$. For the scalar loop integrals, the results are compared to the ones calculated numerically in the limit of large widths, *e.g.* $\Gamma_{t,W} = 100\text{GeV}$. Furthermore, for the scalar box integrals the results can be checked by using the segmentation technique described in [119]. The idea is the following. At the boundary of the phase space, the 4- point functions can be written as a sum of 4 three point functions. The 3-point functions with complex masses can be calculated by using LoopTools. In this way, we have verified that the results of the scalar 4-point functions are correct at the boundary of

⁴The implementation for the case of one massless external momentum is straight forward. However, we have not done this yet since it is not necessary for our present calculation.

phase space. We have also carried out a comparison with a purely numerical approach based on an extension of the ϵ -extrapolation technique [120]. We have found perfect agreement⁵.

For the whole calculation, we have performed two checks at the amplitude level. First, by taking the limit $widths \rightarrow 0^+$ we have observed that the results approach to the results calculated with real internal masses. This again is just a consistency check. Second and it is the most important check where we have verified that the results calculated with complex internal masses are QCD gauge invariant.

As the LLS is integrable at interference level, the NLO calculation with $\lambda_{bbH} \neq 0$ performed in chapter 3 can be trivially extended to the region of $M_H \geq 2M_W$ by using the same method without introducing widths for unstable internal particles. However, there is a small problem related to the universal correction $(\delta Z_H^{1/2} - \delta v)$ where $\delta Z_H^{1/2}$ related to the derivative of the Higgs two-point function becomes singular when M_H equal to $2M_W$ or $2M_Z$. This problem is separately treated by introducing the widths of the W and the Z . To be complete, the results are given in section 5.6.

5.5 Results in the limit of vanishing λ_{bbH}

The input parameters and kinematical cuts are the same as given in section 3.5. We write here additional parameters related to the widths of unstable particles appearing in the calculation:

$$\Gamma_W = 2.1\text{GeV}, \quad \Gamma_Z = 2.4952\text{GeV}, \quad (5.39)$$

the top-quark width is calculated at the tree level in the SM

$$\Gamma_t = \frac{G_\mu(m_t^2 - M_W^2)^2(m_t^2 + 2M_W^2)}{8\pi\sqrt{2}m_t^3} \approx 1.5\text{GeV} \quad (5.40)$$

where the bottom-quark mass has been neglected.

⁵We thank F. Yuasa for sending us the results of the extrapolation technique.

5.5.1 Total cross section

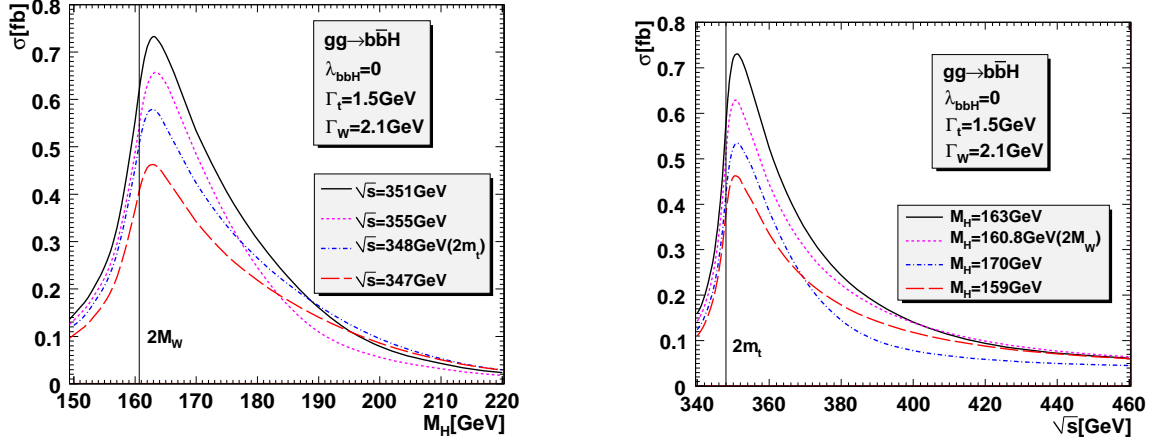


Figure 5.10: *Left: the cross section for the subprocess $gg \rightarrow b\bar{b}H$ as functions of M_H for various values of \sqrt{s} including the case $\sqrt{s} = 2m_t = 348\text{ GeV}$. Right: the cross section for the subprocess $gg \rightarrow b\bar{b}H$ as functions of \sqrt{s} for various values of M_H including the case $M_H = 2M_W = 160.7532\text{ GeV}$.*

We start with the cross section in the case where $\lambda_{bbH} = 0$. In section 3.5 we reported on results up to $M_H = 150\text{ GeV}$ that showed that this cross section was rising fast as one approached the threshold $M_H = 2M_W$. Beyond this threshold our integrated cross sections showed large instabilities. As discussed in subsection 5.2.2 this is due to the appearance of a leading singularity which as we have advocated can be cured by the introduction of a width for the unstable top-quark and W gauge boson. Before convoluting with the gluon distribution function let us briefly look at the behaviour of the partonic cross section $gg \rightarrow b\bar{b}H$ paying a particular attention to this leading Landau singularity region shown in Fig. 5.7, see also Eq. 5.31.

Figs 5.10 show that indeed the widths do regulate the cross section. Moreover it is within the range of LLS that the cross section is largest. The (highest) peak of the cross section occurs for a Higgs mass about 163 GeV (slightly higher than the normal threshold value $2M_W = 160.7532\text{ GeV}$) and for $\sqrt{s} \approx 351\text{ GeV}$ (slightly higher than the

normal threshold value $2m_t = 348\text{GeV}$). The peak positions are slightly shifted from the normal threshold values, this is due to the width effect. The reason for the peak to occur at the normal threshold position is that *all* Landau singularities (leading and sub-leading) start showing up at this point and the size of Landau singularity region is largest at the position of normal threshold, see Fig. 5.7. To see the LLS effect, we look at the two curves $\sqrt{s} = 347\text{GeV}$ and $\sqrt{s} = 2m_t = 348\text{GeV}$ of Fig. 5.10(left). For the former, there is no LLS and the peak effect is due to sub-LLSs (the normal thresholds and 3-point sub-LLSs). The later includes additional LLS contribution, which is significant even after being regulated. We emphasize that although the 4-point LLS is special in the sense that it is not integrable at the level of one-loop amplitude squared one should not overlook this point and use it as an account for the bulk of the large correction around the normal threshold position. The 3-point (sub-) LLSs and normal thresholds have also significant contributions.

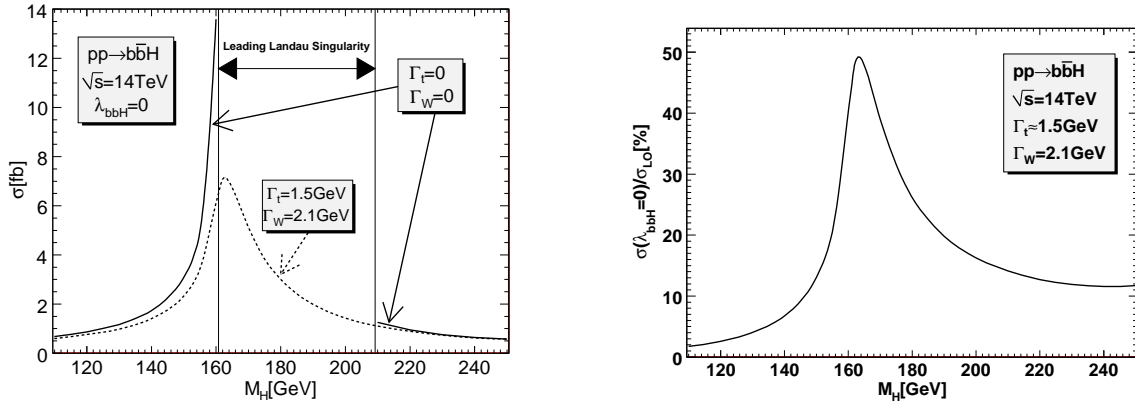


Figure 5.11: *Left: the one-loop induced cross section as a function of M_H in the limit of vanishing bottom-Higgs Yukawa coupling for two cases: with and without widths. Right: the percentage correction of the contribution with widths relative to the tree level cross section calculated with $\lambda_{b\bar{b}H} \neq 0$.*

The cross section at the pp level for the 14TeV centre of mass energy (LHC) as a function of the Higgs mass is shown in Fig. 5.11 taking into account the width

of the top-quark and the W gauge boson. For comparison we also show the cross section without the width effect outside the leading Landau singularity range of M_H . The sharp rise above $M_H > 150\text{GeV}$ is nicely tamed. On the other hand note that on leaving the leading Landau singularity region around $M_H = 211\text{GeV}$, the width effect is much smaller and the figures suggest that one could have entered this region from the right without having recourse to introducing a width. Indeed our numerical integration routine over phase space with the default LoopTools library does not show any bad behaviour until we venture around values of $2M_W < M_H < 200\text{GeV}$. The reason for this can be understood by taking a glance at Fig. 5.7. For $200\text{GeV} < M_H < 211\text{GeV}$ the singularity region is considerably shrunk so that one is integrating over an almost zero measure. The effect of the widths outside the singularity region is to reduce the cross section for $M_H = 120\text{GeV}$, 140GeV and 150GeV by⁶ respectively 15%, 24% and 33% while for $M_H = 210\text{GeV}$, 230GeV and 250GeV the reduction is comparatively more modest with respectively 15%, 5% and 2%.

The relative correction to the tree level cross section is shown in Fig. 5.11 (right). It amounts to 2.6% for $M_H = 120\text{GeV}$, increases to as much as 49% when $M_H = 163\text{GeV}$ and finally becomes almost constant at about 10% for large values of M_H . Large contribution is due to the effect of Landau singularities.

5.5.2 Distributions

⁶The relative difference is defined by $[\sigma(\Gamma = 0) - \sigma(\Gamma \neq 0)]/\sigma(\Gamma \neq 0)$.

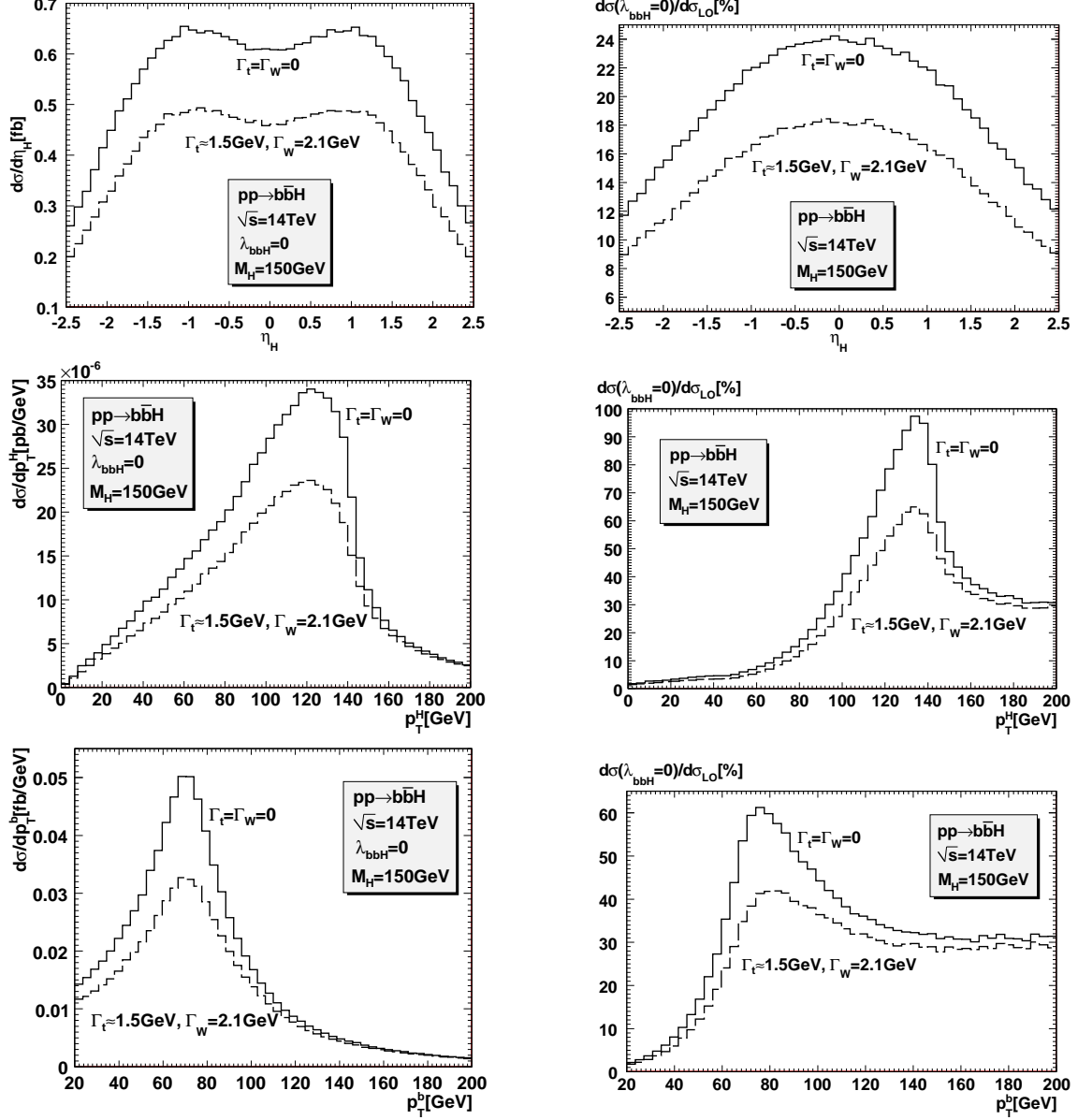


Figure 5.12: Left: The pseudo-rapidity of the Higgs and transverse momentum distributions of the Higgs and the bottom for $M_H = 150\text{GeV}$ arising from the purely one-loop contribution in the limit of vanishing LO ($\lambda_{bbH} = 0$) for two cases: with and without widths. Right: Its relative percentage contribution $d\sigma(\lambda_{bbH} = 0)/d\sigma_{LO}$ is also shown.

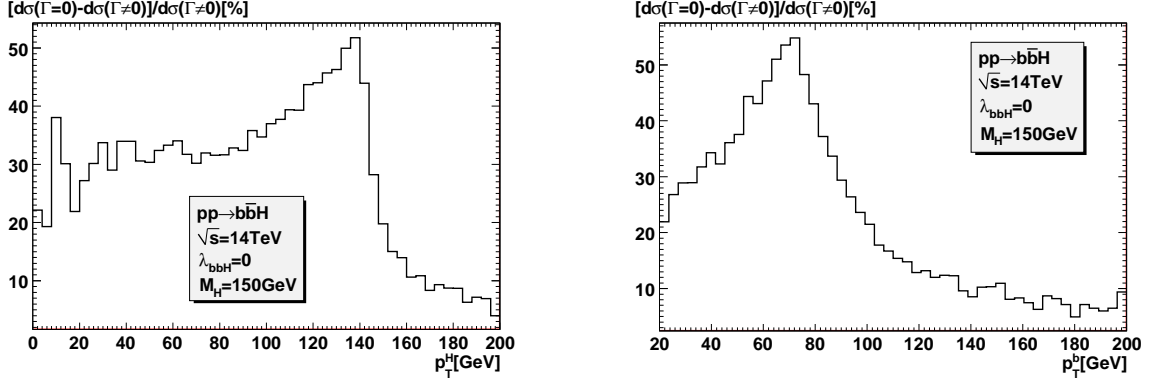


Figure 5.13: The relative difference between two cases: with and without widths, defined by $[d\sigma(\Gamma = 0) - d\sigma(\Gamma \neq 0)]/d\sigma(\Gamma \neq 0)[\%]$, for the transverse momentum distributions of the Higgs and the bottom quark.

In order to see the width effect on distributions, we first consider the case where $M_H = 150\text{GeV} < 2M_W$ (no LLS in this case). Figures 5.12 and 5.13 show the difference between the two cases: with and without widths. The relative difference is rather uniform, about 33%, on the Higgs pseudorapidity distribution. For the transverse momentum distributions, the relative difference is not uniform but has structure as shown in Figure 5.13. We remark that the peaks in the transverse momentum distributions occur at the position where the width effect is largest, hence are related to the opening of sub-leading Landau singularities as discussed in the previous subsection.

The largest relative corrections to the tree level distributions are shown in Fig. 5.14 for the case $M_H = 163\text{GeV} > 2M_W$ (LLS does occur here) which corresponds to the maximum value of the cross section in the limit $\lambda_{bbH} = 0$ as displayed in Fig. 5.11 (right). The correction to the Higgs pseudorapidity distribution is about 60% around the center region. The corrections to the p_T distributions can be enormous in some region of phase space, up to 200% for the Higgs and about 170% for the bottom-quark case. These huge corrections to the distributions in some region of phase space are again due to the effect of Landau singularities.

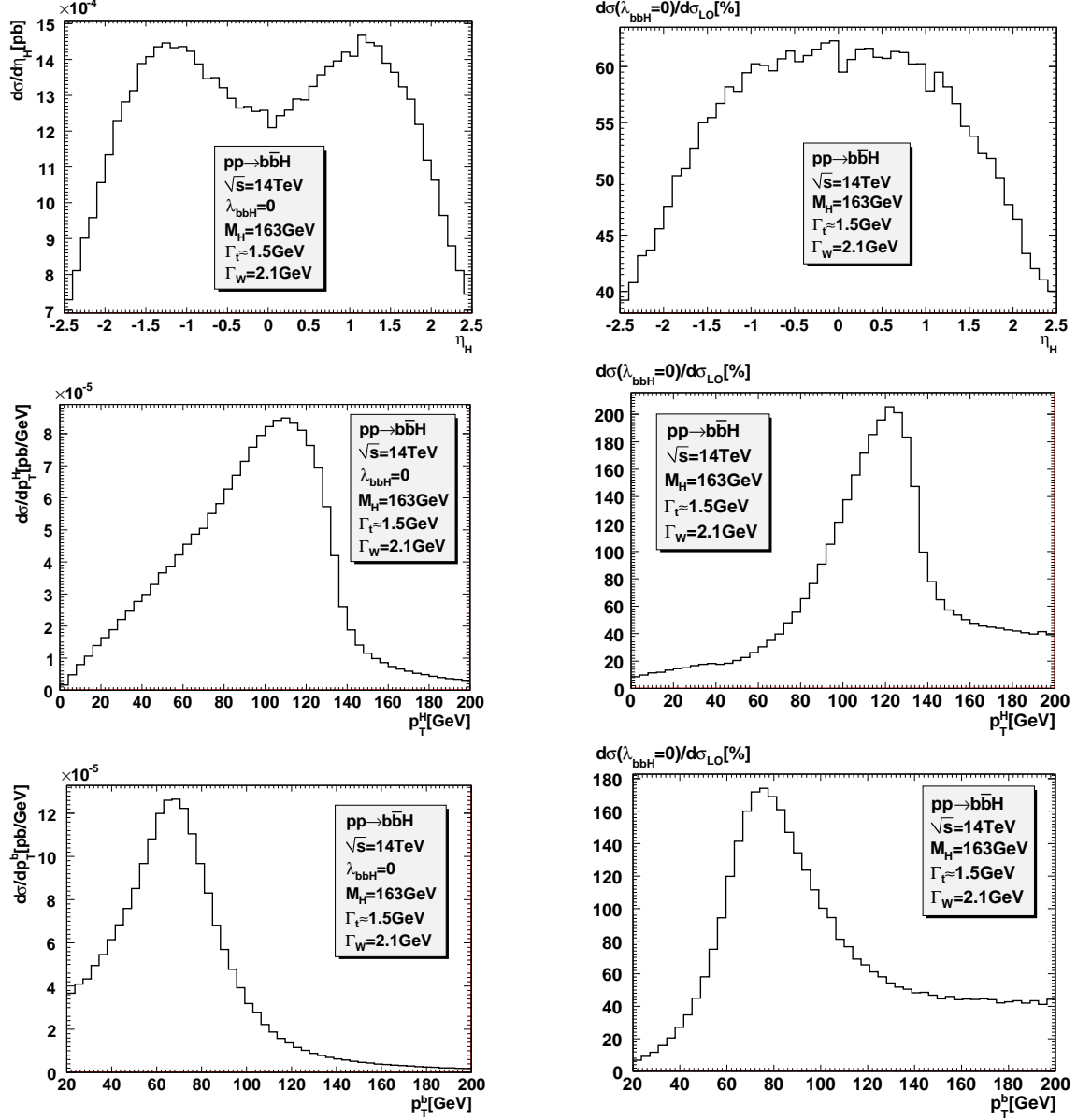


Figure 5.14: Left: The pseudo-rapidity of the Higgs and transverse momentum distributions of the Higgs and the bottom for $M_H = 163 \text{ GeV}$ arising from the purely one-loop contribution in the limit of vanishing LO ($\lambda_{bbH} = 0$). Right: Its relative percentage contribution $d\sigma(\lambda_{bbH} = 0)/d\sigma_{LO}$ is also shown

5.6 Results at NLO with $\lambda_{bbH} \neq 0$

The purpose of this section is to complete the study of subsection 3.5.2, to cover higher values of Higgs mass. Moreover, we would like to know the width effect at NLO in the presence of Landau singularities in various one-loop diagrams. We recall that the LLS is integrable at NLO.

As discussed in subsection 3.2.3 the NLO Yukawa corrections consist of 3 gauge invariant classes, see Fig. 3.4. The study of subsection 3.5.2 revealed that class (a) gives a totally negligible correction below 0.1%. We will not discuss this contribution any further here. Moreover, leading Landau singularities we have discussed only show up in class (c). We will therefore study separately the NLO correction due to class (c) and weigh the effect of implementing the width of the internal particles. Class (b) does not develop any leading Landau singularity and therefore the width effect will be marginal.

5.6.1 Width effect at NLO

The class (c) has problem with the 4-point LLS. However, this LLS is integrable at NLO. Thus one can calculate the NLO cross section without introducing widths for unstable particles in loops. However, one can still expect some effect of Landau singularities (leading and sub-leading) and wonder if the width effect is significant in this case? The answer to this question is given in Fig. 5.15.

The results in this plot are calculated by setting $m_b = 0$ in the kinematics (spinors and propagators) and loop integrals while keeping $m_b = 4.62\text{GeV}$ only in the λ_{bbH} coupling which can be regarded as an independent parameter. The first remark is that if $M_H < 158\text{GeV}$ or $M_H > 165\text{GeV}$ then the NLO width effect is below 5%. For $M_H < 158\text{GeV}$ the W-Goldstone bosons in the loops can never be on-shell and thus the width effect is completely small. For $M_H > 165\text{GeV}$ the W-Goldstone bosons can be on-shell and thus the width effect is a bit bigger than in the former case. Indeed

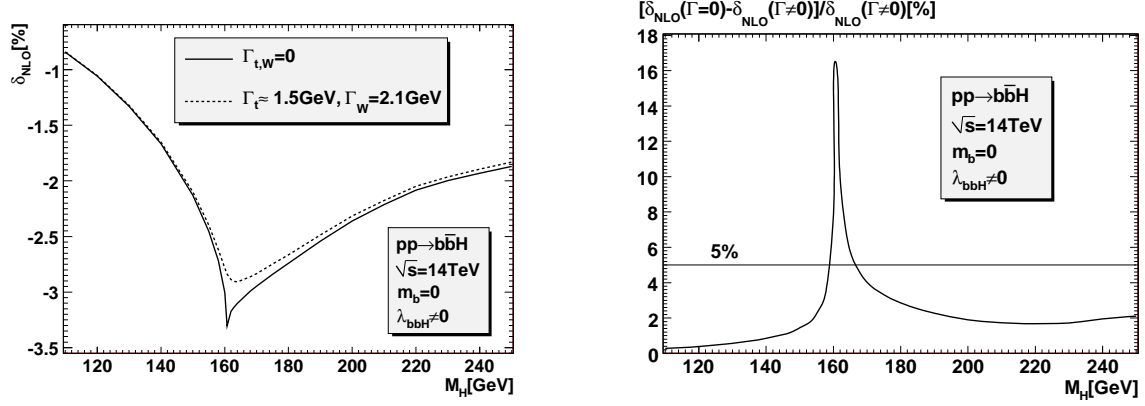


Figure 5.15: The relative difference between two cases: with and without widths, defined by $[d\sigma(\Gamma = 0) - d\sigma(\Gamma \neq 0)]/d\sigma(\Gamma \neq 0)[\%]$, for the NLO correction of the class (c) where the LLS occurs. The tree-level amplitude is calculated with massive bottom quark. The one-loop amplitude is calculated by keeping m_b only in the λ_{bbH} coupling.

even at the peak $M_H = 2M_W$ the width effect is just about 17%. From this analysis we conclude that the width effect at the NLO is small and can be neglected.

5.6.2 NLO corrections with $m_b \neq 0$

The results for the NLO corrections are shown in Fig. 5.16 (left). For classes (b) and (c) the widths of unstable particles are neglected. For the universal correction, $(\delta Z_H^{1/2} - \delta v)$ where $\delta Z_H^{1/2}$ involving the derivative of the two-point function Higgs self-energy diverges when M_H is equal to $2M_W$ or $2M_Z$, all the widths of unstable particles are kept ⁷.

The effect of Landau singularities is obvious if one compares the (c)-curve to the (b)-curve. The contribution from class (b) where the Higgs couples to the internal top decreases very slowly as the Higgs mass increases from 110GeV to 250GeV, as expected there is no structure as would be the case if this contribution were sensitive

⁷Note that $\delta Z_H^{1/2}$ does not diverge when $M_H = 2m_t$ and the top-quark width thus has a marginal effect.

to any threshold or singularity. Class (c) on the other hand does, as expected, reveal some structure around $M_H = 2M_W$ where we see a fall in the relative correction. The correction is however, despite this fall, quite modest ranging from about -1% for $M_H = 160\text{GeV}$ to about -4% for $M_H = 210\text{GeV}$.

The universal correction, $(\delta Z_H^{1/2} - \delta v)$, contributes from -1% to -3% , where the highest correction is at the $H \rightarrow WW$ threshold ($M_H = 2M_W$).

The detailed structure of the class (c) is shown in Fig. 5.16 (right). It consists of two independent helicity structures where the helicities of two bottom quarks in the final state are the same or different. We call them $\delta_{\lambda_3, \lambda_4}$ and $\delta_{\lambda_3, -\lambda_4}$ structures. In the massless bottom limit whose result is displayed in Fig. 5.15, only the $\delta_{\lambda_3, -\lambda_4}$ structure survives. It is remarked that the behaviors of two different helicity structures as functions of M_H are very different despite the fact that they both have a common denominator.

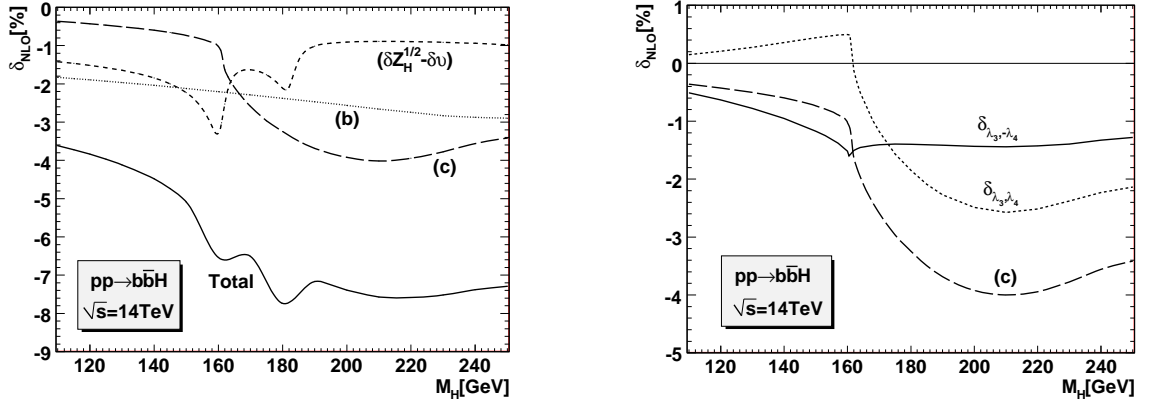


Figure 5.16: *Left: The relative NLO EW corrections normalized to the tree-level cross section. (b) and (c) correspond to the two classes of diagrams displayed in Fig. 3.4. $(\delta Z_H^{1/2} - \delta v)$ is the universal correction contained in the renormalization of the $b\bar{b}H$ vertex. "Total" refers to the sum of those 3 corrections. $\delta Z_H^{1/2}$ is calculated by taking into account the widths of W , Z and the top quark. Right: the structure of (c)-correction which is a sum of two independent helicity configurations.*

5.7 Summary

We have extended the study of section 3.5 to cover higher values of M_H . This study is important and highly nontrivial due to the appearance of Landau singularities in various one-loop Feynman diagrams when $M_H \geq 2M_W$.

We have applied the general study of Landau singularities, presented in chapter 4, to the specific case of $gg \rightarrow b\bar{b}H$. Namely, we have studied in detail the LLS in the case of one-loop 3-point and 4-point functions. The nature of those LLS is carefully explained by using two different methods. On one hand, we used the general formulae (which are for the singular part only) obtained in section 4.4. On the other hand, we used explicit results obtained by performing loop integrals using the traditional method of 't Hooft and Veltman. The latter results in various plots of real and imaginary parts of scalar loop integrals. This indeed helped us to understand much better the various structures of Landau singularities.

We have performed a detailed study to understand how the LLS terminates. From this, we got the upper bounds of external parameters.

We have argued that the problem of 4-point LLS, which is not integrable at the level of one-loop amplitude squared, is solved by introducing a width for internal unstable particles. In order to do so, we have applied the loop calculation method of 't Hooft and Veltman to write down explicitly two formulae to calculate scalar box integrals with complex internal masses (see Appendix E). The restriction is that at least two external momenta are lightlike. We have implemented those two formulae into the library LoopTools.

We have studied the width effect in the presence of Landau singularities in various one-loop diagrams. At NLO, the width effect is negligible. At NNLO, the width effect is extremely important around the normal threshold position ($M_H = 2M_W$).

We have shown various results of one-loop corrections to the cross section as well as important distributions. NNLO corrections, calculated in the limit $\lambda_{b\bar{b}H} = 0$,

can be very large in some region of phase space or parameter space where Landau singularities show up. For the p_T distribution, those corrections can be enormous. NLO corrections remain small although some structure related to Landau singularities does show up.

Chapter 6

Conclusions

In the previous chapters, we have explained how to calculate one-loop Yukawa corrections to the process of SM Higgs production associated with two high p_T bottom quarks at the LHC and their physical content. In particular, we have studied one-loop Landau singularities and shown how to handle them in practice for our process. The properties and effect of the Landau singularities in the process $pp \rightarrow b\bar{b}H$ were also carefully investigated.

The entirely dominant contribution to the process $pp \rightarrow b\bar{b}H$ is the sub-process $gg \rightarrow b\bar{b}H$. The physics of one-loop Yukawa corrections to this sub-process is very rich due to the fact that the bottom-quark and the top-quark are in the same $SU(2)_L$ doublet with a large mass splitting. At tree level, the Higgs boson couples directly to bottom quarks with a small Yukawa coupling λ_{bbH} . At one-loop level, the Higgs can couple to heavy particles like the top-quark or W Goldstone bosons. Thus, it is easy to see that, if we do the expansion in the small coupling λ_{bbH} , the one-loop corrections can still give some contribution when this coupling vanishes. The salient property of the one-loop corrections is related to the smallness of m_b and is best seen if we take the limit $m_b \rightarrow 0$ while keeping λ_{bbH} (which can be regarded as a different parameter) unchanged. In this limit, the tree level contribution contains

only *even* helicity configurations ("even" means that both bottom-quarks have the same helicity) while the one-loop contribution includes both even and *odd* helicity configurations ("odd" means that the two bottom-quarks have opposite helicities). The even one-loop contribution is proportional to the small λ_{bbH} while the odd one, which comes from m_t insertion in loops, is independent of λ_{bbH} and proportional to large couplings like λ_{ttH} and λ_{HHH} . We remark immediately that the NLO correction is proportional to λ_{bbH}^2 hence must be small. However, the most interesting thing is that the purely one-loop contribution which can be extracted by setting $\lambda_{bbH} = 0$ consists of only odd helicity configurations. Thus, this new loop induced contribution can be very different from the tree level or NLO contributions. Moreover, the best way to understand Landau singularities, which are intrinsic analytic properties of loop integral, is to look at purely loop corrections.

The numerical results of chapters 3 and 5 confirm those qualitative conclusions. The NLO correction is small and changes from -4% for $M_H = 120\text{GeV}$ to -8% at $M_H = 2M_Z$ stabilising to around -7% for larger values of M_H up to 250GeV , despite the appearance of various Landau singularities. The purely one-loop contribution (NNLO), calculated by taking into account the widths of the top-quark and W gauge boson, amounts to 2.6% for $M_H = 120\text{GeV}$, increases to as much as 49% when $M_H = 163\text{GeV}$ and finally becomes almost constant at about 10% for large values of M_H . The difference between the two corrections becomes clearest when one looks at the p_T distributions. The NNLO correction to p_T distributions can be enormous in some region of phase space for M_H about $2M_W$ while the NLO correction is modest. Large NNLO corrections are due to the effect of Landau singularities and occur around the normal threshold position $M_H = 2M_W$.

Calculating one-loop corrections contains a lot of technical features. The amplitude squared was calculated by using the helicity amplitude method (HAM) where each helicity amplitude, which is a complex number, is numerically calculated. In order to do so, we have reduced all loop integrals (up to five-point function) in terms of Passarino-Veltman loop functions. This was easily done with the help of LoopTools.

After doing so, we obtained a huge algebraic expression for each helicity configuration which takes a lot of computer time to calculate. The problem was how to optimise the calculation. We found a systematic way to do this by using FORM based on the fact that each helicity amplitude can be factorised in terms of independent blocks. The advantage is that some complicated blocks which appear several times in the computation can be put in a common sector hence just need to be calculated once.

In our calculation with two gluons as external particles, the HAM leads to a very easy and convenient way to check the QCD gauge invariance which means that the amplitude squared is independent of the reference vectors needed to define the gluon polarization vectors. Indeed, this is a very powerful way to check the correctness of the results and can be used for other processes with at least one external gluon/photon.

Another advantage of HAM is that since the tree-level and one-loop helicity amplitudes are calculated separately, the one-loop amplitude squared is immediately obtained when the NLO calculation is done.

There is a special class of one-loop $gg \rightarrow b\bar{b}H$ diagrams where the Higgs boson is produced by W gauge boson fusion. If the Higgs mass is heavy enough for this normal threshold to open ($M_H \geq 2M_W$), then all Landau singularities of two-, three-, four- point functions show up. In particular, the four-point leading Landau singularity leads to severe numerical instabilities when we calculate the cross section involving the square of a one-loop amplitude. We have solved this problem by taking into account the fact that W gauge boson and the top-quark are unstable particles hence have a width. For this, we have followed the standard technique of 't Hooft and Veltman to calculate scalar four-point functions with complex internal masses. The restriction is that at least two external momenta are lightlike. We have implemented those formulae into the library LoopTools. Various checks have been performed to make sure that this implementation is correct. We have also observed that the same implementation can be done for the case of one lightlike external momentum. However, the calculation of the scalar four-point functions with complex internal masses in the most general case

with no restriction on the external momenta is not tractable if one uses the method of 't Hooft and Veltman. Another disadvantage of this method is that the results, even in some special cases with massless external particle, contain many Spence functions. It may be better to find another way.

Although the main calculation of this thesis is for a very specific process, it is quite obvious for us that some of the results discussed above can be used or generalised for other complicated one-loop calculations.

Appendix A

The helicity amplitude method

A.1 The method

We use a combination of helicity amplitude methods as described in [36, 121] to calculate the total cross section. In the following we only want to highlight some key features that were most useful for our calculation, for details of the method we refer to [36, 121]. For our process $g(p_1, \lambda_1) + g(p_2, \lambda_2) \rightarrow b(p_3, \lambda_3) + \bar{b}(p_4, \lambda_4) + H(p_5)$ where the particles are denoted by their momentum p_i and helicity λ_i we write the corresponding helicity amplitude as $\mathcal{A}(\lambda_1, \lambda_2; \lambda_3, \lambda_4)$.

$$\begin{aligned}\mathcal{A}(\lambda_1, \lambda_2; \lambda_3, \lambda_4) &= \epsilon_\mu(p_1, \lambda_1; q_1) \epsilon_\nu(p_2, \lambda_2; q_2) \mathcal{M}^{\mu\nu}(\lambda_3, \lambda_4), \\ \mathcal{M}^{\mu\nu}(\lambda_3, \lambda_4) &= \bar{u}(p_3, \lambda_3) \Gamma^{\mu\nu} v(p_4, \lambda_4).\end{aligned}\tag{A.1}$$

$\Gamma^{\mu\nu}$ is a string of Dirac γ matrices. These γ matrices represent either interaction vertices or momenta from the fermion propagators. In our case the interaction vertices are the vectorial gluon vertices in which case they represent $\not{\epsilon}_i$, the scalar Higgs vertex and at one-loop the pseudo-scalar Goldstone coupling. For the momenta, in our implementation we re-express them in terms of the independent external momenta p_1, p_2, p_3, p_4 . This applies also to the loop momenta after the reduction formalism

of the tensor integrals has been performed. The first step in the idea of the helicity formalism we follow is to turn each of these γ matrices (apart from the pseudo-scalar and the trivial scalar) into a combination of spinor function $u\bar{u}$. We therefore transform our helicity amplitude into products of spinors such as the helicity amplitude could be written like a product $\bar{u} u \bar{u} \dots u \bar{u} v$ with the possible insertion of γ_5 's in the string. The different u, \bar{u}, v in the string we have written have of course, in general, different arguments. Nonetheless one can turn each spinor product of two adjacent $\bar{u}u$, etc into a complex number written in terms of the momenta in our problem as we will see.

In the first step, for the momentum \not{p}_i with $p_i^2 = m_i^2$ we use

$$\not{p}_i = u(p_i, -)\bar{u}(p_i, -) + u(p_i, +)\bar{u}(p_i, +) - m_i. \quad (\text{A.2})$$

The transverse polarization vector of the initial gluon i , $\epsilon_\mu(p_i, \lambda_i; q_i)$, is also first expressed in terms of spinors such as

$$\epsilon_\mu(p_i, \lambda_i; q_i) = \frac{\bar{u}(p_i, \lambda_i)\gamma_\mu u(q_i, \lambda_i)}{[4(p_i \cdot q_i)]^{1/2}}, \quad (\text{A.3})$$

where q_i is an *arbitrary* reference vector satisfying the following conditions

$$q_i^2 = 0, \quad p_i \cdot q_i \neq 0. \quad (\text{A.4})$$

Using the trace technique one can easily prove that definition (A.3) indeed satisfies the physical polarisation sum identity given in Eq. (1.4), namely

$$\sum_{\lambda=\pm} \epsilon_\mu(p, \lambda; q) \epsilon_\nu(p, \lambda; q)^* = -g_{\mu\nu} + \frac{p_\mu q_\nu + p_\nu q_\mu}{p \cdot q}. \quad (\text{A.5})$$

Gauge invariance (transversality condition) requires that the cross sections are independent of the choice of the reference vector as we will see later. This acts as an important check of the calculation, see later. It is not difficult to prove that the choice (A.3) satisfies all the conditions for a transverse polarization vector. In particular,

$$\begin{aligned} p_i \cdot \epsilon(p_i, \lambda_i) &= 0, \quad \epsilon(p_i, \lambda_i) \cdot \epsilon(p_i, \lambda_i) = 0, \\ \epsilon_\mu(p_i, -\lambda_i) &= \epsilon_\mu(p_i, \lambda_i)^*, \quad \epsilon(p_i, \lambda_i) \cdot \epsilon(p_i, -\lambda_i) = -1, \end{aligned} \quad (\text{A.6})$$

where the reference vector is not written down explicitly. $i = 1, 2$ and no sum over i must be understood. Then for $\not{\epsilon}_i = \epsilon_\mu \gamma^\mu$ one uses the so-called Chisholm identity

$$\bar{u}(p, \lambda) \gamma_\mu u(q, \lambda) \gamma^\mu = 2[u(p, -\lambda) \bar{u}(q, -\lambda) + u(q, \lambda) \bar{u}(p, \lambda)], \quad (\text{A.7})$$

where all the spinors in Eq. (A.7) are for massless states in view of the lightlike condition on the reference frame vector and of course the momentum of the real gluon.

With $U(p_i, \lambda_i)$ representing either $u(p_i, \lambda_i)$ or $v(p_i, \lambda_i)$ one uses the general formulae

$$\begin{aligned} \bar{U}(p_i, \lambda_i) \gamma_5 U(p_j, \lambda_j) &= -\lambda_i \frac{A_{\lambda_i \lambda_j}(p_i, p_j) - M_i B_{\lambda_i \lambda_j}(p_i, p_j) + M_j C_{\lambda_i \lambda_j}(p_i, p_j)}{\sqrt{(p_i \cdot k_0)(p_j \cdot k_0)}}, \\ \bar{U}(p_i, \lambda_i) U(p_j, \lambda_j) &= \frac{A_{\lambda_i \lambda_j}(p_i, p_j) + M_i B_{\lambda_i \lambda_j}(p_i, p_j) + M_j C_{\lambda_i \lambda_j}(p_i, p_j)}{\sqrt{(p_i \cdot k_0)(p_j \cdot k_0)}}, \end{aligned} \quad (\text{A.8})$$

where

$$\begin{aligned} M_i &= +m_i \quad \text{if } U(p_i, \lambda_i) = u(p_i, \lambda_i), \\ M_i &= -m_i \quad \text{if } U(p_i, \lambda_i) = v(p_i, \lambda_i), \\ A_{\lambda_i \lambda_j} &= \delta_{\lambda_i - \lambda_j} \lambda_i ((k_0 \cdot p_i)(k_1 \cdot p_j) - (k_0 \cdot p_j)(k_1 \cdot p_i) - i \lambda_i \epsilon_{\mu\nu\rho\sigma} k_0^\mu k_1^\nu p_i^\rho p_j^\sigma), \\ B_{\lambda_i \lambda_j} &= \delta_{\lambda_i \lambda_j} (k_0 \cdot p_j), \quad C_{\lambda_i \lambda_j} = \delta_{\lambda_i \lambda_j} (k_0 \cdot p_i), \end{aligned} \quad (\text{A.9})$$

with $k_{0,1}$ being auxiliary vectors such that $k_0^2 = 0$, $k_1^2 = -1$ and $k_0 \cdot k_1 = 0$. No sum over repeated indices must be understood. For instance, we can choose $k_0 = (1, 0, 1, 0)$ and $k_1 = (0, 1, 0, 0)$. With this choice, it is obvious to see that the denominator in Eq. (A.8) can never vanish if the bottom mass is kept. If one would like to neglect m_b , that choice can bring $p_3 \cdot k_0$ or $p_4 \cdot k_0$ to zero in some cases. If this happens, one can tell the code to choose $k_0 = (1, 0, -1, 0)$ instead of the above choice. In fact, that is what we did in our codes.

In the case of spinors representing a massless state, the helicity formalism simplifies considerably. Only $A_{\lambda_i \lambda_j}$ is needed. Traditionally we introduce the C -numbers $s(p, q)$

and $t(p, q)$,

$$\begin{aligned} s(p, q) &\equiv \bar{u}(p, +)u(q, -) = A_{+-}(p, q), \quad t(p, q) \equiv \bar{u}(p, -)u(q, +) = -s(p, q)^*, \\ |s(p_1, p_2)|^2 &= s(p_1, p_2)t(p_2, p_1) = 2p_1 \cdot p_2. \end{aligned} \quad (\text{A.10})$$

These are the functions that appear in our code for the massless b quark. The massless case is also used when expressing the gluon polarisation vector to which we now turn.

A.2 Transversality and gauge invariance

The reference vector used for the polarisation of the gluon can be changed at will. Changing the reference vector from q to q' amounts essentially to a gauge transformation. Indeed one has [36]

$$\epsilon^\mu(p, \lambda; q') = e^{i\phi(q', q)} \epsilon^\mu(p, \lambda; q) + \beta(q', q) p^\mu, \quad (\text{A.11})$$

where

$$\begin{aligned} e^{i\phi(q', q)} &= \left[\frac{s(p, q)}{t(p, q)} \frac{t(p, q')}{s(p, q')} \right]^{1/2}, \\ \beta(q', q) &= \frac{2}{[4(q' \cdot p)]^{1/2}} \frac{t(q, q')}{t(q, p)}. \end{aligned} \quad (\text{A.12})$$

Therefore up to the phase factor, the difference is contained in the momentum vector of the gluon. QCD gauge invariance for our process leads to the important identity

$$|\mathcal{A}(\lambda_1, \lambda_2; \lambda_3, \lambda_4; q_1, q_2)|^2 = |\mathcal{A}(\lambda_1, \lambda_2; \lambda_3, \lambda_4; q'_1, q'_2)|^2, \quad (\text{A.13})$$

as long as $q'_{1,2}$ satisfy condition (A.4). We have carefully checked that the numerical result for the norm of each helicity amplitude at various point in phase space is independent of the reference vectors $q_{1,2}$ up to 12 digits using double precision. By default, our numerical evaluation is based on the use of $q_{1,2} = (p_2, p_1)$. For the checks in the case of massive b quarks the result with $q_{1,2} = (p_2, p_1)$ is compared with the one

using any $q_{1,2}$ such as conditions (A.4) are obeyed. In the case of massless b quarks it is simplest to take $q_{1,2} = (p_3, p_4)$.

This check is a an important check on many ingredients that enter the calculation: the Dirac spinors, the gluon polarization vectors, the propagators, the Lorentz indices, the tensorial loop integrals. It has been used extensively in our numerical calculation.

Appendix B

Optimization with FORM

B.1 Optimization

Each helicity amplitude $\mathcal{A}(\lambda_1, \lambda_2; \lambda_3 \lambda_4) \equiv \mathcal{A}(\hat{\lambda})$, a C-number, is calculated numerically in the Fortran code. The price to pay is that the number of helicity amplitudes to be calculated can be large, 16 in our case for the electroweak loop part. Some optimisation is necessary. The categorisation of the full set of diagrams into three gauge invariant classes as shown in section 3.2.3 is a first step. We have sought to write each diagram as a compact product of blocks and structures containing different properties of the amplitude. We write the amplitude according to a colour ordering pattern that defines three channels. The ordering is in a one-to-one correspondance with the three channels or diagrams shown in Fig. 3.1. The T -type is the direct channel, the U -type is the crossed one obtained from the T -type by interchanging the two gluons and the S -type is the one involving the triple gluon vertex. The helicity amplitude for each diagram can thus be represented as¹

$$\mathcal{A}(\hat{\lambda})^{T,U,S} = CME(a, b) \times Cc \times \sum [FFE \times SME(\lambda_i)], \quad (\text{B.1})$$

where

¹The method we use here is very similar to the one described by Denner in [51].

- $CME(a, b)$ is the colour matrix element. a, b are the colour indices of the two initial gluons². The colour products can be $(T^a T^b)$, $(T^b T^a)$ or $[T^a, T^b]$ corresponding to the three T, U, S channels respectively
- Cc contains all the common coefficients like the strong coupling constant g_s or factors common to all diagrams and amplitudes such as the normalisation factor entering the representation of the polarisation vector of the gluon, see Eq. (A.3). Cc is the same for all diagrams and is included at the very end of the numerical evaluation stage.
- FFE , form factor element, contains all the denominators of propagators, loop functions as well as various scalar products of external momenta $\{p_1, p_2, p_3, p_4\}$ *i.e.* all the scalar objects which do not depend on the helicity λ_i
- $SME(\hat{\lambda})$, standard matrix element, is a product of the scalar spinor functions $A_{\lambda_i \lambda_j}$, $B_{\lambda_i \lambda_j}$ and $C_{\lambda_i \lambda_j}$ defined in Appendix A.

For each channel, say $\mathcal{A}(\hat{\lambda})^T$, the most complicated and time-consuming part is the FFE . That is why we want to factorise it out and put it in a common block so that in order to calculate all the 16 helicity configurations of $\mathcal{A}(\hat{\lambda})^T$ we just need to calculate FFE once. This is done at every point in phase space. This kind of factorisation can be easily carried out in FORM (see section B.2).

$SME(\hat{\lambda})$ is also complicated because the bottom quark is massive and γ_5 occurs in the “helicity strings”. Thus we have to optimize this part as well. The way we do it for all the 3 groups is as follows. In FORM, we have to find out all the generic expressions of $SME(\hat{\lambda})$. There are 12 of them at tree level and 68 at one-loop if we choose $q_{1,2} = p_{2,1}$ for the reference vectors. For instance,

$$\begin{aligned}
SME_1 &= [\bar{u}(\lambda_3, p_3) v(\lambda_4, p_4)] \times [\epsilon_\mu(\lambda_1, p_1, p_2) p_4^\mu] \times [\epsilon_\nu(\lambda_2, p_2, p_1) p_4^\nu], \\
&= BME_1(\lambda_3, \lambda_4) \times BME_2(\lambda_1) \times BME_3(\lambda_2),
\end{aligned} \tag{B.2}$$

²Other colour indices of the bottom quarks are omitted here for simplicity

can be expressed in terms of 3 basic matrix elements (*BME*). Each *BME* occurs several times when calculating all the *SME*($\hat{\lambda}$). The number of *BME* is 31. Each *BME* is written in terms of scalar spinor functions $A_{\lambda_i \lambda_j}$, $B_{\lambda_i \lambda_j}$, $C_{\lambda_i \lambda_j}$. All the *SME* or *BME* can be found and abbreviated in FORM. As an alternative, we can use Perl for such an operation. The FORM output is converted directly into a Fortran code for numerical evaluation. Needless to say, all the abbreviations of *SME* or *BME* must be put in common blocks.

To get the final result, we have to sum over all the channels. The grouping can be re-arranged in terms of an Abelian part and a non-Abelian part according to

$$\begin{aligned} \mathcal{A}(\hat{\lambda}) &= \mathcal{A}(\hat{\lambda})^T + \mathcal{A}(\hat{\lambda})^U + \mathcal{A}(\hat{\lambda})^S, \\ &\equiv \{T^a, T^b\} \tilde{\mathcal{A}}(\hat{\lambda})^{Abel} + [T^a, T^b] \tilde{\mathcal{A}}(\hat{\lambda})^{NAbel}, \end{aligned} \quad (\text{B.3})$$

where

$$\begin{aligned} \tilde{\mathcal{A}}(\hat{\lambda})^{Abel} &= \frac{1}{2}(\tilde{\mathcal{A}}(\hat{\lambda})^T + \tilde{\mathcal{A}}(\hat{\lambda})^U), \\ \tilde{\mathcal{A}}(\hat{\lambda})^{NAbel} &= \tilde{\mathcal{A}}(\hat{\lambda})^S + \frac{1}{2}(\tilde{\mathcal{A}}(\hat{\lambda})^T - \tilde{\mathcal{A}}(\hat{\lambda})^U) \end{aligned} \quad (\text{B.4})$$

corresponding to the Abelian and Non-Abelian parts respectively. Amplitudes without color factor are denoted by a tilde. The amplitude squared then contains no interference term between the Abelian and Non-Abelian parts:

$$|\mathcal{A}(\hat{\lambda})|^2 = \frac{1}{256} \left(\frac{28}{3} |\tilde{\mathcal{A}}(\hat{\lambda})^{Abel}|^2 + 12 |\tilde{\mathcal{A}}(\hat{\lambda})^{NAbel}|^2 \right) \quad (\text{B.5})$$

where $\frac{1}{256} = \frac{1}{4} \times \frac{1}{8} \times \frac{1}{8}$ is the spin- and colour- averaging factor.

The task of our FORM code is to calculate $\sum_{T\text{-diagrams}} \tilde{\mathcal{A}}(\hat{\lambda})^T$, $\sum_{U\text{-diagrams}} \tilde{\mathcal{A}}(\hat{\lambda})^U$ and $\sum_{S\text{-diagrams}} \tilde{\mathcal{A}}(\hat{\lambda})^S$ as functions of *FFE*s and *SME*s. These algebraic expressions are fed into a Fortran code which uses Eqs. (B.4) and (B.5) to calculate the total amplitude squared.

B.2 Technical details

What we actually do in our FORM code to find all FFE and $SME(\lambda_i)$ is the following. Consider, for example, a pentagon diagram in the class (b) of Fig. 3.4. In the FORM code, we have to write a subroutine to calculate the loop integral given by

$$\begin{aligned}
 E_r^{\mu\nu}(k_i, m_i) &= \int d^D q \\
 &\times \frac{N^{\mu\nu}}{(q^2 - m_0^2)[(q + k_1)^2 - m_1^2][(q + k_2)^2 - m_2^2][(q + k_3)^2 - m_3^2][(q + k_4)^2 - m_4^2]}, \\
 N^{\mu\nu} &= (1 + A\gamma_5)(m_1 + \not{q} + \not{k}_1)(m_2 + \not{q} + \not{k}_2) \\
 &\times \gamma^\mu(m_3 + \not{q} + \not{k}_3)\gamma^\nu(m_4 + \not{q} + \not{k}_4)(1 - A\gamma_5),
 \end{aligned} \tag{B.6}$$

where A is just some coupling constant; $k_1 = p_5$, $k_2 = p_5 + p_3$, $k_3 = k_2 - p_1$, $k_4 = k_3 - p_2$, $m_0 = M_W$, $m_1 = m_2 = m_3 = m_4 = m_t$. In order to write $E_r^{\mu\nu}$ in terms of Passarino-Veltman functions $E_{ijk\dots}$, $D_{ij\dots}$ and $C_{i\dots}$ we have to expand the numerator $N^{\mu\nu}$. We then use Dirac algebra to re-organise $N^{\mu\nu}$ such that each term has the form $\gamma_5(\dots)^\nu \times q^\mu$ or $\gamma_5(\dots)^{\mu\nu} \times \not{q}$. For terms with q^2 , q^4 or $q.k_i$, we use

$$\begin{aligned}
 q^2 &= (q^2 - m_0^2) + m_0^2, \\
 q.k_1 &= \frac{1}{2} \{ [(q + k_1)^2 - m_1^2] - (q^2 - m_0^2) + (m_1^2 - m_0^2 - k_1^2) \}, \\
 q^2 &= [(q + k_1)^2 - m_1^2] + (m_1^2 - k_1^2) - 2k_1^\eta q_\eta.
 \end{aligned} \tag{B.7}$$

D and C functions appear when terms in the right-hand-side cancel with denominator factors. The advantage of using Eq. (B.7) is that the rank of tensorial functions is reduced. In the present example, Eq. (B.7) helps us avoid tensorial five-point functions with rank 4, which are very complicated. Obviously, numerical evaluation is much faster this way. However, there may be a problem when using Eq. (B.7) if the library of scalar loop integrals is not complete. This is the situation of section 5.5. In that calculation, we have to deal with complex internal masses and our library for scalar four-point functions includes only special cases with 2 lightlike external momenta. If we use Eq. (B.7), it will create four-point functions with 3 or 4 massive external

particles since the momenta in the denominator of Eq. (B.6) are shifted: $k_i \rightarrow k_i - k_1$, $i = 2, 3, 4$ and $(k_i - k_1)^2$ are not necessarily zero. We then have a problem with these four-point functions. In this situation, one should not use Eq. (B.7) but simply write $q^2 = g_{\eta\rho} q^\eta q^\rho$, $q \cdot k_i = k_i^\eta q_\eta$ instead. The first aim is to write $E_r^{\mu\nu}$ as the following generic expression

$$E_r^{\mu\nu}(k_i, m_i) = \sum_s f_s^{\mu\nu}(\gamma_5, k_i) T_s(k_i^2, m_i^2), \quad (\text{B.8})$$

where T_s are Passarino-Veltman loop functions, $f_s^{\mu\nu}(\gamma_5, k_i)$ are complicated functions of $g^{\mu\nu}$, γ^μ , k_i^μ and γ_5 .

In order to write helicity amplitudes in simple forms, we have to choose a good momentum basis. In the calculation of $pp \rightarrow b\bar{b}H$ our basis is $\{p_1, p_2, p_3, p_4\}$. We have to replace k_i by p_i to get $E_r^{\mu\nu}(p_i, m_i)$. One can then use the on-shell condition to simplify $E_r^{\mu\nu}$. In practice, one knows that each $T_s(p_i^2, m_i^2)$ appears several times in the calculation and has a very lengthy expression. For optimization and having compact expression of $E_r^{\mu\nu}(p_i, m_i)$ we introduce abbreviations for $T_s(k_i^2, m_i^2)$. Those abbreviations serve as the library of Passarino-Veltman loop functions for the present calculation. The way to do this in FORM is as follows.

```
local F = sum E_r^{\mu\nu}(p_i, m_i); bracket T_s; .sort
collect cfl; .sort
polyfun cfl; .sort
polyfun; id cfl(x?)=1; .sort
print +s F; .end
```

The result of this simple FORM script is that F is a sum of independent Passarino-Veltman loop functions $T_s(k_i^2, m_i^2)$. One can use the command "#write" to produce an output file if one wishes. Now one can use Perl [122] to introduce an abbreviation for each term: $T_s(k_i^2, m_i^2) \rightarrow fT_s$. We have

$$E_r^{\mu\nu}(p_i, m_i) = \sum_s f_s^{\mu\nu}(\gamma_5, p_i) \times fT_s. \quad (\text{B.9})$$

Apart from CME and Cc , a generic T -channel helicity amplitude is calculated in FORM as

$$\tilde{\mathcal{A}}(\hat{\lambda})^T = \bar{u}(\lambda_3, p_3) \left(\sum_r E_r^{\mu\nu} \right) \epsilon_\mu(p_1, q_1) \epsilon_\nu(p_2, q_2) v(\lambda_4, p_4). \quad (\text{B.10})$$

We can now simplify this expression by using the transversality condition for the gluon polarization vectors and Dirac equation. For the latter, we have to re-organise $f_s^{\mu\nu}(\gamma_5, p_i)$ to have the form: $\not{p}_3 \gamma_5 \not{p}_1 \gamma^\mu \gamma^\nu \not{p}_2 \not{p}_4$.

$$\begin{aligned} p_1^\mu \epsilon_\mu(p_1, q_1) &= 0, & p_2^\nu \epsilon_\nu(p_2, q_2) &= 0, \\ \bar{u}(\lambda_3, p_3) \not{p}_3 &= m_b \bar{u}(\lambda_3, p_3), & \not{p}_4 v(\lambda_4, p_4) &= -m_b v(\lambda_4, p_4). \end{aligned} \quad (\text{B.11})$$

Notice that if one chooses $q_1 = p_2$ and $q_2 = p_1$ then $\tilde{\mathcal{A}}(\hat{\lambda})$ is further simplified by using

$$p_2^\mu \epsilon_\mu(p_1, p_2) = 0, \quad p_1^\nu \epsilon_\nu(p_2, p_1) = 0. \quad (\text{B.12})$$

We are now in the position to factorize each term of $\mathcal{A}(\hat{\lambda})^T$ as a product of FFE and $SME(\lambda_i)$. The trick to find all $SME(\lambda_i)$ is the same as above: using the combination (bracket, collect, polyfun).

```

local FT =  $\tilde{\mathcal{A}}(\hat{\lambda})^T$ ; local FU =  $\tilde{\mathcal{A}}(\hat{\lambda})^U$ ; local FS =  $\tilde{\mathcal{A}}(\hat{\lambda})^S$ ;
bracket  $\bar{u}, v, \epsilon, \gamma$ ; .sort
collect cf0; .sort
local FTUS = FT + FU + FS; .sort
polyfun cf0; .sort
polyfun; id cf0(x?)=1; .sort
print +s FTUS; .end

```

The result of this simple FORM script is that $FTUS$ is a sum of independent helicity structures $\bar{u}(\lambda_3, p_3) f_s^{\mu\nu}(\gamma_5, p_i) \epsilon_\mu(p_1, q_1) \epsilon_\nu(p_2, q_2) v(\lambda_4, p_4)$. Now one can use Perl to give each term a name $SME(\lambda_i)$. For FFE , it is just slightly more complicated

```

local FT =  $\tilde{\mathcal{A}}(\hat{\lambda})^T$ ; local FU =  $\tilde{\mathcal{A}}(\hat{\lambda})^U$ ; local FS =  $\tilde{\mathcal{A}}(\hat{\lambda})^S$ ;
bracket  $\bar{u}, v, \epsilon, \gamma$ ; .sort
collect cf0; normalize cf0; .sort
local FTUS = FT + FU + FS; bracket cf0; .sort
collect cf1; .sort
polyfun cf1; .sort
polyfun; id cf1(x?)=1; .sort
print +s FTUS; .end

```

where the command "normalize cf0;" is very important. The result of this FORM script is that $FTUS$ is a sum of $cf0[\sum(X_s(p_i.p_j) \times fT_s)]$ where $X_s(p_i.p_j)$ are just simple algebra expressions, fT_s are loop functions. We can then use Perl to give the argument of each function $cf0$ a name FFE . Thus $FFE \equiv \sum(X_s(p_i.p_j) \times fT_s)$.

To sum up, the working stream of our FORM code is the following. Input: all expressions of helicity amplitudes for all Feynman diagrams. This is just simply applying the Feynman rules. Output: $\sum_{T-diagrams} \tilde{\mathcal{A}}(\hat{\lambda})^T$, $\sum_{U-diagrams} \tilde{\mathcal{A}}(\hat{\lambda})^U$ and $\sum_{S-diagrams} \tilde{\mathcal{A}}(\hat{\lambda})^S$ as functions of FFE s and SME s. The major source of bugs is at the beginning when we type in the Feynman-rule-amplitude-expressions. The rest is almost automatic. One might wonder about the connection between FORM and Perl. This is semi-automatic in our code, *i.e.* we have to run FORM and Perl separately. The three FORM scripts described above generate their output files. We write three very simple Perl scripts to read those files and introduce abbreviations. Those Perl scripts also prepare three output files to be read by FORM. Indeed if one does not like using Perl and wants to do everything automatically within FORM, this is possible.

B.3 Automation with FORM

In this section, we would like to show that the working stream described in the previous section can be automatized in FORM without invoking Perl. We have not

done this in the $pp \rightarrow b\bar{b}H$ calculation. However, the implementation is straight forward. The only difficulty is "How to introduce abbreviations?". The answer is in the following FORM example³.

```

Symbol a,b,c,d,e,x,y,n; CFunction f1,f2,f3;
Local F = x*(1+a+b+c)^3+y*(1+a+b+c)^2;
AntiBracket x,y; .sort
Collect f1; Makeinteger f1; Bracket f1; .sort

*** which terms to be abbreviated? ***

Keep Brackets;
id f1(x?) = f1(terms_(x),x);
id f1(1,x?) = x;
id f1(n?,x?) = f1(-termsinbracket_(0),x);
id f1(-1,x?) = x;
Bracket f1; .sort

*** give it a name and store it by using $ variable ***

Keep Brackets;
#$cou = 0;
if ( count(f1,1)!=0 ); $cou = $cou + 1; id f1(n?,x?) = f2($cou)*f3($cou,x);
endif;
Bracket f2,f3; .sort
#do i = 1,$cou id f3('i',x?$t'i') = 1; #enddo .sort

*** using temporary expressions for writing output file ***
#do i = 1,$cou local XX'i'=$t'i'; #enddo .sort

*** for fortran output files ***
format doublefortran;
#write <abbrf2.F> " Subroutine abbreviation(x,y)"
#write <abbrf2.F> " IMPLICIT DOUBLE PRECISION (A-H, O-Z)"

```

³We have learnt these tricks from a private communication with Vermaseren.

```

#write <abbrf2.F> " DOUBLE PRECISION f2('$cou')
#write <abbrf2.F> " Common/abbr/f2"
#do i = 1,$cou'
* #write <abbrf2.F> " f2('i') = '$t'i'"
#write <abbrf2.F> " f2('i') = %e",XX'i'
#enddo
#write <abbrf2.F> " End"
#write <funct.F> " Function fun(x,y,a,b,c)"
#write <funct.F> " IMPLICIT DOUBLE PRECISION (A-H, O-Z)"
#write <funct.F> " DOUBLE PRECISION f2('$cou')
#write <funct.F> " Common/abbr/f2"
#write <funct.F> " fun=%e",F(fun)
#write <funct.F> " Return"
#write <funct.F> " End"
.end

```

The working stream of this example is the following. Input: an algebraic expression named F. Output: two Fortran files to calculate F: "funct.F" and "abbrf2.F". The latter computes all abbreviations which are "complicated" functions of (x,y) and appear several times in the final result. This is nothing but the idea of optimization.

Appendix C

Phase space integral

C.1 $2 \rightarrow 3$ phase space integral

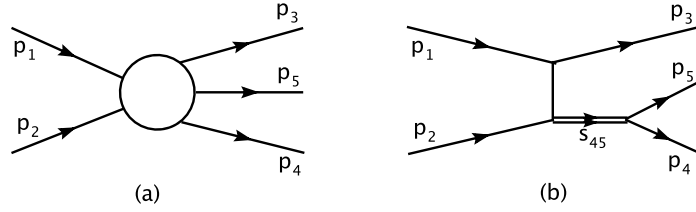


Figure C.1: A typical $2 \rightarrow 3$ Feynman diagram. The arrow gives the momentum direction.

The phase space integral is given by

$$R_3 = \int \frac{d^3 \mathbf{p}_3}{2e_3} \frac{d^3 \mathbf{p}_4}{2e_4} \frac{d^3 \mathbf{p}_5}{2e_5} \delta^4(p_1 + p_2 - p_3 - p_4 - p_5). \quad (\text{C.1})$$

There are 9 integration variables with 4 constraints from the Dirac delta function. All the interactions we consider are spherically symmetric, it means that there is one trivial variable ϕ corresponding to rotation around the z -axis. Integration over ϕ gives a factor of 2π . Thus, there are 4 essential final state variables¹. We define the

¹For a $2 \rightarrow n$ process, the number of essential final state variables is $3n - 5$.

kinematical function

$$\lambda(x, y, z) \equiv x^2 + y^2 + z^2 - 2xy - 2xz - 2yz. \quad (\text{C.2})$$

R_3 can be factorized into $2 \rightarrow 2$ and $1 \rightarrow 2$ processes (see Fig. C.1b)

$$R_3 = \int ds_{45} R_2(s, s_{45}, m_b^2) R_2(s_{45}, m_b^2, m_H^2), \quad (\text{C.3})$$

with

$$R_2(s_{ij}, m_i^2, m_j^2) = \frac{\lambda^{1/2}(s_{ij}, m_i^2, m_j^2)}{8s_{ij}} \int d\cos\theta_i^{(ij)} d\phi_i^{(ij)}, \quad (\text{C.4})$$

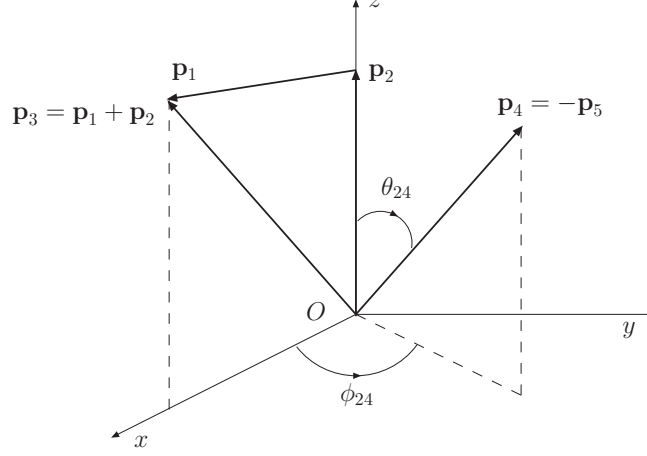
where $\theta(\phi)_i^{(ij)}$ are the angles determined in the rest frame of $(i+j)$, $s_{ij} = (p_i + p_j)^2$ with $i, j = 3, 4, 5$. Clearly, formula (C.3) is just one way of factorizing the phase space integral. We can replace s_{45} by s_{34} or s_{35} . In practice, choosing a good set of integration variables makes the integral convergent much faster. For a complicated calculation it is very difficult to know which choice is the best. In that case, we should always start with the tree level and try all the possibilities of phase space factorization with the same number of Monte Carlo points (if one uses the Monte Carlo method) and compare the integration errors to judge the best choice. That is what we did to find out that Eq. (C.3) is the best way to parameterise the phase space in the case of $gg \rightarrow b\bar{b}H$ calculation.

We choose $Oz \parallel p_2$. In the center-of-mass system (CMS) of $(4+5)$, we call this the CMS45 hereafter, one has $\mathbf{p}_4 + \mathbf{p}_5 = \mathbf{p}_1 + \mathbf{p}_2 - \mathbf{p}_3 = 0$. Thus \mathbf{p}_1 , \mathbf{p}_2 and \mathbf{p}_3 define a plane chosen to be Oxz (see Fig. C.2). \mathbf{p}_4 is defined by two angles θ_{24} and ϕ_{24} .

$$R_2(s_2, m_b^2, M_H^2) = \frac{\lambda^{1/2}(s_2, m_b^2, M_H^2)}{8s_2} \int_{-1}^1 d\cos\theta_{24} \int_0^{2\pi} d\phi_{24}. \quad (\text{C.5})$$

In the CMS of $(1+2)$, we call this the CMSgg hereafter, one gets

$$R_2(s, s_2, m_b^2) = 2\pi \frac{\lambda^{1/2}(s, s_2, m_b^2)}{8s} \int_{-1}^1 d\cos\theta_{23}, \quad (\text{C.6})$$

Figure C.2: *Coordinate system in the frame $\mathbf{p}_4 + \mathbf{p}_5 = 0$.*

where the factor 2π comes from the trivial integration over ϕ_{23} . The range of s_2 is given by

$$\begin{aligned} s &\geq s_2 \geq (m_b + M_H)^2, \\ s_0 \geq s &= x_1 x_2 s_0 \geq (2m_b + M_H)^2, \end{aligned} \quad (\text{C.7})$$

where s_0 is the invariant mass of the initial protons, $x_{1,2} \in [0, 1]$ are the momentum fractions carried by the initial gluons. The second equation in (C.7) implies that

$$1 \geq x_1 \geq \frac{(2m_b + M_H)^2}{s_0}, \quad 1 \geq x_2 \geq \frac{(2m_b + M_H)^2}{s_0 x_1}. \quad (\text{C.8})$$

The integration formula we actually use in the Fortran code, taking into account the convolution of the gluon structure functions, reads

$$\begin{aligned} \hat{R}_3 &= 2\pi \int_0^1 dx'_1 \int_0^1 dx'_2 \int_0^1 ds'_2 \int_{-1}^1 d\cos\theta_{23} \int_{-1}^1 d\cos\theta_{24} \int_0^{2\pi} d\phi_{24}, \\ &\times J \frac{\lambda^{1/2}(s, s_2, m_b^2)}{8s} \frac{\lambda^{1/2}(s_2, m_b^2, M_H^2)}{8s_2} \end{aligned} \quad (\text{C.9})$$

where we have changed the integration variables as follows

$$\begin{aligned} x_1 &= x'_1 \left[1 - \frac{(2m_b + M_H)^2}{s_0} \right] + \frac{(2m_b + M_H)^2}{s_0}, \\ x_2 &= x'_2 \left[1 - \frac{(2m_b + M_H)^2}{s_0 x_1} \right] + \frac{(2m_b + M_H)^2}{s_0 x_1}, \\ s_2 &= s'_2 [s - (m_b + M_H)^2] + (m_b + M_H)^2, \end{aligned} \quad (\text{C.10})$$

and J is the Jacobian

$$J = \left[1 - \frac{(2m_b + M_H)^2}{s_0} \right] \left[1 - \frac{(2m_b + M_H)^2}{s_0 x_1} \right] [s - (m_b + M_H)^2]. \quad (\text{C.11})$$

We should stress again that θ_{24} and ϕ_{24} are defined in the CMS45 while $\cos \theta_{23}$ is defined in the CMSgg. In order to calculate the helicity amplitudes, which are Lorentz invariant, one has to reconstruct from $\{s_2, \cos \theta_{23}, \cos \theta_{24}, \phi_{24}\}$ all the components of 5 external momenta in some reference frame. The way we do this for the CMSgg is as follows. First, the components of p_4 and p_5 can be easily calculated in the CMS45

$$\begin{aligned} \mathbf{p}_5 &= -\mathbf{p}_4, \quad |\mathbf{p}_5| = |\mathbf{p}_4| = \frac{\lambda^{1/2}(s_2, m_b^2, M_H^2)}{2\sqrt{s_2}}, \\ \mathbf{p}_{4z} &= |\mathbf{p}_4| \cos \theta_{24}, \\ \mathbf{p}_{4x} &= |\mathbf{p}_4| \sin \theta_{24} \cos \phi_{24}, \\ \mathbf{p}_{4y} &= |\mathbf{p}_4| \sin \theta_{24} \sin \phi_{24}. \end{aligned} \quad (\text{C.12})$$

In the CMSgg we get

$$\begin{aligned} p_1 &= (\sqrt{s}, 0, 0, -\sqrt{s}), \quad p_2 = (\sqrt{s}, 0, 0, \sqrt{s}), \\ \mathbf{p}_{45} &= \mathbf{p}_4 + \mathbf{p}_5 = -\mathbf{p}_3, \quad |\mathbf{p}_3| = \frac{\lambda^{1/2}(s, s_2, m_b^2)}{2\sqrt{s}}, \quad e_{45} = \sqrt{s_2 + |\mathbf{p}_3|^2}, \\ \mathbf{p}_{3z} &= |\mathbf{p}_3| \cos \theta_{23}, \quad \mathbf{p}_{3x} = |\mathbf{p}_3| \sin \theta_{23}, \quad \mathbf{p}_{3y} = 0. \end{aligned} \quad (\text{C.13})$$

In the CMSgg one sees that the CMS45 is moving with the 4-component momentum $p_{45} = (e_{45}, -\mathbf{p}_3)$. We then boost p_4 calculated above in the CMS45 to be in the CMSgg by using the following general Lorentz transformation

$$\begin{aligned} e' &= \gamma_0 e - \gamma_0 \mathbf{v}_0 \cdot \mathbf{p}, \\ \mathbf{p}' &= \mathbf{p} + \gamma_0 \mathbf{v}_0 \left(\frac{\gamma_0 \mathbf{v}_0 \cdot \mathbf{p}}{\gamma_0 + 1} - e \right), \end{aligned} \quad (\text{C.14})$$

with

$$\gamma_0 = \frac{e_0}{m_0}, \quad m_0 = \sqrt{e_0^2 - \mathbf{p}_0^2}, \quad \mathbf{v}_0 = \frac{1}{e_0}(\mathbf{p}_{0x}, \mathbf{p}_{0y}, \mathbf{p}_{0z}), \quad (\text{C.15})$$

where p_0 is the 4-component momentum of a reference frame K' observed in K , p is any momentum observed in K and p' is the same momentum observed in K' . The inverse of equations (C.14) and (C.15) are obtained by changing \mathbf{v}_0 to $-\mathbf{v}_0$ and by interchanging primed and unprimed variables. Now we have all the components of $p_1, p_2, p_3, p_4, p_5 = p_1 + p_2 - p_3 - p_4$ in one reference frame, CMSgg.

In the CMS of two initial protons (CMSPP), the proton and gluon momenta are

$$\begin{aligned} P_2^\mu &= (\sqrt{s_0}, 0, 0, \sqrt{s_0}), \quad P_1^\mu = (\sqrt{s_0}, 0, 0, -\sqrt{s_0}), \\ p_1 &= x_1 P_1, \quad p_2 = x_2 P_2, \end{aligned} \quad (\text{C.16})$$

where we have neglected the proton mass². All the kinematical cuts are defined in the CMSPP. One can move from the CMSgg to CMSPP by using the following boost matrix along the z axis

$$\Lambda_{gg \rightarrow PP} = \begin{pmatrix} \gamma & 0 & 0 & -\beta\gamma \\ 0 & 1 & 0 & 0 \\ 0 & 0 & 1 & 0 \\ -\beta\gamma & 0 & 0 & \gamma \end{pmatrix}, \quad (\text{C.17})$$

with $\gamma = \frac{x_1+x_2}{2\sqrt{x_1x_2}}$, $\beta = \frac{x_1-x_2}{x_1+x_2}$. This boost matrix can be easily found from the Lorentz transformation of the four vector $(p_1 + p_2)$ from the CMSgg to CMSPP. The helicity amplitudes can be calculated in the CMSgg or CMSPP as one wishes.

For experimental purpose, one has to impose cuts on the transverse momenta and pseudorapidities of the bottom and anti-bottom in CMSPP

$$|\mathbf{p}_{3T}|, |\mathbf{p}_{4T}| \geq |\mathbf{p}_T|_{\min} \quad \text{and} \quad |\eta_{3,4}| \leq \eta_{\max} \quad (\text{C.18})$$

²The proton mass $m_p = 0.9383\text{GeV}$.

where the values of $|\mathbf{p}_T|_{min}$ and η_{max} depend on the experiment, the definition of pseudorapidity is

$$\eta = -\ln \left[\tan \left(\frac{\theta}{2} \right) \right]. \quad (\text{C.19})$$

Those kinematical cuts also help to avoid some possible zero poles associated with some bottom-quark propagators in the massless limit and with some Gram determinants related to the tensorial reduction of loop integrals.

C.2 Numerical integration with BASES

BASES is a Monte Carlo integrator which functions by means of the importance and stratified sampling method [37]. Executions of BASES consists of the grid optimization and integration steps. Both steps are done by performing a number of *iterations*. An iteration is the process of computing the estimate of an integral and its variance. Each iteration is a Monte Carlo integration with N_{call} sample points and is realised as follows. The full multi-dimensional integral volume is covered by a grid of N_{cube} , the number of hypercubes (each hypercube is divided into many subregions). In each hypercube, the integral and its variance are evaluated with $N_{trial} = N_{call}/N_{cube}$ sample points. The results of each iteration are obtained by summing up results of all hypercubes. N_{cube} is calculated as follows

$$N_{cube} = N_{region}^{N_{wild}} < 32768, \quad N_{region} = \left(\frac{N_{call}}{2} \right)^{1/N_{wild}} \leq 25, \quad (\text{C.20})$$

with N_{wild} is the number of *wild variables* on which the integrand depends strongly or exhibits singular behavior. N_{call} and N_{wild} are BASES input parameters. Clearly $N_{wild} \leq N_{dim}$, N_{dim} the number of integration variables, and the maximum number of wild variables is 15. As input information for BASES, one has to decide which are the "wild" variables and place them at the beginning of the integration variable array.

- Grid optimization step: at the first iteration the grid is uniformly defined for each variable axis. After each iteration the grid is adjusted so as to make the size of the subregions narrower at the parts with larger function value and wider at the parts with the smaller one. In this way a suited grid to the integrand is obtained. The number of iterations for this step is denoted $ITMX1$ (default 15), a BASES input parameter.
- Integration step: the probability to select each hypercube and the maximum value of the function in it are calculated as well as the estimate of integral with the frozen grid determined in the former step. The number of iterations for this step is denoted $ITMX2$ (default 100), a BASES input parameter.

The typical BASES input parameters for calculating (C.9) are: $N_{dim} = 6$, $N_{wild} = 2$, $N_{call} = 10^5$, $ITMX1 = 20$ and $ITMX2 = 130$. The two wild variables are $\cos \theta_{23}$ and $\cos \theta_{24}$ placed at the beginning of the integration variable array. With those input parameters, the typical error we obtained for the $pp \rightarrow b\bar{b}H$ calculation is 0.08%.

Appendix D

Mathematics

D.1 Logarithms and Powers

The natural logarithm $\ln(z)$ is defined as

$$\ln(z) = \ln(|z|) + i \arg(z), \quad (\text{D.1})$$

with $-\pi \leq \arg(z) \leq \pi$. The logarithm $\ln z$ has a branch cut along the negative real axis. The general power $w = z^\alpha$ (α is a complex constant) is defined with the aid of the exponential function

$$z^\alpha = (e^{\ln z})^\alpha = e^{\alpha \ln z}. \quad (\text{D.2})$$

With those definitions, one has the following rules

$$\ln(z_1 z_2) = \ln(z_1) + \ln(z_2) + \eta(z_1, z_2), \quad (\text{D.3})$$

$$\begin{aligned} \eta(z_1, z_2) &= 2\pi i [\theta(-\operatorname{Im} z_1)\theta(-\operatorname{Im} z_2)\theta(\operatorname{Im} z_1 z_2) - \theta(\operatorname{Im} z_1)\theta(\operatorname{Im} z_2)\theta(-\operatorname{Im} z_1 z_2)], \\ (z_1 z_2)^\alpha &= e^{\alpha \ln(z_1 z_2)} = e^{\alpha[\ln(z_1) + \ln(z_2) + \eta(z_1, z_2)]} = e^{\alpha \eta(z_1, z_2)} z_1^\alpha z_2^\alpha, \end{aligned} \quad (\text{D.4})$$

which have important consequences

$$\begin{aligned}
\ln(z_1 z_2) &= \ln(z_1) + \ln(z_2) \text{ if } \operatorname{Im} z_1 \text{ and } \operatorname{Im} z_2 \text{ have different sign} \\
\ln \frac{z_1}{z_2} &= \ln(z_1) - \ln(z_2) \text{ if } \operatorname{Im} z_1 \text{ and } \operatorname{Im} z_2 \text{ have the same sign} \\
(z_1 z_2)^\alpha &= z_1^\alpha z_2^\alpha \text{ if } \operatorname{Im} z_1 \text{ and } \operatorname{Im} z_2 \text{ have different sign.}
\end{aligned} \tag{D.5}$$

For $-z = a - i\rho$ with a real and $\rho \rightarrow 0^+$ we have

$$\begin{aligned}
\ln(-z) &= \begin{cases} \ln|a| & \text{if } a > 0 \\ \ln|a| - i\pi & \text{if } a < 0 \end{cases} \\
\arg(-z) &= \arg(z) - \pi, \\
\ln(-z) &= \ln(|z|) + i \arg(-z) = \ln(|z|) + i \arg(z) - i\pi = \ln(z) - i\pi, \\
(-z)^\alpha &= e^{-i\pi\alpha} e^{\alpha \ln(z)} = e^{-i\pi\alpha} z^\alpha.
\end{aligned} \tag{D.6}$$

If A and B are real then

$$\ln(AB - i\rho) = \ln(A - i\rho') + \ln(B - i\rho/A), \tag{D.7}$$

where ρ' is infinitesimal and has the same sign as ρ . From this we get

$$(AB - i\rho)^\alpha = e^{\alpha \ln(AB - i\rho)} = e^{\alpha [\ln(A - i\rho') + \ln(B - i\rho/A)]} = (A - i\rho')^\alpha (B - i\rho/A)^\alpha. \tag{D.8}$$

D.2 Dilogarithms

The dilogarithm or Spence function is defined by [118, 123, 124]

$$\operatorname{Sp}(z) = - \int_0^1 dt \frac{\ln(1 - zt)}{t}, \tag{D.9}$$

where z may be complex. The logarithm has a branch cut along the negative real axis, implying for the Spence function a cut along the positive real axis from 1 to $+\infty$. When one is in a problematic situation, the following transformation formulae may be helpful

$$\operatorname{Sp}(z) = -\operatorname{Sp}\left(\frac{1}{z}\right) - \frac{1}{6}\pi^2 - \frac{1}{2}\ln^2(-z), \tag{D.10}$$

$$\operatorname{Sp}(z) = -\operatorname{Sp}(1 - z) + \frac{1}{6}\pi^2 - \ln(1 - z) \ln(z). \tag{D.11}$$

More transformation formulae can be found in [123, 124].

D.3 Gamma and Beta functions

The gamma function $\Gamma(z)$ is a function of the complex variable z . For $\text{Re } z > 0$ it is defined by

$$\Gamma(z) = \int_0^\infty dt e^{-t} t^{z-1} \quad (\text{D.12})$$

where the principal value of t^{z-1} is to be taken. For $\text{Re } z \leq 0$ the alternative definition reads [125]

$$\Gamma(z) = \frac{1}{2i \sin \pi z} \int_C dt e^t t^{z-1}, \quad (\text{D.13})$$

where the path of integration C starts at $-\infty$ on the real axis, circles the origin once in the positive direction, and returns to $-\infty$; the initial and final arguments of t are to be $-\pi$ and π , respectively. The latter defines an analytic function for all z other than $0, \pm 1, \pm 2, \dots$. For positive integers n definition (D.12) gives

$$\Gamma(n+1) = n\Gamma(n) = n!. \quad (\text{D.14})$$

$\Gamma(z)$ is analytic everywhere, except at the points $z = 0, -1, -2, \dots$. The following properties of the gamma function are very useful

$$\begin{aligned} \Gamma(z+1) &= z\Gamma(z), \\ \Gamma(z)\Gamma(1-z) &= \frac{\pi}{\sin \pi z}, \\ \Gamma(\epsilon) &= \frac{1}{\epsilon} - \gamma_E + \mathcal{O}(\epsilon), \quad \epsilon \rightarrow 0, \end{aligned} \quad (\text{D.15})$$

where γ_E is Euler constant.

The beta function is defined by

$$B(p, q) = \int_0^1 dt t^{p-1} (1-t)^{q-1} \quad (\text{D.16})$$

where $\text{Re } p > 0$ and $\text{Re } q > 0$; the principal values of the various powers are to be taken. The analytic continuation of $B(p, q)$ onto the left halves of the p and q planes is achieved by using

$$B(p, q) = \frac{\Gamma(p)\Gamma(q)}{\Gamma(p+q)}. \quad (\text{D.17})$$

D.4 Integrals

Formulae to move to spherical coordinates:

$$\int dt_1 \cdots dt_K = \int r^{K-1} dr d\Omega_{K-1}, \quad \int d\Omega_{K-1} = \frac{2\pi^{K/2}}{\Gamma(K/2)}. \quad (\text{D.18})$$

The following integral formula is very useful in many cases

$$\int_0^\infty ds \frac{s^{\alpha-1}}{(z+s)^\beta} = z^{(\alpha-\beta)} \frac{\Gamma(\beta-\alpha)\Gamma(\alpha)}{\Gamma(\beta)}, \quad (\text{D.19})$$

where z can be complex.

The following integral usually appears in loop calculation [118]

$$S_3 = \int_0^1 dy \frac{\ln(ay^2 + by + c) - \ln(ay_0^2 + by_0 + c)}{y - y_0}, \quad (\text{D.20})$$

where a is real, while b , c and y_0 may be complex, with the restriction that $\text{Im}(ay^2 + by + c)$ has the same sign for $0 \leq y \leq 1$.

Let ϵ and ρ be infinitesimally real quantities having the opposite sign to $\text{Im}(ay^2 + by + c)$ and $\text{Im}(ay_0^2 + by_0 + c)$ respectively. Using Eq. (D.7) we get

$$\begin{aligned} \ln(ay^2 + by + c) &= \ln(a - i\epsilon) + \ln[(y - y_1)(y - y_2)], \\ \ln(ay_0^2 + by_0 + c) &= \ln(a - i\rho) + \ln[(y_0 - y_1)(y_0 - y_2)], \end{aligned} \quad (\text{D.21})$$

where $y_{1,2}$ are two roots of equation

$$y^2 + \frac{b}{a}y + \frac{c}{a} = 0. \quad (\text{D.22})$$

We then use Eq. (D.3) to get

$$S_3 = \int_0^1 dy \frac{\ln[(y-y_1)(y-y_2)] - \ln[(y_0-y_1)(y_0-y_2)]}{y-y_0} - \eta(a-i\epsilon, \frac{1}{a-i\rho}) \ln \frac{y_0-1}{y_0}. \quad (D.23)$$

We write

$$\begin{aligned} \ln[(y_0-y_1)(y_0-y_2)] &= \ln(y_0-y_1) + \ln(y_0-y_2) + \eta(y_0-y_1, y_0-y_2) \\ \ln[(y-y_1)(y-y_2)] &= \ln(y-y_1) + \ln(y-y_2) + \eta(y-y_1, y-y_2) \end{aligned} \quad (D.24)$$

with

$$\eta(y-y_1, y-y_2) = \eta(-y_1, -y_2) \quad (D.25)$$

since y is real and $\text{Im}[(y-y_1)(y-y_2)] = \text{Im}(\frac{b}{a}y + \frac{c}{a}) = \text{Im}(\frac{c}{a}) = \text{Im}(y_1y_2)$ as we assumed at the beginning. We have

$$S_3 = \int_0^1 dy \frac{\ln(y-y_1) - \ln(y_0-y_1) + \ln(y-y_2) - \ln(y_0-y_2)}{y-y_0} + \left[\eta(-y_1, -y_2) - \eta(y_0-y_1, y_0-y_2) - \eta(a-i\epsilon, \frac{1}{a-i\rho}) \right] \ln \frac{y_0-1}{y_0}. \quad (D.26)$$

For this, we have to calculate

$$R(y_1, y_0) = \int_0^1 dy \frac{\ln(y-y_1) - \ln(y_0-y_1)}{y-y_0}. \quad (D.27)$$

We change the integration variable $y = y' + y_1$ to get

$$R = \int_{-y_1}^{1-y_1} dy \frac{\ln y - \ln(y_0-y_1)}{y-y_0+y_1}. \quad (D.28)$$

Since the residue of the pole is zero and the logarithmic cut along the negative real axis is outside the triangle $[0, -y_1, 1-y_1]$, we can write

$$\int_{-y_1}^{1-y_1} = \int_0^{1-y_1} - \int_0^{-y_1}. \quad (D.29)$$

We then make the substitutions $y = (1 - y_1)y'$ and $y = -y_1y'$ to get

$$\begin{aligned} R &= \int_0^1 dy \frac{d}{dy} \left[\ln \left(1 + y \frac{1 - y_1}{y_1 - y_0} \right) \right] \{ \ln[(1 - y_1)y] - \ln(y_0 - y_1) \} \\ &\quad - \int_0^1 dy \frac{d}{dy} \left[\ln \left(1 - y \frac{y_1}{y_1 - y_0} \right) \right] \{ \ln(-y_1y) - \ln(y_0 - y_1) \}. \end{aligned} \quad (\text{D.30})$$

Since y is real and positive the logarithmic arguments never cross the cut along the negative real axis. We do partial integration to get

$$\begin{aligned} R &= \ln \left(\frac{1 - y_0}{y_1 - y_0} \right) [\ln(1 - y_1) - \ln(y_0 - y_1)] - \ln \left(\frac{-y_0}{y_1 - y_0} \right) [\ln(-y_1) - \ln(y_0 - y_1)] \\ &\quad - \text{Sp} \left(\frac{y_1}{y_1 - y_0} \right) + \text{Sp} \left(\frac{1 - y_1}{y_0 - y_1} \right). \end{aligned} \quad (\text{D.31})$$

One uses Eq. (D.11) to obtain

$$\begin{aligned} R(y_1, y_0) &= \text{Sp} \left(\frac{y_0}{y_0 - y_1} \right) - \text{Sp} \left(\frac{y_0 - 1}{y_0 - y_1} \right) + \ln \left(\frac{y_0}{y_0 - y_1} \right) \eta(-y_1, \frac{1}{y_0 - y_1}) \\ &\quad - \ln \left(\frac{1 - y_0}{y_1 - y_0} \right) \eta(1 - y_1, \frac{1}{y_0 - y_1}). \end{aligned} \quad (\text{D.32})$$

The result for S_3 reads

$$\begin{aligned} S_3 &= R(y_1, y_0) + R(y_2, y_0) \\ &\quad + \left[\eta(-y_1, -y_2) - \eta(y_0 - y_1, y_0 - y_2) - \eta(a - i\epsilon, \frac{1}{a - i\rho}) \right] \ln \frac{y_0 - 1}{y_0} \end{aligned} \quad (\text{D.33})$$

which contains 4 Spence functions.

Appendix E

Scalar box integrals with complex masses

The calculation of the scalar one-loop function for the box ($N = 4$) with imaginary internal masses in the most general case with no restriction on the external invariants is not tractable. The standard technique of 't Hooft and Veltman [118] (see also [126]) has some restriction on the values of external momenta. In particular, the method works if at least one of the external momenta is lightlike. In our present calculation, there are at least 2 lightlike external momenta in all boxes. We explain here our derivation based on the method given in [118] for this special case.

With $N = D = 4$, from Eq. (4.55) we get

$$D_0 \equiv (4\pi)^2 T_0^4 = \int_0^1 dx \int_0^x dy \int_0^y dz \frac{1}{(ax^2 + by^2 + gz^2 + cxy + hxz + jyz + dx + ey + kz + f)^2}, \quad (\text{E.1})$$

where we have changed the integration variables as $t = \sum_{i=1}^4 x_i$, $x = \sum_{i=1}^3 x_i$, $y =$

$x_1 + x_2, z = x_1$; and

$$\begin{aligned}
a &= \frac{1}{2}(Q_{33} + Q_{44} - 2Q_{34}) = p_3^2, & b &= \frac{1}{2}(Q_{22} + Q_{33} - 2Q_{23}) = p_2^2, \\
g &= \frac{1}{2}(Q_{11} + Q_{22} - 2Q_{12}) = p_1^2, & c &= Q_{23} + Q_{34} - Q_{33} - Q_{24} = 2p_2 \cdot p_3, \\
h &= Q_{13} + Q_{24} - Q_{14} - Q_{23} = 2p_1 \cdot p_3, & j &= Q_{12} + Q_{23} - Q_{22} - Q_{13} = 2p_1 \cdot p_2, \\
d &= Q_{34} - Q_{44} = m_3^2 - m_4^2 - p_3^2, & e &= Q_{24} - Q_{34} = m_2^2 - m_3^2 - p_2^2 - 2p_2 \cdot p_3, \\
k &= Q_{14} - Q_{24} = m_1^2 - m_2^2 + p_1^2 + 2p_1 \cdot p_4, & f &= \frac{Q_{44}}{2} - i\epsilon = m_4^2 - i\epsilon,
\end{aligned} \tag{E.2}$$

with Q_{ij} is defined in Eq. (4.25). d, e, k, f are complex while other parameters are real. There are two cases corresponding to the fact that the positions of two lightlike momenta are opposite or adjacent.

E.1 Integral with two opposite lightlike external momenta

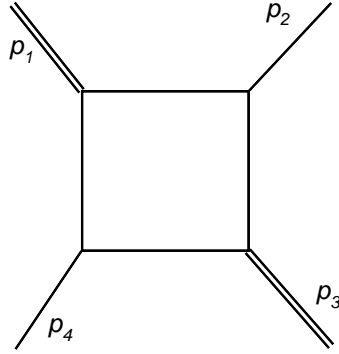


Figure E.1: A box diagram with two opposite lightlike external momenta p_1 and p_3 . Double line means massless.

For the box shown in Fig. E.1 with $p_1^2 = p_3^2 = 0$ one gets $a = g = 0$ and writes

$$D_0^{(13)} = \int_0^1 dx \int_0^x dy \int_0^y dz \frac{1}{(by^2 + cxy + hxz + jyz + dx + ey + kz + f)^2}. \tag{E.3}$$

Integrating over z to get

$$D_0^{(13)} = \int_0^1 dx \int_0^x dy \frac{y}{(Ax+B)(Cx+D)}. \quad (\text{E.4})$$

with

$$\begin{aligned} A &= cy + d, \quad B = by^2 + ey + f, \\ C &= (c+h)y + d, \quad D = (b+j)y^2 + (e+k)y + f. \end{aligned} \quad (\text{E.5})$$

One changes the integration order as

$$\int_0^1 dx \int_0^x dy = \int_0^1 dy \int_y^1 dx. \quad (\text{E.6})$$

We get

$$D_0^{(13)} = \int_0^1 dy y \int_y^1 dx \frac{1}{(Ax+B)(Cx+D)}, \quad (\text{E.7})$$

where A, B, C, D are complex. Integrating over x as follows

$$\begin{aligned} \int_y^1 dx \frac{1}{(Ax+B)(Cx+D)} &= \frac{1}{AC} \int_y^1 \frac{dx}{(x + \frac{B}{A})(x + \frac{D}{C})} \\ &= \frac{1}{AD - BC} \int_y^1 \left(\frac{1}{x + \frac{B}{A}} - \frac{1}{x + \frac{D}{C}} \right) dx \\ &= \frac{1}{AD - BC} \left(\ln \frac{1 + \frac{B}{A}}{y + \frac{B}{A}} - \ln \frac{1 + \frac{D}{C}}{y + \frac{D}{C}} \right) \\ &= \frac{1}{AD - BC} \left(\ln \frac{A+B}{Ay+B} - \ln \frac{C+D}{Cy+D} \right), \end{aligned} \quad (\text{E.8})$$

where we have made sure that the arguments of the logarithms never cross the cut along the negative real axis. One easily gets

$$\begin{aligned} D_0^{(13)} &= \int_0^1 dy \\ &\times \frac{1}{(cj - bh)y^2 + (dj + ck - eh)y + dk - fh} \left(\ln \frac{A+B}{Ay+B} - \ln \frac{C+D}{Cy+D} \right) \end{aligned} \quad (\text{E.9})$$

where the discriminant of the quadratic denominator in the prefactor is nothing but the Landau determinant

$$\det(Q_4) = (dj + ck - eh)^2 - 4(cj - bh)(dk - fh). \quad (\text{E.10})$$

We write

$$D_0^{(13)} = \frac{1}{(cj - bh)(y_2 - y_1)} \int_0^1 \left(\frac{1}{y - y_2} - \frac{1}{y - y_1} \right) \left(\ln \frac{A + B}{Ay + B} - \ln \frac{C + D}{Cy + D} \right) \quad (\text{E.11})$$

with

$$y_{1,2} = \frac{-(dj + ck - eh) \mp \sqrt{\det(Q_4)}}{2(cj - bh)}, \quad (\text{E.12})$$

where the indices 1, 2 correspond to $-$ and $+$ signs respectively.

Now we have to look at the imaginary parts of the arguments of the logarithms in Eq. (E.11). We write them explicitly

$$\begin{aligned} A + B &= by^2 + (c + e)y + d + f, \\ Ay + B &= (b + c)y^2 + (e + d)y + f, \\ C + D &= (b + j)y^2 + (e + k + c + h)y + d + f, \\ Cy + D &= (b + j + c + h)y^2 + (e + k + d)y + f. \end{aligned} \quad (\text{E.13})$$

Imaginary parts read

$$\begin{aligned} \text{Im}(A + B) &= \text{Im}(ey + d + f) = \text{Im}[ym_2^2 + (1 - y)m_3^2 - i\epsilon] < 0, \\ \text{Im}(Ay + B) &= \text{Im}(ey + dy + f) = \text{Im}[ym_2^2 + (1 - y)m_4^2 - i\epsilon] < 0, \\ \text{Im}(C + D) &= \text{Im}[(e + k)y + d + f] = \text{Im}[ym_1^2 + (1 - y)m_3^2 - i\epsilon] < 0, \\ \text{Im}(Cy + D) &= \text{Im}[(e + k)y + dy + f] = \text{Im}[ym_1^2 + (1 - y)m_4^2 - i\epsilon] < 0. \end{aligned} \quad (\text{E.14})$$

Using formula $\ln(a/b) = \ln a - \ln b$ for $\text{Im}(a) \text{Im}(b) > 0$, we rewrite Eq. (E.11) as

$$D_0^{(13)} = \frac{1}{\sqrt{\det(Q_4)}} \sum_{i=1}^2 \sum_{j=1}^4 (-1)^{i+j} \int_0^1 dy \frac{1}{y - y_i} \ln(A_j y^2 + B_j y + C_j) \quad (\text{E.15})$$

with

$$\begin{aligned}
A_1 &= b + c, & B_1 &= e + d, & C_1 &= f, \\
A_2 &= b, & B_2 &= c + e, & C_2 &= d + f, \\
A_3 &= b + j, & B_3 &= e + k + c + h, & C_3 &= d + f, \\
A_4 &= b + j + c + h, & B_4 &= e + k + d, & C_4 &= f.
\end{aligned} \tag{E.16}$$

We would like to make an important remark here. From Eq. (E.14) we can re-write Eq. (E.11) in the form

$$D_0^{(13)} = \frac{1}{(cj - bh)(y_2 - y_1)} \int_0^1 \left(\frac{1}{y - y_2} - \frac{1}{y - y_1} \right) \left(\ln \frac{A + B}{C + D} - \ln \frac{Ay + B}{Cy + D} \right). \tag{E.17}$$

We notice that if $y = y_{1,2}$ then $AD = BC$ which means

$$\frac{A + B}{C + D} \Big|_{y=y_{1,2}} = \frac{Ay + B}{Cy + D} \Big|_{y=y_{1,2}} = \frac{B}{D} \Big|_{y=y_{1,2}}. \tag{E.18}$$

Thus, we get

$$\int_0^1 \left(\frac{1}{y - y_2} - \frac{1}{y - y_1} \right) \left(\ln \frac{A + B}{C + D} \Big|_{y=y_{1,2}} - \ln \frac{Ay + B}{Cy + D} \Big|_{y=y_{1,2}} \right) = 0. \tag{E.19}$$

Subtracting this zero contribution from Eq. (E.15) we get another form

$$\begin{aligned}
D_0^{(13)} &= \frac{1}{\sqrt{\det(Q_4)}} \sum_{i=1}^2 \sum_{j=1}^4 (-1)^{i+j} \\
&\times \int_0^1 dy \frac{\ln(A_j y^2 + B_j y + C_j) - \ln(A_j y_i^2 + B_j y_i + C_j)}{y - y_i}
\end{aligned} \tag{E.20}$$

which is more convenient for the evaluation in terms of Spence functions.

Each integral in Eq. (E.15) or (E.20) can be written in terms of 4 Spence functions as given in Eq. (D.33). Thus $D_0^{(13)}$ can be written in terms of 32 Spence functions.

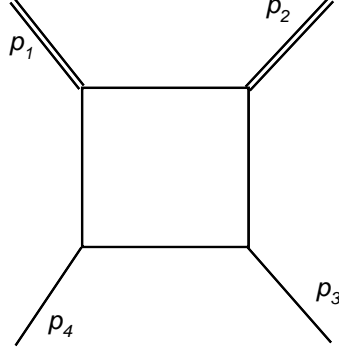


Figure E.2: A box diagram with two adjacent lightlike external momenta p_1 and p_2 . Double line means massless.

E.2 Integral with two adjacent lightlike external momenta

For the box shown in Fig. E.2 with $p_1^2 = p_2^2 = 0$ one gets $b = g = 0$ and writes

$$D_0^{(12)} = \int_0^1 dx \int_0^x dy \int_0^y dz \frac{1}{(ax^2 + cxy + hzx + jyz + dx + ey + kz + f)^2}. \quad (\text{E.21})$$

As in the case of $D_0^{(13)}$, integrating over z gives

$$D_0^{(12)} = \underbrace{\int_0^1 dx \int_0^x dy \frac{1}{a_1 b_1}}_{I_1} + s_k \underbrace{\int_0^1 dx \int_0^x dy \frac{1}{-s_k a_1 (a_1 y + b_1)}}_{I_2}, \quad (\text{E.22})$$

with

$$\begin{aligned} s_k &= \text{sign}(\text{Im}(k)), \quad -s_k a_1 = -s_k(hx + jy + k) - i\epsilon', \\ b_1 &= ax^2 + cxy + dx + ey + f, \\ a_1 y + b_1 &= ax^2 + jy^2 + (c + h)xy + dx + (e + k)y + f - i\epsilon, \end{aligned} \quad (\text{E.23})$$

where we have used the fact that $\text{Im}(a_1 y + b_1) = \text{Im}[dx + (e + k)y + f] = \text{Im}[(x - y)m_3^2 + (1 - x)m_4^2 + ym_1^2 - i\epsilon] < 0$ because $0 \leq y \leq x \leq 1$. ϵ and ϵ' are infinitesimally

positive and carry the sign of the imaginary parts of $-s_k a_1$ and $a_1 y + b_1$. For I_1 , we integrate over y , similar to Eq. (E.8), to get

$$I_1 = \int_0^1 dy \frac{1}{(ja - hc)y^2 + (jd - he - kc)y + jf - ke} \times \left[\ln \frac{(j + h)y + k - i\epsilon'}{hy + k - i\epsilon'} - \ln \frac{(a + c)y^2 + (d + e)y + f}{ay^2 + dy + f} \right]. \quad (\text{E.24})$$

Consider the prefactor

$$\begin{aligned} \det(Q_4) &= (jd - he - kc)^2 - 4(ja - hc)(jf - ke), \\ y_{11(12)} &= \frac{(he + kc - jd) \mp \sqrt{\det(Q_4)}}{2(ja - hc)}, \end{aligned} \quad (\text{E.25})$$

where the indices 11, 12 correspond to $-$ and $+$ signs respectively. We rewrite I_1 as

$$\begin{aligned} I_1 &= \frac{1}{\sqrt{\det(Q_4)}} \sum_{i=1}^2 (-1)^i \int_0^1 dy \frac{1}{y - y_{1i}} \left[\ln \frac{(j + h)y + k - i\epsilon'}{hy + k - i\epsilon'} - \ln \frac{(a + c)y^2 + (d + e)y + f}{ay^2 + dy + f} \right] \\ &= \frac{1}{\sqrt{\det(Q_4)}} \sum_{i=1}^2 \sum_{j=1}^4 (-1)^{i+j} \int_0^1 dy \frac{1}{y - y_{1i}} \ln(A_{1j}y^2 + B_{1j}y + C_{1j}) \end{aligned} \quad (\text{E.26})$$

with

$$\begin{aligned} A_{11} &= 0, \quad B_{11} = h, \quad C_{11} = k, \\ A_{12} &= 0, \quad B_{12} = j + h, \quad C_{12} = k, \\ A_{13} &= a + c, \quad B_{13} = d + e, \quad C_{13} = f, \\ A_{14} &= a, \quad B_{14} = d, \quad C_{14} = f. \end{aligned} \quad (\text{E.27})$$

Thus I_1 can be written in terms of 24 Spence functions. For I_2 we shift $y = y + \alpha x$, α such that

$$j\alpha^2 + (c + h)\alpha + a = 0. \quad (\text{E.28})$$

There are, in general, two values of α . The final result does not depend on which value of α we take. We have used this freedom to find bugs in the numerical calculation and

it turns out to be a very powerful method to check the correctness of the imaginary part which can be very tricky for the case of equal masses. One gets

$$I_2 = \int_0^1 dx \int_{-\alpha x}^{(1-\alpha)x} dy \frac{1}{(Gx + H - i\epsilon')(Ex + F - i\epsilon)}, \quad (\text{E.29})$$

with

$$\begin{aligned} G &= -s_k h - s_k j \alpha, \quad H = -s_k j y - s_k k, \\ E &= (2j\alpha + c + h)y + d + \alpha(e + k), \quad F = jy^2 + (e + k)y + f. \end{aligned} \quad (\text{E.30})$$

For real α we have

$$\begin{aligned} \int_0^1 dx \int_{-\alpha x}^{(1-\alpha)x} dy &= \int_0^1 dx \int_0^{(1-\alpha)x} dy - \int_0^1 dx \int_0^{-\alpha x} dy \\ &= \int_0^{1-\alpha} dy \int_{y/(1-\alpha)}^1 dx - \int_0^{-\alpha} dy \int_{-y/\alpha}^1 dx. \end{aligned} \quad (\text{E.31})$$

We write

$$\frac{1}{(Gx + H - i\epsilon')(Ex + F - i\epsilon)} = \frac{1}{GF - HE} \left(\frac{G}{Gx + H - i\epsilon'} - \frac{E}{Ex + F - i\epsilon} \right). \quad (\text{E.32})$$

Integrating over x , we get

$$\begin{aligned} I_2 &= \int_{-\alpha}^{1-\alpha} \frac{dy}{GF - HE} \ln \frac{G + H}{E + F} - \int_0^{1-\alpha} \frac{dy}{GF - HE} \ln \frac{\frac{Gy}{1-\alpha} + H}{\frac{Ey}{1-\alpha} + F} \\ &+ \int_0^{-\alpha} \frac{dy}{GF - HE} \ln \frac{\frac{Gy}{-\alpha} + H}{\frac{Ey}{-\alpha} + F}. \end{aligned} \quad (\text{E.33})$$

The prefactor

$$\begin{aligned} \frac{GF - HE}{s_k} &= j(j\alpha + c)y^2 + (2\alpha jk + jd - he + kc)y + \alpha(ke + k^2 - jf) + kd - hf \\ &= j(j\alpha + c)(y - y_{21})(y - y_{22}), \end{aligned} \quad (\text{E.34})$$

with

$$y_{21(22)} = \frac{-(2\alpha jk + jd - he + kc) \mp \sqrt{\det(Q_4)}}{2j(j\alpha + c)}, \quad (\text{E.35})$$

where the indices 21, 22 correspond to $-$ and $+$ signs respectively. We rewrite I_2 as

$$\begin{aligned}
I_2 &= \frac{1}{s_k \sqrt{\det(Q_4)}} \sum_{i=1}^2 (-1)^i I_2^{(i)}, \\
I_2^{(i)} &= \int_{-\alpha}^{1-\alpha} \frac{dy}{y - y_{2i}} \ln \frac{G + H}{E + F} - \int_0^{1-\alpha} \frac{dy}{y - y_{2i}} \ln \frac{\frac{Gy}{1-\alpha} + H}{\frac{Ey}{1-\alpha} + F} \\
&\quad + \int_0^{-\alpha} \frac{dy}{y - y_{2i}} \ln \frac{\frac{Gy}{-\alpha} + H}{\frac{Ey}{-\alpha} + F}.
\end{aligned} \tag{E.36}$$

We make the substitutions $y = y - \alpha$ for the first integral, $y = (1 - \alpha)y$ for the second integral and $y = -\alpha y$ for the third integral to get

$$\begin{aligned}
I_2^{(i)} &= \int_0^1 \frac{dy}{y - \alpha - y_{2i}} \ln \frac{-s_k j y - s_k h - s_k k - i\epsilon'}{j y^2 + (c + h + e + k)y + a + d + f - i\epsilon} \\
&\quad - \int_0^1 \frac{(1 - \alpha)dy}{(1 - \alpha)y - y_{2i}} \ln \frac{-s_k(j + h)y - s_k k - i\epsilon'}{(a + c + j + h)y^2 + (d + e + k)y + f - i\epsilon} \\
&\quad + \int_0^1 \frac{-\alpha dy}{-\alpha y - y_{2i}} \ln \frac{-s_k h y - s_k k - i\epsilon'}{a y^2 + d y + f - i\epsilon}.
\end{aligned} \tag{E.37}$$

Consider the arguments of the three logarithms, as demonstrated in Eq. (E.14), it is easy to see that the sign of the imaginary parts of the denominators is negative as indicated by $-i\epsilon$. The derivation is for real α . However, this result is also correct if α is complex as proven in [118]. We can now rewrite I_2 as

$$I_2 = \frac{1}{s_k \sqrt{\det(Q_4)}} \sum_{i=1}^2 \sum_{j=1}^6 (-1)^i \int_0^1 dy \frac{c_j}{a_j y - b_j - y_{2i}} \ln(A_{2j} y^2 + B_{2j} y + C_{2j}) \tag{E.38}$$

with

$$\begin{aligned}
c_1 &= 1, & a_1 &= 1, & b_1 &= \alpha, \\
c_2 &= -(1 - \alpha), & a_2 &= 1 - \alpha, & b_2 &= 0, \\
c_3 &= -\alpha, & a_3 &= -\alpha, & b_3 &= 0, \\
c_4 &= -1, & a_4 &= 1, & b_4 &= \alpha, \\
c_5 &= 1 - \alpha, & a_5 &= 1 - \alpha, & b_5 &= 0, \\
c_6 &= \alpha, & a_6 &= -\alpha, & b_6 &= 0, \\
A_{21} &= 0, & B_{21} &= -s_k j, & C_{21} &= -s_k k - s_k h, \\
A_{22} &= 0, & B_{22} &= -s_k(j + h), & C_{22} &= -s_k k, \\
A_{23} &= 0, & B_{23} &= -s_k h, & C_{23} &= -s_k k, \\
A_{24} &= j, & B_{24} &= c + h + e + k, & C_{24} &= a + d + f, \\
A_{25} &= a + c + j + h, & B_{25} &= d + e + k, & C_{25} &= f, \\
A_{26} &= a, & B_{26} &= d, & C_{26} &= f.
\end{aligned} \tag{E.39}$$

I_2 can be written in terms of 36 Spence functions. Thus

$$D_0^{(12)} = I_1 + s_k I_2 \tag{E.40}$$

contains 60 Spence functions. For the evaluation of $D_0^{(12)}$ in terms of Spence functions, it is better to do the following replacement for each logarithm in $I_{1,2}$:

$$\begin{aligned}
\ln(A_{1j}y^2 + B_{1j}y + C_{1j}) &\rightarrow \ln(A_{1j}y^2 + B_{1j}y + C_{1j}) - \ln(A_{1j}y_{1i}^2 + B_{1j}y_{1i} + C_{1j}), \\
\ln(A_{2j}y^2 + B_{2j}y + C_{2j}) &\rightarrow \ln(A_{2j}y^2 + B_{2j}y + C_{2j}) - \ln(A_{2j}\hat{y}_{2i}^2 + B_{2j}\hat{y}_{2i} + C_{2j}),
\end{aligned} \tag{E.41}$$

with $\hat{y}_{2i} = (y_{2i} + b_j)/a_j$. The argument for this is similar to that explained in the previous section, see Eq. (E.20).

For the boxes with one lightlike external momentum, the result is written in terms of 72 Spence functions by using exactly the same method.

Bibliography

- [1] S. L. Glashow. Partial Symmetries of Weak Interactions. *Nucl. Phys.*, 22:579–588, 1961.
- [2] Steven Weinberg. A Model of Leptons. *Phys. Rev. Lett.*, 19:1264–1266, 1967.
- [3] A. Salam, in Elementary Particle Theory, ed. N. Svartholm (Almqvist and Wiksell, Stockholm, 1968), *Weak and electromagnetic interactions*.
- [4] Murray Gell-Mann. A Schematic Model of Baryons and Mesons. *Phys. Lett.*, 8:214–215, 1964.
- [5] H. Fritzsch, Murray Gell-Mann, and H. Leutwyler. Advantages of the Color Octet Gluon Picture. *Phys. Lett.*, B47:365–368, 1973.
- [6] D. J. Gross and Frank Wilczek. ULTRAVIOLET BEHAVIOR OF NON-ABELIAN GAUGE THEORIES. *Phys. Rev. Lett.*, 30:1343–1346, 1973.
- [7] H. David Politzer. RELIABLE PERTURBATIVE RESULTS FOR STRONG INTERACTIONS? *Phys. Rev. Lett.*, 30:1346–1349, 1973.
- [8] W.-M. *et. al.* Yao. Review of Particle Physics. *Journal of Physics G*, 33:1+, 2006.
- [9] The LEP Collaborations ALEPH, DELPHI, L3, OPAL, and the LEP Electroweak Working Group,[arXiv:hep-ex/0612034v2] (December 2006).

- [10] <http://lhc.web.cern.ch/lhc/>.
- [11] Abdelhak Djouadi. The anatomy of electro-weak symmetry breaking. I: The Higgs boson in the standard model. *Phys. Rept.*, 457:1–216, 2008, hep-ph/0503172.
- [12] A. Denner and S. Dittmaier. Reduction of one-loop tensor 5-point integrals. *Nucl. Phys.*, B658:175–202, 2003, hep-ph/0212259.
- [13] A. Denner and S. Dittmaier. Reduction schemes for one-loop tensor integrals. *Nucl. Phys.*, B734:62–115, 2006, hep-ph/0509141.
- [14] A. Denner, S. Dittmaier, M. Roth, and L. H. Wieders. Complete electroweak $O(\alpha)$ corrections to charged-current $e^+ e^- \rightarrow 4$ fermion processes. *Phys. Lett.*, B612:223–232, 2005, hep-ph/0502063.
- [15] A. Denner, S. Dittmaier, M. Roth, and L. H. Wieders. Electroweak corrections to charged-current $e^+ e^- \rightarrow 4$ fermion processes: Technical details and further results. *Nucl. Phys.*, B724:247–294, 2005, hep-ph/0505042.
- [16] Zvi Bern, Lance J. Dixon, and David A. Kosower. On-Shell Methods in Perturbative QCD. *Annals Phys.*, 322:1587–1634, 2007, 0704.2798.
- [17] C. F. Berger et al. An Automated Implementation of On-Shell Methods for One- Loop Amplitudes. 2008, 0803.4180.
- [18] Carola F. Berger, Zvi Bern, Lance J. Dixon, Darren Forde, and David A. Kosower. All one-loop maximally helicity violating gluonic amplitudes in QCD. *Phys. Rev.*, D75:016006, 2007, hep-ph/0607014.
- [19] Carola F. Berger, Zvi Bern, Lance J. Dixon, Darren Forde, and David A. Kosower. Bootstrapping one-loop QCD amplitudes with general helicities. *Phys. Rev.*, D74:036009, 2006, hep-ph/0604195.

- [20] Ruth Britto, Freddy Cachazo, Bo Feng, and Edward Witten. Direct proof of tree-level recursion relation in Yang- Mills theory. *Phys. Rev. Lett.*, 94:181602, 2005, hep-th/0501052.
- [21] Ruth Britto, Freddy Cachazo, and Bo Feng. New recursion relations for tree amplitudes of gluons. *Nucl. Phys.*, B715:499–522, 2005, hep-th/0412308.
- [22] Z. Bern et al. The NLO multileg working group: summary report. 2008, 0803.0494.
- [23] Ruth Britto, Freddy Cachazo, and Bo Feng. Generalized unitarity and one-loop amplitudes in $N = 4$ super-Yang-Mills. *Nucl. Phys.*, B725:275–305, 2005, hep-th/0412103.
- [24] Darren Forde. Direct extraction of one-loop integral coefficients. *Phys. Rev.*, D75:125019, 2007, 0704.1835.
- [25] Ruth Britto and Bo Feng. Unitarity cuts with massive propagators and algebraic expressions for coefficients. *Phys. Rev.*, D75:105006, 2007, hep-ph/0612089.
- [26] R. P. Feynman. Quantum theory of gravitation. *Acta Phys. Polon.*, 24:697–722, 1963.
- [27] R. P. Feynman. Closed loop and tree diagrams. In *Magic Without Magic*, Ed. J. R. Klauder, San Francisco 1972, 355–375.
- [28] Stefano Catani, Tanju Gleisberg, Frank Krauss, German Rodrigo, and Jan-Christopher Winter. From loops to trees by-passing Feynman’s theorem. 2008, 0804.3170.
- [29] R. J. Eden, P. V. Landshoff, D. I. Olive and J. C. Polkinghorne. The analytic S-matrix. CUP, Cambridge, 1966.
- [30] L. D. Landau. On analytic properties of vertex parts in quantum field theory. *Nucl. Phys.*, 13:181–192, 1959.

- [31] S. Coleman and R. E. Norton. Singularities in the physical region. *Nuovo Cim.*, 38:438–442, 1965.
- [32] G. Passarino and M. J. G. Veltman. One Loop Corrections for $e^+ e^-$ Annihilation Into $\mu^+ \mu^-$ in the Weinberg Model. *Nucl. Phys.*, B160:151, 1979.
- [33] T. Hahn and M. Perez-Victoria. Automatized one-loop calculations in four and D dimensions. *Comput. Phys. Commun.*, 118:153–165, 1999, hep-ph/9807565.
- [34] Thomas Hahn and Michael Rauch. News from FormCalc and LoopTools. *Nucl. Phys. Proc. Suppl.*, 157:236–240, 2006, hep-ph/0601248.
- [35] G. J. van Oldenborgh and J. A. M. Vermaseren. New Algorithms for One Loop Integrals. *Z. Phys.*, C46:425–438, 1990.
- [36] R. Kleiss and W. James Stirling. Spinor Techniques for Calculating $p \text{ anti-}p \rightarrow W^{+-} / Z^0 + \text{Jets}$. *Nucl. Phys.*, B262:235–262, 1985.
- [37] Setsuya Kawabata. A New version of the multidimensional integration and event generation package BASES/SPRING. *Comp. Phys. Commun.*, 88:309–326, 1995.
- [38] S. L. Glashow, J. Iliopoulos, and L. Maiani. Weak Interactions with Lepton-Hadron Symmetry. *Phys. Rev.*, D2:1285–1292, 1970.
- [39] Chen-Ning Yang and Robert L. Mills. Conservation of isotopic spin and isotopic gauge invariance. *Phys. Rev.*, 96:191–195, 1954.
- [40] Peter W. Higgs. Broken symmetries, massless particles and gauge fields. *Phys. Lett.*, 12:132–133, 1964.
- [41] Peter W. Higgs. Spontaneous Symmetry Breakdown Without Massless Bosons. *Phys. Rev.*, 145:1156–1163, 1966.
- [42] F. Englert and R. Brout. BROKEN SYMMETRY AND THE MASS OF GAUGE VECTOR MESONS. *Phys. Rev. Lett.*, 13:321–322, 1964.

- [43] G. S. Guralnik, C. R. Hagen, and T. W. B. Kibble. GLOBAL CONSERVATION LAWS AND MASSLESS PARTICLES. *Phys. Rev. Lett.*, 13:585–587, 1964.
- [44] T. W. B. Kibble. Symmetry breaking in non-Abelian gauge theories. *Phys. Rev.*, 155:1554–1561, 1967.
- [45] Guido Altarelli. New Physics and the LHC. 2008, 0805.1992.
- [46] K. I. Aoki, Z. Hioki, M. Konuma, R. Kawabe, and T. Muta. Electroweak Theory. Framework of On-Shell Renormalization and Study of Higher Order Effects. *Prog. Theor. Phys. Suppl.*, 73:1–225, 1982.
- [47] G. Belanger et al. Automatic calculations in high energy physics and Grace at one-loop. *Phys. Rept.*, 430:117–209, 2006, hep-ph/0308080.
- [48] L. D. Faddeev and V. N. Popov. Feynman diagrams for the Yang-Mills field. *Phys. Lett.*, B25:29–30, 1967.
- [49] A. Bassetto, G. Nardelli, and R. Soldati. Yang-Mills theories in algebraic non-covariant gauges: Canonical quantization and renormalization. Singapore, Singapore: World Scientific (1991) 227 p.
- [50] Michael Edward Peskin and Daniel V. Schroeder. An Introduction to quantum field theory. Reading, USA: Addison-Wesley (1995) 842 p.
- [51] Ansgar Denner. Techniques for calculation of electroweak radiative corrections at the one loop level and results for W physics at LEP-200. *Fortschr. Phys.*, 41:307–420, 1993, arXiv:0709.1075 [hep-ph].
- [52] F. Boudjema and E. Chopin. Double Higgs production at the linear colliders and the probing of the Higgs selfcoupling. *Z. Phys.*, C73:85–110, 1996, hep-ph/9507396.
- [53] A. Sirlin. Radiative Corrections in the SU(2)-L x U(1) Theory: A Simple Renormalization Framework. *Phys. Rev.*, D22:971–981, 1980.

- [54] W. J. Marciano and A. Sirlin. Radiative Corrections to Neutrino Induced Neutral Current Phenomena in the $SU(2)_L \times U(1)$ Theory. *Phys. Rev.*, D22:2695, 1980.
- [55] A. Sirlin and W. J. Marciano. Radiative Corrections to $\nu_\mu + N \rightarrow \mu^- + X$ and their Effect on the Determination of ρ^2 and $\sin^2 \theta_W$. *Nucl. Phys.*, B189:442, 1981.
- [56] Gerard 't Hooft. Renormalization of Massless Yang-Mills Fields. *Nucl. Phys.*, B33:173–199, 1971.
- [57] Gerard 't Hooft. RENORMALIZABLE LAGRANGIANS FOR MASSIVE YANG-MILLS FIELDS. *Nucl. Phys.*, B35:167–188, 1971.
- [58] Stephen P. Martin. A supersymmetry primer. 1997, hep-ph/9709356.
- [59] Abdelhak Djouadi. The anatomy of electro-weak symmetry breaking. II: The Higgs bosons in the minimal supersymmetric model. *Phys. Rept.*, 459:1–241, 2008, hep-ph/0503173.
- [60] L. Girardello and Marcus T. Grisaru. Soft Breaking of Supersymmetry. *Nucl. Phys.*, B194:65, 1982.
- [61] Ali H. Chamseddine, R. Arnowitt, and Pran Nath. Locally Supersymmetric Grand Unification. *Phys. Rev. Lett.*, 49:970, 1982.
- [62] Riccardo Barbieri, S. Ferrara, and Carlos A. Savoy. Gauge Models with Spontaneously Broken Local Supersymmetry. *Phys. Lett.*, B119:343, 1982.
- [63] Savas Dimopoulos and David W. Sutter. The Supersymmetric flavor problem. *Nucl. Phys.*, B452:496–512, 1995, hep-ph/9504415.
- [64] Lawrence J. Hall, Joseph D. Lykken, and Steven Weinberg. Supergravity as the Messenger of Supersymmetry Breaking. *Phys. Rev.*, D27:2359–2378, 1983.

- [65] J. F. Gunion and Howard E. Haber. Higgs Bosons in Supersymmetric Models. 1. *Nucl. Phys.*, B272:1, 1986.
- [66] John F. Gunion, Howard E. Haber, Gordon L. Kane, and Sally Dawson. THE HIGGS HUNTER'S GUIDE. SCIPP-89/13.
- [67] John F. Gunion, Howard E. Haber, Gordon L. Kane, and Sally Dawson. Errata for the Higgs hunter's guide. 1992, hep-ph/9302272.
- [68] (Ed.) Bruning, O. et al. LHC design report. Vol. I: The LHC main ring. CERN-2004-003-V-1; <http://ab-div.web.cern.ch/ab-div/Publications/LHC-DesignReport.html>.
- [69] <http://lhc-machine-outreach.web.cern.ch/lhc-machine-outreach/collisions.htm>.
- [70] D. Rainwater. Searching for the Higgs boson. 2007, hep-ph/0702124.
- [71] F. Gianotti. Physics at the LHC. *Phys. Rept.*, 403:379–399, 2004.
- [72] Fabiola Gianotti and Monica Pepe-Altarelli. Precision physics at the LHC. *Nucl. Phys. Proc. Suppl.*, 89:177–189, 2000, hep-ex/0006016.
- [73] V. Drollinger and A. Sopczak. Comparison of Higgs boson mass and width determination of the LHC and a linear collider. *Eur. Phys. J. direct*, C3:N1, 2001, hep-ph/0102342.
- [74] Fawzi Boudjema and Le Duc Ninh. Leading Yukawa corrections to Higgs production associated with a tagged bottom anti-bottom pair in the Standard Model at the LHC. *Phys. Rev.*, D77:033003, 2008, 0711.2005.
- [75] Le Duc Ninh. Leading electroweak corrections to the process $pp \rightarrow b\bar{b}H$ in the Standard Model at the LHC. *Acta Physica Polonica B Proceedings Supplement No 2, 1 (2008) 411*, presented at the Symposium "Physics in Collision 2007", Annecy, France.

- [76] Le Duc Ninh. Yukawa corrections to Higgs production associated with two bottom quarks at the LHC. *Proceedings of the 43rd Rencontres de Moriond on Electroweak Interactions and Unified Theories*, 2008, 0804.4025.
- [77] R. Michael Barnett, Howard E. Haber, and Davison E. Soper. Ultraheavy Particle Production from Heavy Partons at Hadron Colliders. *Nucl. Phys.*, B306:697, 1988.
- [78] Duane A. Dicus and Scott Willenbrock. Higgs Boson Production from Heavy Quark Fusion. *Phys. Rev.*, D39:751, 1989.
- [79] Stefan Dittmaier, Michael Kramer, and Michael Spira. Higgs radiation off bottom quarks at the Tevatron and the LHC. *Phys. Rev.*, D70:074010, 2004, hep-ph/0309204.
- [80] S. Dawson, C. B. Jackson, L. Reina, and D. Wackeroth. Exclusive Higgs boson production with bottom quarks at hadron colliders. *Phys. Rev.*, D69:074027, 2004, hep-ph/0311067.
- [81] S. Dawson, C. B. Jackson, L. Reina, and D. Wackeroth. Higgs production in association with bottom quarks at hadron colliders. *Mod. Phys. Lett.*, A21:89–110, 2006, hep-ph/0508293.
- [82] C. Buttar et al. Les Houches physics at TeV colliders 2005, standard model, QCD, EW, and Higgs working group: Summary report. 2006, hep-ph/0604120.
- [83] D. Dicus, T. Stelzer, Z. Sullivan, and S. Willenbrock. Higgs boson production in association with bottom quarks at next-to-leading order. *Phys. Rev.*, D59:094016, 1999, hep-ph/9811492.
- [84] Robert V. Harlander and William B. Kilgore. Higgs boson production in bottom quark fusion at next-to- next-to-leading order. *Phys. Rev.*, D68:013001, 2003, hep-ph/0304035.

- [85] Stefan Dittmaier, Michael Kramer, Alexander Muck, and Tobias Schluter. MSSM Higgs-boson production in bottom-quark fusion: Electroweak radiative corrections. *JHEP*, 03:114, 2007, hep-ph/0611353.
- [86] Guangping Gao, Robert J. Oakes, and Jin Min Yang. Heavy supersymmetric particle effects in Higgs boson production associated with a bottom quark pair at LHC. *Phys. Rev.*, D71:095005, 2005, hep-ph/0412356.
- [87] Wolfgang Hollik and Michael Rauch. Higgs-boson production in association with heavy quarks. *AIP Conf. Proc.*, 903:117–120, 2007, hep-ph/0610340.
- [88] S. Dawson and C. B. Jackson. SUSY QCD Corrections to Associated Higgs-bottom Quark Production. *Phys. Rev.*, D77:015019, 2008, 0709.4519.
- [89] J. A. M. Vermaseren. New features of FORM. 2000, math-ph/0010025.
- [90] A.C. Genz and A.A. Malik. An adaptive algorithm for numerical integration over an N-dimensional rectangular region. *J. Comput. Appl. Math.* 6 (1980) 295–302; <http://wwwasdoc.web.cern.ch/wwwasdoc/shortwrupsdir/d120/top.html>.
- [91] A. Pukhov. CalcHEP: a package for evaluation of Feynman diagrams and integration over multi-particle phase space.
<http://www.ifh.de/pukhov/calchep.html>.
- [92] <http://user.pa.msu.edu/wkt/cteq/cteq6/cteq6pdf.html>.
- [93] J. Pumplin et al. New generation of parton distributions with uncertainties from global QCD analysis. *JHEP*, 07:012, 2002, hep-ph/0201195.
- [94] Daniel Stump et al. Inclusive jet production, parton distributions, and the search for new physics. *JHEP*, 10:046, 2003, hep-ph/0303013.
- [95] S. Kretzer, H. L. Lai, F. I. Olness, and W. K. Tung. CTEQ6 parton distributions with heavy quark mass effects. *Phys. Rev.*, D69:114005, 2004, hep-ph/0307022.

- [96] K. A. Assamagan et al. The Higgs working group: Summary report 2003. 2004, hep-ph/0406152.
- [97] C. Itzykson and J. B. Zuber. QUANTUM FIELD THEORY. New York, Usa: McGraw-hill (1980) 705 P.(International Series In Pure and Applied Physics).
- [98] G. Sterman. An Introduction to quantum field theory. Cambridge, UK: Univ. Pr. (1993) 572 p.
- [99] J. D. Bjorken and S. D. Drell. Relativistic Quantum Fields. McGraw-Hill Book Company, New York, 1965.
- [100] http://www.ph.unito.it/~maina/scuola08/program_2008.html.
- [101] D. Fotiadi, M. Froissart, J. Lascoux, and F. Pham. Applications of an isotopy theorem. *Topology*, 4:159–191, 1965.
- [102] E.R. Speer and M.J. Westwater. Generic Feynman amplitudes. 1971.
- [103] Zoltan Nagy and Davison E. Soper. Numerical integration of one-loop Feynman diagrams for N- photon amplitudes. *Phys. Rev.*, D74:093006, 2006, hep-ph/0610028.
- [104] Y. Kurihara and T. Kaneko. Numerical contour integration for loop integrals. *Comput. Phys. Commun.*, 174:530–539, 2006, hep-ph/0503003.
- [105] J. C. Polkinghorne and G. R. Screaton. The analytic properties of perturbation theory. II. *Nuovo Cimento (10)*, 15:925–931, 1960.
- [106] From a private communication with Eric Pilon.
- [107] R. J. Eden. Lectures on the use of perturbation methods in dispersion theory. College Park, Md.: University of Maryland, (1961).
- [108] J. Cunningham. Some properties of the landau curves. *Rev. Mod. Phys.*, 36(3):833–843, Jul 1964.

- [109] J. Tarski. Analyticity of the Fourth Order Scattering Amplitude with Two Complex Invariants. *J. Math. Phys.*, 1:149, 1960.
- [110] T. Kinoshita. Mass singularities of Feynman amplitudes. *J. Math. Phys.*, 3:650–677, 1962.
- [111] R. Keith Ellis and Giulia Zanderighi. Scalar one-loop integrals for QCD. *JHEP*, 02:002, 2008, 0712.1851.
- [112] See for example: T. Binoth, M. Ciccolini, N. Kauer, and M. Kramer. Gluon-induced W-boson pair production at the LHC. *JHEP*, 12:046, 2006, hep-ph/0611170.
- [113] See for example: C. Bernicot and J. Ph. Guillet. Six-Photon Amplitudes in Scalar QED. *JHEP*, 01:059, 2008, 0711.4713.
- [114] Fawzi Boudjema and Le Duc Ninh. $b\bar{b}H$ production at the LHC: Yukawa corrections and the leading Landau singularity. 2008, 0806.1498, submitted to Phys. Rev. D.
- [115] H. W. Turnbull. The Theory of Determinants, Matrices, and Invariants. Blackie and Son Ltd., London, 1945. 2nd edition, p. 77.
- [116] A. Denner, S. Dittmaier, M. Roth, and D. Wackeroth. Predictions for all processes $e^+ e^- \rightarrow \text{fermions} + \text{gamma}$. *Nucl. Phys.*, B560:33–65, 1999, hep-ph/9904472.
- [117] www.to.infn.it/maina/network/scuola/index.html.
- [118] Gerard 't Hooft and M. J. G. Veltman. Scalar One Loop Integrals. *Nucl. Phys.*, B153:365–401, 1979.
- [119] F. Boudjema, A. Semenov, and D. Temes. Self-annihilation of the neutralino dark matter into two photons or a Z and a photon in the MSSM. *Phys. Rev.*, D72:055024, 2005, hep-ph/0507127.

- [120] E. de Doncker, Y. Shimizu, J. Fujimoto, and F. Yuasa. Computation of loop integrals using extrapolation. *Comput. Phys. Commun.*, 159:145–156, 2004.
- [121] Alessandro Ballestrero and Ezio Maina. A New method for helicity calculations. *Phys. Lett.*, B350:225–233, 1995, hep-ph/9403244.
- [122] <http://www.perl.com/>.
- [123] L. C. Maximon. The dilogarithm function for complex argument. *Royal Society of London Proceedings Series A*, 459:2807–2819, November 2003.
- [124] L. Lewin. *Polylogarithms and Associated Functions*. North-Holland, New York, 1981.
- [125] George F. Carrier, Max Krook, and Carl E. Pearson. *Functions of a Complex Variable: Theory and Technique (Classics in Applied Mathematics)*. Society for Industrial and Applied Mathematics, Philadelphia, PA, USA, 2005.
- [126] Ansgar Denner, U. Nierste, and R. Scharf. A Compact expression for the scalar one loop four point function. *Nucl. Phys.*, B367:637–656, 1991.